A MICROFLUIDIC IN VITRO MODEL OF THE BLOOD-BRAIN BARRIER

by

Ross Hunter Booth

A dissertation submitted to the faculty of
The University of Utah
in partial fulfillment of the requirements for the degree of

Doctor of Philosophy

Department of Bioengineering

The University of Utah

December 2014

The University of Utah Graduate School

STATEMENT OF DISSERTATION APPROVAL

The dissertation of **Ross Hunter Booth**

has been approved by the following supervisory committee members:

Hanseup Kim	, Chair	**07/21/2014** Date Approved
Alan Dorval	, Member	**07/21/2014** Date Approved
Hamid Ghandehari	, Member	**07/21/2014** Date Approved
Carlos Mastrangelo	, Member	**07/21/2014** Date Approved
Florian Solzbacher	, Member	**07/21/2014** Date Approved

and by **Patrick Tresco** , Chair/Dean of

the Department/College/School of **Bioengineering**

and by David B. Kieda, Dean of The Graduate School.

ABSTRACT

The blood-brain barrier (BBB) limits entry of most molecules into the brain and complicates the development of brain-targeting compounds, necessitating novel BBB models. This dissertation describes the first microfluidic BBB model allowing the study of BBB properties in relation to various chemical compounds by enabling tunable wall shear stress (WSS) via dynamic fluid flow, cell-cell interaction through a thin co-culture membrane, time-dependent delivery of test compounds, and integration of sensors into the system, resulting in significant reduction of reagents and cells required and shorter cell seeding time. Use of parallel channels first enabled simultaneous monitoring of multiple cell populations under a wide range (~x15) of WSS.

The microfluidic model formed the BBB by incorporating brain endothelial (b.End3) and glial (C6/C8D1A) cells at the intersection of two crossing microchannels, respectively representing luminal and abluminal sides, fabricated in a transparent polydimethylsiloxane (PDMS) substrate utilizing high-precision soft lithography techniques. The utilized cells were adopted from immortalized cells for high consistency over repeated passages and pure and proliferative culture.

The developed microfluidic BBB model was validated by (1) expression of tight junction protein ZO-1 and glial protein GFAP by fluorescence imaging, and P-gp activity by Calcein AM, confirming key BBB proteins; (2) high trans-endothelial electrical

resistance (TEER) of co-cultures exceeding 250Ωcm^2 confirming sufficiently contiguous cell layer formation; (3) chemically-induced barrier modulation, with transient TEER loss by 150μM histamine (~50% for 8-15min), and increase in permeability at elevated pH (10.0); (4) size-dependent (668-70,000Da) compound permeability mimicking *in vivo* trends; and (5) highly linear correlation (R^2>0.85) of clearance rates of seven selected neural drugs with *in vivo* brain/plasma ratios. We demonstrated the effects of WSS (0-86dyn/cm^2) on bEnd.3 properties under increasing WSS, including increase in (6) TEER, (7) cell re-alignment toward flow direction, and (8) protein expression of ZO-1/P-gp, and (9) decrease in tracer permeability.

The developed *in vitro* microfluidic BBB model provides distinct advantages for monitoring and modulating barrier functions and prediction of compound permeability. Thus, it would provide an innovative platform to study mechanisms and pathology of barrier function as well as to assess novel pharmaceuticals early in development for their BBB clearance capabilities.

TABLE OF CONTENTS

LIST OF FIGURES

LIST OF TABLES

ABBREVIATIONS

µBBB	microfluidic *in vitro* blood brain barrier model
µCCA	microscale cell culture analogue
µNVU	microfluidic *in vitro* neurovascular unit
µTAS	micro total analysis system
AD	Alzheimer's Disease
ABC	ATP-binding cassette
ADMET	absorption, distribution, metabolism, excretion, toxicity
APTES	aminopropyltriethoxysilane
AUC	are under the curve
B/P	brain/plasma ratio
BBB	blood-brain barrier
BCRP	breast cancer resistance protein
bEnd.3	brain endothelial cell line
BMEC	brain microvascular endothelial cell
BSA	bovine serum albumin
C8-D1A	astrocyte type I cell line
CAD	computer-aided drafting
CMC	Comparative Medicine Center

CNS	central nervous system
CVD	chemical vapor deposition
DAPI	4’,6-diamidino-2-phenylindole
DMEM	Dulbecco’s Modified Eagle Medium
DRIE	deep reactive-ion etching
EC	endothelial cell
ECS	extracellular space
ELS	elastin-like polypeptide
ESEM	environmental scanning electron microscopy
F12	Ham’s Nutrient Mixture F12
FBS	fetal bovine serum
FITC	fluorescein isothiocyanate
GDNF	glial-derived neurotrophic factor
GFAP	glial fibrillary acidic protein
HBSS	Hanks’ Balanced Salt Solution
HEPES	4-(2-hydroxyethyl)-1-piperazineethanesulfonic acid
HPLC	high-performance liquid chromatography
IGF-I	insulin-like growth factor I
K_p	brain uptake ratio
LC	liquid chromatography
LC-MS	liquid chromatography-mass spectrometry
LogP	logarithm of the octanol/water partition coefficient
$LogP_e$	logarithm of endothelial permeability coefficient

LPCVD	low-pressure chemical vapor deposition
LRP-1	low density lipoprotein receptor-related protein 1
MDR1	multidrug resistance protein 1, P-glycoprotein
MEA	multi-electrode array
MEMS	microelectromechanical systems
MMD	multilayered microfluidic device
MRP	multidrug resistance protein
MS	mass spectrometry
NBM	neurobasal medium
NMDA	N-Methyl-D-aspartate
Nrf2-ARE	NF-E2-related factor 2-antioxidant response element
NVU	neurovascular unit
P-gp	P-glycoprotein
PAμBBB	parallel array *in vitro* blood brain barrier model
PC	polycarbonate
PD	pharmacodynamic
PDMS	polydimethylsiloxane
PECVD	plasma-enhance chemical vapor deposition
PFA	paraformaldehyde
PBPK	physiologically-based pharmacokinetic models
PI	propidium idodie
PK	Pharmacokinetic
P_S	permeability surface area product

PVDF	polyvinylidene fluoride
RAM	random access memory
RIE	reactive-ion etching
SEM	scanning electron microscope
SI	shape index
siRNA	small interfering ribonucleic acid
SMBB	Sorenson Molecular Biotechnology Building
TCD	thermal conductivity detector
TEER	trans-endothelial electrical resistance
TJ	tight junctions
TNF-α	tumor necrosis factor alpha
VEC	vascular endothelial cells
WB	western blot
WSS	wall shear stress
ZO-1	zonal occludin-1

ACKNOWLEDGEMENTS

I would foremost like to thank my advisor and mentor, Dr. Hanseup Kim, for continuous guidance and support throughout the described studies, and for having faith in my abilities to conduct such research independently. Thank you for your continual motivation and drive. I would like to thank my advisory committee members, Chuck Dorval, Hamid Ghandehari, Carlos Mastrangelo, and Florian Solzbacher. I would also like to acknowledge Moses Noh, whose work on the micro-flow sensor contributed to the study in Chapter 4. The majority of this research was funded by USTAR startup fund, without which it may not have been possible. Finally, I wish to thank my friends and family for their continuous support, especially my wife Stella, for her patience during all my late nights away at the lab.

CHAPTER 1

INTRODUCTION

This dissertation aims to address the feasibility of modeling the blood-brain barrier (BBB) by developing an innovative chip-based microfluidic platform. This chapter describes the significance of such a system, and overviews the project and approach taken in this dissertation to develop and characterize the described platforms.

1.1 Motivation and Significance

There is currently a prevalent and increasing burden on the healthcare industry over the growing number of patients suffering from neurodegenerative disorders of the central nervous system (CNS), notably Alzheimer's Disease (AD), which is diagnosed in an estimated 24 million patients worldwide, and is projected to double every 20 years [1]. However, CNS drug development progress is comparatively slower than other healthcare areas [2,3]. The distinguishing pharmacokinetic hurdle [4] to drug development for CNS disorders is the BBB [3], which effectively blocks nearly all nonpolar compounds larger than ~500Da from entering neural tissue [5]. Due to this prevalent role in drug development, innovative preclinical models of the BBB are in high demand. BBB models primarily have two applications: (1) to monitor barrier function and investigate changes

induced by chemical and physical stimuli; and to (2) predict the rate of delivery of compounds across the BBB. The first application is extremely useful for basic research on BBB physiological mechanisms, and to study the BBB's role in CNS disease progression [6]; the second application can be used to test the passage of novel drugs [7] or drug delivery vehicles [8] across the BBB during stages of prescreening and optimization of CNS treatments prior to animal and clinical studies [9]. This dissertation aims to include feasibility of the use of the innovative system for both of these applications within its scope.

In vitro models are a valuable precursor to animal models due to lower cost, time, and ethical constraints [10], and enable more focused, controllable, and repeatable experimentation, as well as more massively-parallel environments. The validity of an *in vitro* model is dependent on how closely it reproduces the key physiological characteristics of its *in vivo* archetype. The key characteristics of the BBB include: Structurally, (1) a contiguous monolayer of endothelial cells containing strongly expressed tight junctions [11]; (2) astrocytes in close contact with the endothelial monolayer, which play a key role in modulating barrier function through cell signaling from endfoot processes [12]; functionally having strong expression of (3) membrane-bound transport components for receptor-mediated transport and efflux transport [13]; a microenvironment experiencing (4) fluidic shear stress, which is known to have a mechanotransductive effect on endothelial cell phenotype [14,15]; Model conditions should show highly (5) selective permeability from the constituted structures to dissolved compounds; and (6) maintenance of high electrical resistance indicating the contiguity of the endothelial cell monolayer and soundness of tight junctions. Additionally, the reliable,

rapid measurement of these physiological conditions is an important component to a valid BBB model. This is particularly the case for trans-membrane properties, thus an effective BBB model must allow reliable measurement of tracer compound permeability and trans-endothelial electrical resistance (TEER).

The commercially-available current state-of-the art *in vitro* models comprises a simple transwell insert [16]. Transwell inserts comprise of a porous membrane attached to a cup-shaped insert for placement in multiwell plates of multiple sizes. However, they are limited to represent only static environments, without continuous luminal flows. Luminal flows are known to cause fluid shear stress [5] that imposes mechanotransductive effects on endothelial cell phenotypes *in vitro* and *in vivo* [17], thus influencing a myriad of molecular pathways [18] activated via membrane-bound receptors [19], inducing proliferative responses including tight junction proteins [20], membrane efflux transporters [14], and cytoskeletal restructuring and cell reorientation [15] in a manner dependent on flow direction [21]. Thus, a truly representative *in vitro* model should have physiologically relevant flow conditions.

In 1996, a dynamic *in vitro* BBB (DIV-BBB) [22-24] model was developed which utilizes hollow fibers to mimic BBB architecture and flow conditions. However, the DIV-BBB has wall thickness (150μm) significantly higher than transwell membranes (10μm), discouraging cell-cell interaction and decreasing background permeability, take significantly longer (~3x) to reach steady-state barrier permeability [10,22] than 2D models, and lack the potential for integration of biosensors and compartmentalized or parallel array setups due to the simplicity of their design and fabrication as simple hollow fiber bundles in a bulky cartridge [10,22], having diameters of approximately 1mm, more

than 10x larger than brain capillaries, failing to accurately represent *in vivo* flow conditions.

To address these short-comings of existing systems, this dissertation presents a microfluidic *in vitro* BBB model (μBBB) [25] that includes several practical advantages: (A) Significantly lower costs, timescales, and ethical issues than *in vivo* studies; (B) Massively-parallel, controlled and repeatable environments, and easier elucidation of molecular mechanisms than *in vivo* models; (C) Dynamic microenvironment providing shear stress stimulation to cultured endothelial cells, allowing controlled delivery of test compounds and improved permeability analysis compared to *in vitro* static models; (D) Much thinner culture membrane, decreasing the distance between co-cultured cells for compound diffusion, compared to *in vitro* DIV-BBB models. (E) Smaller functional volumes for quicker media exchange, material conservation, and scales closer to true *in vivo* dimensions; (F) A 2D culture surface allowing complete initial seeding and shorter times to steady-state barrier resistance for a more rapid turn-around time, shortening experiments and allowing a more high-throughput approach to experimentation.

The impact of this dissertation involves development of an innovative platform for BBB modeling with the aforementioned practical advantages, and characterization and validation of such a system in both scientific and engineering aspects for use in basic research and pharmaceutical drug development for the following two applications: (1) The system was developed and utilized to test responses of the cultured cells to chemical and physical stimuli, including chemical stimulation [26] and shear stress [27]. (2) The system was also used for proof-of-concept as a drug delivery test platform for predicting clinical clearance through the BBB. The combined impact of these studies will prove the

validity of a microfluidic BBB platform for use by both the scientific community, to study BBB physiological functions and responses to various chemical or physical stimuli in basic research, and the industry community, for prescreening of BBB clearance of novel pharmaceuticals as a predictive tool. It is our educated opinion that microfluidic systems will inevitably be commercialized for heavy use in these applications in the coming years, and the work in this dissertation is intended as the launching point.

1.2 Summary of Innovation

This dissertation reports the first published chip-based microfluidic cell culture model for the BBB [28], the first published microfluidic platform allowing simultaneous testing of endothelial cell trans-membrane and morphological properties under multiple distinct shear stresses [29], and the first multidrug (>3) correlation of a microfluidic BBB model with *in vivo* brain penetration results [30]. The multilayered microfluidic device (MMD) comprises two base polydimethylsiloxane (PDMS) substrates, two glass layers, and a free-standing porous membrane [31] fixed between the PDMS layers. It houses two perpendicularly-crossing channels to introduce dynamic flows, and the functional barrier area is located on free-standing membrane at the channel junction, enabling the ability to conduct flow-based permeability assays. This is particularly advantageous because it allows steady-state concentrations to be maintained in both the luminal and abluminal chambers, whereas static transwell concentrations gradually change over time as they reach equilibrium, reducing the accuracy of permeability calculations. Commercial electrode sticks have been used to measure TEER in conventional microfluidic systems [32]; in contrast, the μBBB system is alternately designed with integrated fully-fabricated

thin-film electrodes, fixing the distance between electrodes for measurement repeatability. Nondestructive microscopy of the system is also possible due to transparency of the PDMS substrate. In addition, we developed a novel experimental design employing a parallel array of the luminal channels containing endothelial cells, allowing unprecedented simultaneous measurement of endothelial cell trans-membrane and morphological properties under varying magnitudes of shear stress. In summary, these engineered innovations of the novel platform enable scientific advantages, by allowing mimicry of the dynamic environment found *in vivo,* as well as practical advantages, by providing greater experimental control, high tunability of model conditions, better measurement of BBB functionality, material conservation, and cost.

1.3 Research Objectives

The objective of this dissertation is to introduce, characterize, and validate the first microfluidic BBB, was largely accomplished through three distinct research phases, which are respectively reported in Chapters 3-5. The forthcoming chapters will be structured as follows, describing the complete scope of this dissertation.

Chapter 2 provides the background necessary for understanding the studies described in the following chapters, including (1) underlying biology of the BBB, (2) review of previous models of the BBB, (3) review of microfluidics systems and fabrication methods used in this dissertation, (4) characteristics of the BBB model used in this dissertation, and (5) methods of model validation used in this dissertation.

Chapter 3 describes initial development and characterization of the μBBB model using the techniques and methods described in Chapter 2, establishing the μBBB system

as a low-cost, polymeric alternative to previous dynamic hollow-fiber based systems, with particular discussion comparing these systems. The foundational concepts of the μBBB are covered in this chapter, and the methods of observing trans-membrane properties were developed. Cell lines bEnd.3 and C8-D1A were used in this study, and the effects of chemical modulation (histamine, pH elevation) on trans-membrane barrier properties (TEER, tracer permeability) were observed.

Chapter 4 describes the development of a modified version of the device designed for observation of quantitatively-dependent effects of shear stress stimulation on endothelial cell physiological properties, in an unprecedently high-throughput manner. This was done to test for any flow-rate limitations for the BBB model with the bEnd.3 cell line, and to observe mechanical modulation effects on both trans-membrane barrier properties (TEER, tracer permeability) and morphometric properties (cell alignment, shape), as well as on BBB protein expression (zonal occludin-1, P-glycoprotein).

Chapter 5 describes a proof-of-concept study of the system as a predictive tool for drug clearance, by running 7 CNS-targeting drugs currently under development through the BBB model prepared with bEnd.3 cells in monoculture and in co-culture with C6 astrocytes. Concentration-specific cytotoxicity of these compounds were measured to establish acceptable permeability assay concentrations, and permeated concentrations of the drugs were measured with chromatographic methods. Permeability results were compared *in vivo* data from literature to confirm *in vivo* correlation.

Chapter 6 summarizes the project's impact, and stature within the current, new body of microfluidic BBB platforms, presents some unpublished results relating to P-glycoprotein and glial fibrillary acidic protein expression by the selected cell lines bEnd.3

and C6, and discusses several future directions and applications for the model characterized in this dissertation.

1.4 References

[1] Ferri, C. P., M. Prince, C. Brayne, H. Brodaty, L. Fratiglioni, M. Ganguli, K. Hall, K. Hasegawa, H. Hendrie, and Y. Huang. Global prevalence of dementia: A delphi consensus study. *The Lancet*. **366**(9503):2112-2117, 2006.

[2] Pangalos, M. N., L. E. Schechter, and O. Hurko. Drug development for cns disorders: Strategies for balancing risk and reducing attrition. *Nat Rev Drug Discov*. **6**(7):521-532, 2007.

[3] Pardridge, W. M., W. H. Oldendorf, P. Cancilla, and H. J. Frank. Blood-brain barrier: Interface between internal medicine and the brain. *Ann Intern Med*. **105**(1):82-95, 1986.

[4] Pardridge, W. M. Blood-brain barrier drug targeting: The future of brain drug development. *Mol Interv*. **3**(2):90-105, 151, 2003.

[5] Cardoso, F. L., D. Brites, and M. A. Brito. Looking at the blood-brain barrier: Molecular anatomy and possible investigation approaches. *Brain Res Rev*. **64**(2):328-363, 2010.

[6] Hawkins, B. T. and T. P. Davis. The blood-brain barrier/neurovascular unit in health and disease. *Pharmacol Rev*. **57**(2):173-185, 2005.

[7] Reichel, A. Addressing central nervous system (cns) penetration in drug discovery: Basics and implications of the evolving new concept. *Chem Biodivers*. **6**(11):2030-2049, 2009.

[8] Pathan, S. A., Z. Iqbal, S. M. Zaidi, S. Talegaonkar, D. Vohra, G. K. Jain, A. Azeem, N. Jain, J. R. Lalani, R. K. Khar, and F. J. Ahmad. Cns drug delivery systems: Novel approaches. *Recent Pat Drug Deliv Formul*. **3**(1):71-89, 2009.

[9] Cucullo, L., B. Aumayr, E. Rapp, and D. Janigro. Drug delivery and in vitro models of the blood-brain barrier. *Curr Opin Drug Discov Devel*. **8**(1):89-99, 2005.

[10] Frampton, J. P., M. L. Shuler, W. Shain, and M. R. Hynd. Biomedical technologies for in vitro screening and controlled delivery of neuroactive compounds. *Cent Nerv Syst Agents Med Chem*. **8**(3):203-219, 2008.

[11] Wolburg, H. and A. Lippoldt. Tight junctions of the blood-brain barrier:

Development, composition and regulation. *Vascul Pharmacol*. **38**(6):323-337, 2002.

[12] Haseloff, R. F., I. E. Blasig, H. C. Bauer, and H. Bauer. In search of the astrocytic factor(s) modulating blood-brain barrier functions in brain capillary endothelial cells in vitro. *Cell Mol Neurobiol*. **25**(1):25-39, 2005.

[13] Taylor, E. M. The impact of efflux transporters in the brain on the development of drugs for cns disorders. *Clin Pharmacokinet*. **41**(2):81-92, 2002.

[14] Cucullo, L., M. Hossain, V. Puvenna, N. Marchi, and D. Janigro. The role of shear stress in blood-brain barrier endothelial physiology. *BMC Neurosci*. **12**(40, 2011.

[15] Galbraith, C. G., R. Skalak, and S. Chien. Shear stress induces spatial reorganization of the endothelial cell cytoskeleton. *Cell Motil Cytoskeleton*. **40**(4):317-330, 1998.

[16] Rubin, L. L., D. E. Hall, S. Porter, K. Barbu, C. Cannon, H. C. Horner, M. Janatpour, C. W. Liaw, K. Manning, J. Morales, and et al. A cell culture model of the blood-brain barrier. *J Cell Biol*. **115**(6):1725-1735, 1991.

[17] Chien, S., S. Li, and Y. J. Shyy. Effects of mechanical forces on signal transduction and gene expression in endothelial cells. *Hypertension*. **31**(1 Pt 2):162-169, 1998.

[18] Acevedo, A. D., S. S. Bowser, M. E. Gerritsen, and R. Bizios. Morphological and proliferative responses of endothelial cells to hydrostatic pressure: Role of fibroblast growth factor. *J Cell Physiol*. **157**(3):603-614, 1993.

[19] Chien, S. Molecular basis of rheological modulation of endothelial functions: Importance of stress direction. *Biorheology*. **43**(2):95-116, 2006.

[20] Siddharthan, V., Y. V. Kim, S. Liu, and K. S. Kim. Human astrocytes/astrocyte-conditioned medium and shear stress enhance the barrier properties of human brain microvascular endothelial cells. *Brain Res*. **1147**(39-50, 2007.

[21] Chien, S. Effects of disturbed flow on endothelial cells. *Ann Biomed Eng*. **36**(4):554-562, 2008.

[22] Santaguida, S., D. Janigro, M. Hossain, E. Oby, E. Rapp, and L. Cucullo. Side by side comparison between dynamic versus static models of blood-brain barrier in vitro: A permeability study. *Brain Res*. **1109**(1):1-13, 2006.

[23] Cucullo, L., M. S. McAllister, K. Kight, L. Krizanac-Bengez, M. Marroni, M. R. Mayberg, K. A. Stanness, and D. Janigro. A new dynamic in vitro model for the multidimensional study of astrocyte-endothelial cell interactions at the blood-

brain barrier. *Brain Res*. **951**(2):243-254, 2002.

[24] Neuhaus, W., R. Lauer, S. Oelzant, U. P. Fringeli, G. F. Ecker, and C. R. Noe. A novel flow based hollow-fiber blood-brain barrier in vitro model with immortalised cell line pbmec/c1-2. *J Biotechnol*. **125**(1):127-141, 2006.

[25] Booth, R. and H. Kim. A multi-layered microfluidic device for in vitro blood-brain barrier permeability studies. *International Conference on Miniaturized Systems for Chemistry and Life Sciences*. **15**(1388-1390, 2011.

[26] Stamatovic, S. M., R. F. Keep, and A. V. Andjelkovic. Brain endothelial cell-cell junctions: How to "open" the blood brain barrier. *Current Neuropharmacology*. **6**(179-192, 2008.

[27] Krizanac-Bengez, L., M. R. Mayberg, E. Cunningham, M. Hossain, S. Ponnampalam, F. E. Parkinson, and D. Janigro. Loss of shear stress induces leukocyte-mediated cytokine release and blood–brain barrier failure in dynamic in vitro blood–brain barrier model. *Journal of Cellular Physiology*. **206**(1):68-77, 2006.

[28] Booth, R. and H. Kim. Characterization of a microfluidic in vitro model of the blood-brain barrier ([small mu]bbb). *Lab on a Chip*. 2012.

[29] Booth, R., S. Noh, and H. Kim. A multiple-channel, multiple-assay platform for characterization of full-range shear stress effects on vascular endothelial cells. *Lab on a Chip*. **14**(11):1880-1890, 2014.

[30] Booth, R. and H. Kim. Permeability analysis of neuroactive drugs through a dynamic microfluidic in vitro blood–brain barrier model. *Annals of biomedical engineering*. 1-13, 2014.

[31] Chueh, B. H., D. Huh, C. R. Kyrtsos, T. Houssin, N. Futai, and S. Takayama. Leakage-free bonding of porous membranes into layered microfluidic array systems. *Anal Chem*. **79**(9):3504-3508, 2007.

[32] Douville, N. J., Y. C. Tung, R. Li, J. D. Wang, M. E. El-Sayed, and S. Takayama. Fabrication of two-layered channel system with embedded electrodes to measure resistance across epithelial and endothelial barriers. *Anal Chem*. **82**(6):2505-2511, 2010.

CHAPTER 2

BACKGROUND

2.1 Structure and Function of the Blood-Brain Barrier

The distinguishing characteristic in the process of drug delivery to the central nervous system (CNS), consisting of the brain and spinal cord, is the blood-brain barrier (BBB). Around the end of the 19th century, it was first noted by Paul Ehrlich that intravenous injections of dye elucidate a clear lack of staining in the CNS [1]. A few years later, the term BBB was first coined by Lewandowski et al. when studying the limitations of perfusion of potassium ferrocyanate into the CNS [2]. The invention of the electron microscope in the 1960s allowed the anatomical structure of the BBB to be observed and described using intravascular horseradish peroxidase injections [3], rapidly progressing our understanding of the structure and function of the BBB.

2.1.1 Introduction to the Neurovascular Unit

The BBB effectively restricts virtually all molecules except small and lipophilic ones – only small lipophilic molecules with molecular weights below ~500 Daltons typically cross the BBB freely [4]. The presence of this uniquely restrictive barrier to compounds in the CNS exists primarily for 4 physiological reasons: (1) Maintenance of homeostasis of the brain, (2) protection of brain tissue from exogenous compounds, (3)

controlling nutrient supply in the brain, and (4) directing inflammatory responses according to changes in the local environment [5].

2.1.2 BBB Physiological Features

The physical characteristics of the BBB are dictated by a dynamic interaction between multiple cell types, primarily the brain endothelial cells lining the capillaries in the brain. Brain endothelial cells are distinct from peripheral endothelial cells in several ways, including reduced pinocytic activity [6], lack of fenestrations [7], higher mitochondrial density [8], and higher expression of membrane transporters [9]. These distinct characteristics are highly dependent on the interactions with surrounding glial cells, thus the neurovascular unit is considered to consist of multiple types of cells. Anatomically, the neurovascular unit is comprised of both the endothelial cells and the surrounding pericytes and astrocytes [10], though there is evidence that neurons may also play a role in endothelial phenotype as well [11] (Figure 2.1).

The BBB's barrier properties are primarily governed by a combination of the physical barrier provided by the tight junctions, the transport barrier provided by the membrane transport efflux mechanisms including ATP-binding Casette transporter proteins such as P-gp or other multidrug resistance proteins (MRPs) such as breast cancer resistance protein (BCRP) [12], as well as a metabolic barrier component. Additionally, the BBB maintains the ionic composition of the brain for optimal synaptic functions of neurons, largely via specific ion channels and transporters [13]. Thus, the BBB is important for protecting the CNS from neurotoxic and xenobiotic compounds, in addition to the homeostasis necessary for CNS function and nutrient supply.

Structure of Brain Capillaries

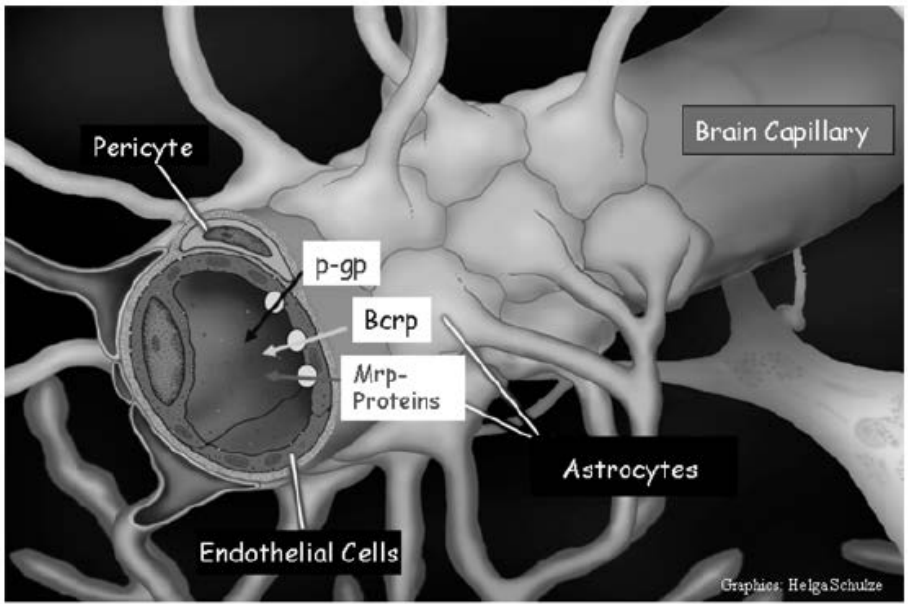

Figure 2.1 Structure of brain capillaries. Structurally, brain capillaries are made up of brain microvascular endothelial cells the endfeet of astrocytes, and pericytes within the basement membrane. In addition to tight junctions between endothelial cells, the blood-brain barrier is functionally controlled by ATP-binding cassette (ABC) transporters such as p-gp, or other multidrug resistance proteins (MRPs) such as breast cancer resistance protein (Bcrp). Figure from Fricker [12].

2.1.2.1 Role of Endothelial Cell Tight Junctions

The paracellular route for compounds to pass the endothelial cell layer is primarily regulated by tight junctions, a highly complex structural assembly of proteins [14] which make up the extracellular space between adjacent endothelial cells, effectively abolishing aqueous diffusional pathways between the blood and brain [15,16]. Endothelial cell tight junctions consist of transmembrane proteins [17,18], largely occludins [19], claudins [20], and junctional adhesion molecules (JAMs). These compounds are directly linked to cytoplasmic proteins known as zonal occludins, which are further linked to the actin cytoskeleton [21]. Thus, the zonal occludins (ZO-1, ZO-2, ZO-3) regulate the

effectiveness of tight junctions in barrier function, and are most commonly studied (particularly ZO-1) for validation of BBB properties because they are specific markers for tight junctions and act as an intermediate molecule in the tight junction complex.

In addition to their role as structural barriers, tight junctions have also been observed to be dynamic signaling complexes, involving control of gene expression, cell proliferation, and differentiation in a bi-directional manner [22]. For example, with this mechanism, tight junctions coordinately receive and transmit signal molecules of the Rho class with intracellular mechanisms [23], signaling routes mainly involving protein kinases activated through phosphorylation cascades [24]. Thus, the role of tight junctions in BBB function likely extends beyond guarding the paracellular route for compounds.

2.1.2.2 Role of Membrane Transporters

P-glycoprotein (P-gp), often referred to as the primary multidrug resistance (MDR) protein, is an efflux transporter found on luminal endothelial membranes as well as at astrocyte processes in the brain [25]. While the paracellular route for compounds is guarded by tight junctions, the transcellular route is guarded largely by ABC transporters such as P-gp [26] or Bcrp, effectively expelling a large variety of compounds into the luminal space as a key component in BBB homeostasis. For this reason, P-gp expression is considered to be an essential measure for evaluating cell constituents in *in vitro* BBB models [27].

Also relevant to drug delivery through the BBB is the presence of transporters on endothelium which move the opposite direction from P-gp. These are particularly receptor-mediated systems which make it possible for particular macromolecules which

cannot enter paracellular routes to enter the brain through transcellular routes [10]. Among the best known and characterized are transferrin receptor [28], glucose carrier GLUT-1 [29], and amino acid transporter L1 [30], which exist in higher concentrations than peripheral endothelial cells, providing potential delivery routes to the brain for tailored macromolecules [31]. To date, such macromolecules have not proven to reach the CNS in effective pharmacological concentrations, though such routes are promising for future clinical application, and future study testing the effectiveness of such macromolecules for BBB passage in *in vitro* models should include characterization of the presence of the target receptor in the BBB model in use.

2.1.2.3 Role of Astrocytes

As early as 1967, it has been predicted that astrocytes play a major role in inducing BBB phenotype and specialization [32]. Astrocyte endfeet have been observed to cover the majority of the abluminal surface of brain endothelial cells [33], secreting a number of inducing factors, such as transforming growth factor-β, glial-derived neurotrophic factor (GDNF), basic fibroblast growth factor, and angiopoetin 1 [34]. These processes influence a number of mediating compounds in BBB function [35], including effects on both the paracellular compound pathway, tight junction expression [36], and effects on the transcellular pathway, membrane-bound transporters such as P-gp [37] and GLUT-1 [33]. Astrocytes have been seen to produce factors inducing development of tight junctions through these processes, leading to induction of transcytotic mechanisms such as transferrin receptor [38]. BBB characteristics have even been induced in non-brain endothelial cells such human vein endothelial cells by co-culturing with astrocytes [39].

Furthermore, endothelial cells have been shown to produce factors to facilitate astrocyte differentiation [40]. It is clear that the interaction between these two cell types are highly important to BBB physiology, therefore they are included in most *in vitro* co-culture models.

2.1.2.4 Role of Shear Stress

The exposure to physiological shear stress plays a critical role in modulating endothelial cell morphology [41]. Endothelial cells cultured under shear stress show a number of physiological characteristics more representative of *in situ [42]*, such as an abundance of endocytic vesicles, microfilaments, and clathrin-coated pits [43]. A number of membrane-bound proteins, including integrins [44], caveolae [45], G proteins [46], and ion channels [47,48], have been shown to be involved in mechanotransduction of shear stress into pleiotropic physiological responses, initiated by downstream signal-regulated kinases [49]. Among the physiological functions affected are: (1) production of substances related to vasoactivity and cell adhesion [50,51], (2) increased expression of tight junctions [52], (3) increased cell survival [53], (4) energy metabolism [54], and (5) membrane transport systems [42]. Accordingly, these physiological responses have an effect on barrier activity; therefore, reconstituting a high-shear stress environment is essential for a truly representative BBB model.

2.2 Traditional Models of the Blood-Brain Barrier

The two primary classifications of BBB models are *in vivo,* studies with complete animal models, and *in vitro*, studies with reconstituted cell-based platforms in the

laboratory. While all aspects of the *in vivo* system are yet to be reproduced in an *in vitro* model [55], they have contributed significantly to our current understanding of endothelial transport and regulation. Indeed, the principle advantages of *in vitro* models include (1) higher capacity and higher throughput, (2) lower costs and reagents required, (3) the ability to quantify compounds directly in physiological buffers, (4) feasible identification of cell toxicity, (5) and lesser ethical constraints [56]. Nevertheless, to increase their experimental advantage, *in vitro* models must be developed to mimic the *in vivo* microenvironment as closely as possible to ensure their predictive accuracy.

2.2.1 *In Vivo* Models

Direct *in vivo* brain uptake techniques provide reliable characterization of drug BBB penetration [57]. Studies of *in vivo* brain penetration look at both the permeability surface area product P_S, as well as brain uptake ratio K_p, which includes equilibration of the compound in neural tissue over time [58]. K_p is based on the ratio of brain and plasma concentrations under steady-state biodistribution [59]. P_S is particularly advantageous in terms of permeability information, because it is not compromised by drug metabolism, protein binding, or nonspecific brain binding [60]. P_S is measured by perfusing the brain directly with the tracer via the carotid artery, allowing short-term measurement of permeability. However, P_S is a highly technically demanding product to measure, and is considerably lower-throughput than K_p, often only measured in late stages of compound development. Though these methodologies are comparably low-throughput compared to *in vitro* measurements, their results are particularly important for validating *in vitro* models.

In addition to full-animal *in vivo* experiments, isolated brain capillaries from various sources, including human and bovine, rat, rabbit, and pig [61], have been studied *ex vivo* for studying drug accumulation, transporter activity , and gene expression [62,63]. However, such *ex vivo* studies are technically demanding and ethically limiting, the preparation procedures tend to modify barrier functions [64], while access to the luminal surface of microvessels is nearly impossible [65]. Thus, the development of *in vitro* models was deemed necessary.

2.2.2 *In Vitro* Models

Cells used in *in vitro*-based BBB models are commonly derived from one of many mammalian species, including bovine, porcine, rat, murine, or human [66]. High costs and laborious, time-consuming isolation procedures lead to the necessity for use of immortalized cell lines. These cell lines have the advantage of undergoing a large number of passages without any change in phenotype, and enable ultra-high yield and homogeneity [67]. However, these cell lines have a disadvantage in that they typically show higher leakiness and lower expression levels of tight junction and transporter proteins than primary cells [55]. Overall, the utilization of immortalized cell lines have been widely accepted for *in vitro* models due to high consistency from passage to passage as well as in intralaboratory-comparison, highly repeatable physiological behaviors and rapid, low-cost model characterization.

2.2.2.1 Transwell Systems

The current state-of-the-art for BBB models, and epithelial/endothelial cell culture models in general, is the simple transwell system (Figure 2.2A). Transwells are comprised of porous inserts for well plates, available in many sizes (6-, 12-, 24-, or 48-wells). These systems are unique over the universal polystyrene-surface cell culture vessels in that they allow interaction between multiple chambers through a porous barrier which restricts migration of cells of a certain size, while allowing all components of the cellular media [69]. Another, perhaps more significant way these models transcend basic

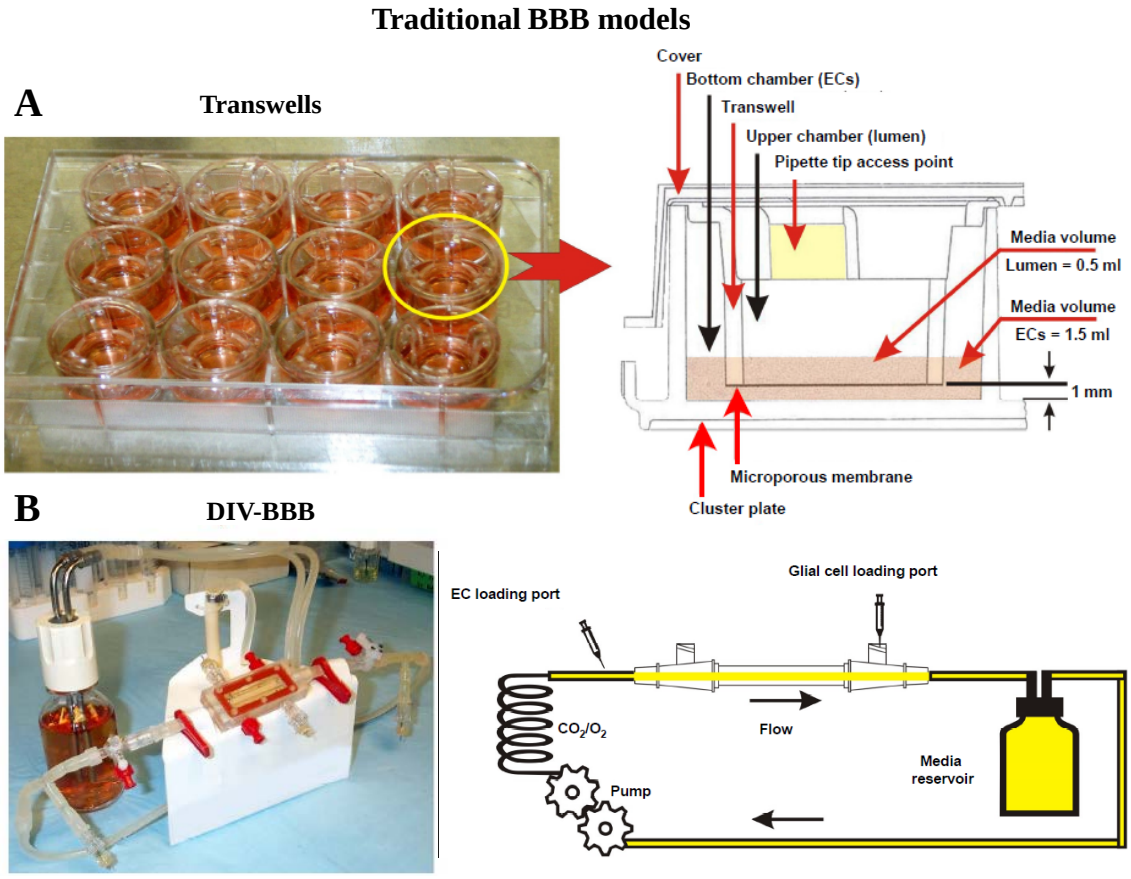

Figure 2.2 Traditional *in vitro* BBB models. (A) The majority of *in vitro* BBB models use transwells, in static condition with a porous insert in a multi-well setup. (B) Hollow fiber bundled systems represent a dynamic *in vitro* for introducing flow-based environments while allowing co-culture with astrocytes. Figure from Cucullo [68].

cell culture vessels is that they allow modeling of cooperative interaction between the multiple cell types, while keeping the cells of different type isolated from each other physically [70]. However, the overly simplistic transwell platform lacks the exposure to intraluminal shear stress. This is critical for the vascular endothelium to develop and/or maintain intrinsic BBB properties observed *in vivo*; therefore, integration of a shear stress component to the system is crucial. In addition, experimental control over delivered permeability compounds is insufficient for accurate permeability measurement, as concentrations in the luminal and abluminal chambers change over time, contradicting assumptions of linearity of membrane flux during permeability assays.

2.2.2.2 Dynamic *In Vitro* BBB Models

To enable the introduction of flow into BBB cell culture models, several types of microfluidic systems have been utilized. The cone-plate apparatus represents the first attempt [71], comprising a rotating cone opposite an endothelial cell monolayer. The angular motion of the cone translates to shear stress exerted on the cell monolayer; however, the shear stress is not entirely uniform along the radius of the cone, resulting in an uneven magnitude of shear stress applied to the cells. In addition, such systems did not contain porous substrates for permeability studies or compartmentalized co-cultures. Nevertheless, many early studies of shear stress effects on cells were conducted with these systems [72].

Artificial capillary-like structures known as hollow fibers, which are made from thermoplastic polymers such as polypropylene or polysulfone, have been adapted to model cell-based vascular systems under flow and have been coined dynamic *in vitro*

BBB (DIV-BBB) systems (Figure 2.2B) [73]. In macroscopic terms, these hollow fiber bundles resemble vessel structures, though at a 10x larger scale. Bundles are typically seeded in the interior with brain microvascular cells, with astrocytes in the exterior space of the bundles, allowing study of physiological response of cells under tunable levels of shear stress [74]. However, due to the 3D structure of these systems, cell growth cannot be evaluated directly with microscopy, and they take significantly longer to reach full confluence than 2D systems. The thicknesses (200 μm) of the hollow fiber walls are far higher than track-etched porous membranes, by more than a factor of 10x. This increase in distance makes the presence of cell-cell interaction via migration of astrocyte processes through the porous substrate far less likely [75]. Finally, in comparison to these hollow fiber systems, much smaller systems with lesser cell and reagent consumption and faster turn-around times can be achieved with microfluidic systems containing tailored 2D culture surfaces and integrated sensors.

2.3 MEMS and Microfluidics

Microfabrication technology, particularly microelectromechanical systems (MEMS) allow the development of a more innovative BBB model. MEMS technologies have stemmed from the methodological foundations provided by the integrated circuit industry, allowing development of mechanical systems at an increasingly smaller scale. Thus far, microfluidic systems have been employed primarily in industry for the applications of analytic devices, miniaturized sensors, flow cytometry, and disposable HPLC chips [76]. More recently, these techniques have garnered increased interest in the pharmaceutical industry due to advantages over simple systems, such as (1) smaller

dimensions with high resolution/sensitivity, (2) incorporation of sensing and actuating function, (3) ease to study interaction of molecules with cells, (4) minimal invasiveness, (5) high portability, (6) shorter analysis time, and (7) high-throughput experimentation [77].

2.3.1 Previous Microfluidic Cell Culture Systems

In terms of flow-based cell culture systems, microfluidics hold several practical advantages over macroscale flow systems, including efficient exploitation of mechanical forces, dominance of viscous and diffusional forces, rapid turn-around times, and low costs [78]. Microfluidic systems permit spatial confinements resulting in biochemical gradients and diffusive profiles more representative of the *in vivo* microenvironment. The advent of microfluidics have generated unprecedented opportunity to study and use biological cells in new, uniquely tailorable microenvironments in a highly parallel experimental manner [79], enabling generation of abundant information. Microfluidic platforms have seen considerable progress for the application of liver cell culture and study [80,81]. Because of the small dimensions and resultantly laminar flows inherent to microfluidic platforms, they are particularly well suited for modeling vascular systems in a high-throughput and environmentally relevant manner; therefore, such systems have been utilized for reconstituting vascular systems [82] and probing artery function [83], proving useful for studying blood circulation dynamics [84], behaviors of vascular endothelial cells under shear stress [85], angiogenesis dynamics [86], and vascularization of tailored scaffolds [87]. However, the system described in this dissertation represents the first reported microfluidic system for the application of BBB modelling [88].

2.3.2 Fabrication Methods

Techniques used in this dissertation involve both hard (silicon, glass) and soft (polymer) micromachining methods. While hard micromachining has its roots in the integrated circuits industry [89], soft lithography methods have been developed more recently, based on fabrication of polymeric substrates [77].

2.3.2.1 Hard Micromachining Methods

The primary thin-film deposition method used in this dissertation is sputtering [90]. Sputtering has some advantages over other thin-film deposition methods, such as evaporation and chemical vapor deposition (CVD): A wide variety of materials are feasible for deposition, and the Denton Discovery 18 system available in our fabrication facility has multiple targets, allowing three metals to be deposited in a single pump-down process. Second, there is relatively low energy and temperature of the sputtered atoms compared with evaporation, which is particularly advantageous for the lift-off process, in which the films are laid directly onto photoresist, which tends to be distorted at high temperatures. However, even with this low-temperature process, distorting does occur at high enough power; therefore, sputtering processes in this dissertation were conducted at no higher than 50W power.

Lithography is used to transfer a master pattern onto the substrate surface. Photolithography is the predominant method for microfabrication, where UV light passing through a mask is used to define the etching pattern on the substrate. The lithography method used for thin-film patterning in this dissertation is the lift-off process, which differs from the etching process in that the photoresist is deposited prior to thin-

film deposition, used the following steps: (1) Generation of the 2D pattern on computer-aided drafting (CAD) software; (2) Fabrication of the mask for these processes were generated on a quartz plate with a chromium absorber metal by e-beam lithography, which has a higher resolution than photolithography; (3) Deposition of the photoresist on a cleaned, prepared glass substrate. A lift-off photoresist (LOR-10B) in addition to patterning positive photoresist (S1813) was used, in that the material is dissolved by the developer when exposed to UV light. Spin-coating of the viscous photoresist solutions was used to uniformly deposit the materials on the substrate, with speeds ranging from 1500-4000 RPM; (4) Soft-baking of the photoresist on a hotplate (190°C for LOR-10B, 110°C for S1813) to ensure success of the pattern transfer; (5) UV exposure through the aligned photomask. A UV lamp projects light through the mask to the substrate in hard contact at the correct dose to achieve proper pattern development; (6) Wet development of the exposed photoresist using liquid developer (MIF-300); (7) Thin-film layer deposition. The sputtering process is low-temperature enough to prevent distortion of the photoresist pattern; (8) Lift-off using acetone under sonication. This process results in the final patterned layers of metal films on the glass substrate.

2.3.2.2 Soft Micromachining Methods

In contrast with traditional hard materials, polymers are inexpensive, easy to handle, have highly tunable mechanical properties, and are largely biocompatible. The silicone-based elastomer polydimethylsiloxane (PDMS) has been adopted as the most popular bioMEMS polymer substrate due to its highly suitable combination of physical and chemical properties [91]. These properties allow (1) high fidelity in pattern transfer;

(2) superior conformability to other surfaces for large-scale integration [92]; (3) good sealing with itself and other surfaces, both reversibly and irreversibly [93]; (4) highly transparent (5) highly permeable to gases [94], facilitating cell-based applications. The PDMS material used in this dissertation was the Sylgard 184 (Dow-Corning), which cures quickly at a mixed ratio of 10:1 at any temperature higher than about 60°C.

Due to the malleable characteristics of uncured PDMS, an enormous variety of shapes can be defined by use of replica molding, enabling high-fidelity 3D pattern generation with exceptionally high aspect ratios [89]. The replica molds for this dissertation were generated using photolithography. In contrast with the lift-off process used for hard micromachining in this project, the replica mold was generated from SU-8, which is a negative photoresist, in that the material is solidified by the developer when exposed to UV light. SU-8 is composed of EPON SU-8 resin, and a photosensitizer triaryl sulfonium salt [95]. Due to the epoxy resin's high stability and high cross-linking density, extremely thick coatings can be achieved. One of the thickest varieties (SU-8 2075) was used in this project to enable the 200 μm thick microfluidic structures.

2.3.2.3 Bonding Methods

Soft substrate bonding is one of the most critical steps for generation of multi-layered microfluidic device. Hard substrate bonding (silicon-silicon, silicon-glass, or glass-glass) were not required for the structures used in this dissertation. The particular soft-substrate bonding methods under concern in this dissertation were PDMS-PDMS, PDMS-glass, and PDMS-polycarbonate membrane. Indeed, errors with bonding are perhaps the most prominent source of leaking in microfluidic devices [96]. Thus, an

important design consideration for microfluidic devices is the method of bonding. The use of oxygen plasma allows simple oxidation of the surface of both PDMS and glass substrates to generate irreversible siloxane bonds (Si-O-Si) for a strong, reliable bond [97].

However, the need to bond the polycarbonate porous membrane between the PDMS substrates limits the feasibility of the plasma oxidation method. More recently, a method was devised where PDMS prepolymer is used as a mortar to enable bonding of porous membranes into layers of PDMS [98], and this method was used for the study presented in Chapter 3. The PDMS prepolymer mixture is diluted in toluene to significantly reduce the viscosity of the mixture in a tunable manner, and is spin-coated onto a Si wafer, which is then pressed to the channel substrate to generate a sufficiently thin layer of PDMS prepolymer to allow bonding of the membrane without clogging the channels. The assembly is pressed together and cured in an oven, generating a strong bond. However, this method requires both heat and pressure, making sufficiently uniform application of pressure to obtain a complete seal around the channel structures, while preventing deformation of the channel structure or the membrane, quite tedious for larger structures leading to frequent failures; therefore, a different method was adopted for the subsequent studies. This method utilizes 3-amino-propyltriethoxysilane (APTES), a biocompatible surface treatment, to modify the surface of the membrane, allowing plasma activation [99]. Following ~20 min of surface activation in a 5% aqueous solution at 80°C, the membrane and PDMS substrates are activated with oxygen plasma, and a strong, irreversible bond is achieved at room temperature in the same manner as conventional plasma bonding [97], after which residual APTES on the free-standing

membrane is dissolved in ethanol. Indeed, this method yielded a more reliable bond than the prepolymer mortar method, as indicated by a significant reduction in the occurrence of leaks.

2.3.2.4 Packaging and Preparation

Packaging methods used in this dissertation pertain primarily to postassembly preparation. A Disco DAD641 dicing machine was used to cut the glass wafers used for electrode inserts into rectangular shapes to be embedded into the channel layers. Prior to bonding, a biopsy punch with 2mm diameter was used to core holes for the inlets and outlets. Following bonding, inlets and outlets were prepared for connection to tubing assemblies. Needles with the sharp edge cut flat were used to connect tubing to the chips due to their low volume, and were embedded inside 25 μL pipette tips to ensure secure connection to the inlet holes. Dow Corning 734 flowable sealant was used for securing inlet connectors due to its high compatibility with PDMS, and lack of any chemical reaction to ethanol, which is used heavily during the sterilization process.

2.4 *In Vitro* Model Characteristics

As it is well known that no existing *in vitro* BBB model has mimicked all BBB functionalities [100], researchers in development of BBB *in vitro* models aim to achieve the most relevant features of the BBB for the particular aim of investigation [101]. Nevertheless, the ultimate goal in the field is to achieve as many BBB characteristics as possible, as is our goal in this dissertation. Inclusion of the right model characteristics are key to generating the best possible model.

2.4.1 Constituent Cell Types

The current standard is co-culture systems with endothelial and glial cells. A third cell type, the pericyte, is present *in vivo* and covers approximately a quarter of the abluminal endothelial surface, playing a role in endothelial proliferation and inflammatory processes [102]. Difficulties in isolating this cell type have limited their use in *in vitro* models. For this dissertation, we have focused on the two standard cell types, brain endothelial and glial cells.

Though advantageous in initial cell phenotype, primary cells are difficult and costly to obtain, and generally lose BBB characteristics after only a few passages, while also being subject to ethical limitations. Conversely, immortalized cell lines retain consistent physiological and morphological characteristics over as many passages as needed. This is due to the immortalization process through viral transformation. These provide advantages in experimental consistency, despite their drawbacks in cell phenotype.

Many immortalized cell lines have been used in BBB models, including brain endothelial cells of bovine, porcine, murine, or rat source, MDCK cells, and CACO-2 cells [103]. Popular endothelial cell lines have been used, including the RBE4 from rat origin [104] or the hCMEC/D3 cell line derived from human origin [105]. In addition, the highly characterized human epithelial cell line Caco-2 has been used in BBB models [106], despite heavy differences from brain endothelial cells in terms of cell phenotype [107]. For this dissertation, we opted to use the bEnd.3 immortalized murine cell line because it has been shown to express levels of ZO-1, claudin-5, and occludin comparative to primary brain microvascular endotheliacl cells (BMECs) [108,109], and exhibits rapid

proliferation. For co-culture, the immortalized rat glial cell line C8-D1A was used in the initial characterization study. However, its proliferative properties were inferior to bEnd.3, thus subsequently the C6 glial cell line was used because it was commonly used in previous co-culture BBB models [110,111] and to generate astrocyte-conditioned medium [112], and because its proliferative properties were comparable to bEnd.3.

2.4.2 Porous Membrane

The most common materials for track-etched porous membranes used in BBB models are polycarbonate and polyethylene terephthalate (PET), each with their own advantages. Polycarbonate membranes have lower nonspecific binding properties and thus less interference with testing compounds, whereas PET membranes are transparent, allowing light-based microscopic observation of cells adhered to them [113]. Another influential property is pore size, where pores of 0.4μm have been seen to produce highest trans-endothelial electrical resistance (TEER) with otherwise similar conditions [114]. Furthermore, 0.4 μm pore size has been shown to restrict astrocyte cell bodies from migrating through the membrane, while allowing end-feet to pass through the pores to interact with the adjacent endothelial cells [115]. Conversely, 3.0 μm pores prompt migration of astrocyte growth on both sides of the membrane, and clogging of pores, preventing passage of astrocytic soluble factors [116,117]. For these reasons, polycarbonate membranes of 0.4 μm pore size (provided by Corning) were used in this dissertation, with a 10 μm membrane thickness, and nominal pore density of $1x10^8$ pores/cm^2, which is significantly higher than the primary alternative PET ($4x10^6$ pores/cm^2).

2.4.3 Adhesion-Promoting Treatments

Coating of the membrane culture surface is a key model condition for achieving optimal model performance, particularly in microfluidic models where adhesion to the substrate is a potential issue. These protein coatings are intended to mimic the basal lamina, a key extracellular component in the BBB [118]. The major components of the basal lamina include type IV collagen and fibronectin [119], which are commonly used in previous BBB models as well as in this dissertation. What concentrations should be used for these coatings have not been clearly established [120]; therefore, some trial-and-error experimentation was required for this study. For example, in Chapter 3, lower concentrations were used (10 μg/mL) during the coating step, and was sufficient for the low flows used in the study. However, increasing concentrations of each protein to 100 μg/mL for coating in Chapter 4 enabled optimal adhesion of endothelial cells at comparatively higher flows (several orders of magntitude), and this coating scheme was also used in Chapter 5.

2.4.4 Cellular Media

An advantage of immortalized cell lines is that they perform consistently well without media supplementation, and the same media formulation was used for all studies in this dissertation: A 50/50 mixture of Dulbecco's Modified Eagle Medium (DMEM) and Ham's Nutrient Mixture F12, supplemented with 0.365 g/L L-glutamine and 5% fetal bovine serum (FBS). In addition, penicillin/streptomycin solution and amphotericin B were added to the media formulation to help prevent bacterial and fungal contamination, respectively.

Many BBB models have opted to replace the presence of astrocytes with astrocyte-conditioned medium, or media bathing astrocyte cell cultures to allow it to contain astrocyte-derived soluble factors secreted by the cells [121]. These astrocyte-conditioned media have been seen to modulate barrier properties relating to expression of tight junction [122] and efflux transporter proteins [123]. Other supplementation includes the addition of hydrocortisone to the cell culture media following seeding, which has been seen to benefit the formation of barrier properties, though the exact mechanism by which hydrocortisone does this remains largely unclear [124]. Another additive commonly used to purify primary cells is puromycin, which eliminates nonendothelial cells from the cultured cells [125].

2.4.5 Microfluidic Structures

The use of microfluidics in this dissertation enabled the application of shear stress to the cells in a highly controllable manner. The microfluidic structure itself went through a number of changes depending on the aims of the study itself. All mask designs were generated using SolidWorks software. For consistency, the depth of the microfluidic structure was kept at a constant 200 μm thickness. Slight variations of SU-8 film thicknesses occur due to imperfect levelling of the hot-plate and occasional presence of bubbles during the sot-bake process [126]. To reduce the occurences of these bubbles, a glass dish was placed over the hot-plate during the soft-bake process following initial spin-coating, and the film was deposited in two 100 μm layers instead of a single 200 μm layer. The degree of error allowed during fabrication of the silicon replica molds was 10 μm; therefore, for quality control, SU-8 thicknesses were measured with a Tencor

Profilometer, and only molds were used where all measurements were between 190-210 µm.

All flow in all versions of the microfluidic structures used in this dissertation are completely laminar [127] and thus viscous-dominant, where dissolved particle motion is dominated by diffusion, as in capillaries: The Reynolds number for a rectangular channel is calculated as:

$$Re = \frac{2\rho V_{ave}(wh)}{\mu(w+h)} \tag{2.1}$$

where ρ and μ are density and viscosity, respectively, and w and h are channel width and height, respectively. Based on this equation, the lowest aspect ratio channel used in this dissertation (and highest Reynolds number) of dimensions 100µmX400µm, has a Reynolds number of ~2.3s/cm*V_{ave}, where V_{ave} is the average velocity. Thus, the minimum velocity for transition to turbulent flow is ~1000 cm/s, several orders of magnitude higher than practical flow-rates used in this dissertation; therefore, it is a valid assumption that flow is completely laminar for all experiments.

2.5 Methods of Model Characterization

This dissertation uses previously established methods of characterization to validate the model in each of the studies described in the forthcoming chapters. The primary methods of model characterization are TEER and compound permeability, as they are direct representations of monolayer tightness and compound diffusion, respectively. Additionally, to look at cell morphologies and specific expression of BBB protein constituents, imaging and protein analysis methods are also used, though they are

more indirect measures of barrier function. Finally, to characterize flow characteristics of the microfluidic component of the model, computational simulations are used. The specific methodological procedures of each of these techniques for the studies in Chapters 3-6 will be described in greater detail as it pertains to the specific study.

2.5.1 TEER Measurement

TEER of endothelial cell monolayers is feasible because the cells may be considered to have a level of resistance to ionic movement through the paracellular pathways (tight junctions), which can be considered as equivalent to a combination of resistors and capacitors in a circuit [128], though the capacitors are typically neglected from the model circuit for simplicity, leaving a series of resistors. Thus, the placement of two electrodes opposite each chamber representing the luminal and abluminal compartments allows measurement of this resistance.

According to consensus in the field of *in vitro* BBB models, a generally accepted level of TEER above 150Ωcm^2 is characteristic of a good *in vitro* model [129-131], while *in vivo* microvessels commonly reach 1800 Ωcm^2 [132]. In contrast, peripheral TEER *in vivo* is typically measured to be less than 100 Ωcm^2. It is worthy of note that TEER results are difficult to compare or repeat across separate laboratories [129]. For example, one group has published TEER values of 400-700 Ωcm^2 [133] with commercial Endohm chambers, significantly lower than data measured with custom equipment in the same laboratory between 1200-1800 Ωcm^2 [134] under the same conditions. Thus, TEER is most useful when used as a quality control measure for experimental consistency, as a comparison of intralaboratory culture conditions, or for monitoring toxicity or barrier

modulation.

2.5.2 Trans-BBB Permeability Methods

The most direct measurement of BBB function of an *in vitro* model is measurement of compound tracers. The relationship between TEER and solute transport is not necessarily linear, since transport depends on a combination of transport through all paracellular pathways (tight junctions), while TEER depends on areas with lowest electrical resistance between cells [135]. Indeed it was shown that at TEER values higher than 130 Ωcm^2, paracellular permeability was independent of TEER status [136]; therefore, paracellular permeability should be monitored with tracer compounds. To be used as a marker of paracellular transport, tracer compounds should not be compounds which work as ligands for transcellular transporters [129]. There are many convenient, fluorescent compounds which fit this category, such as sodium fluorescein [137], lucifer yellow [138], propidium iodide, or fluorescein isothiocyanate (FITC)-labeled dextrans [139]. FITC-Dextran is particularly convenient, and was used in each of the proposed studies, because it comes in many sizes, allowing monitoring of permeability according to size difference with physicochemical consistency.

The flow-based microfluidic permeability assay platform provides diffusive conditions much closer to that of *in vivo* than in large-scale static systems. Because at such sub-mm scales, compound transport is dominated by the convective effect [140] due to the laminar flow profile in capillaries or microchannels, test compounds provided by the steady laminar flow, permeability rates are dependent on the supplied concentration, and not on the time-dependent compound motion that occurs in static diffusion systems.

2.5.3 Imaging Methods

In addition to barrier function measurement with TEER and permeability, cellular function can be monitored using methods of microscopy. Fluorescence microscopy of immobilized, fixed cultures of BBB cells allows monitoring of the localized expression of specific proteins. One of the most important of these compounds is considered to be ZO-1, one of the key components of tight junctions [52]. Expression of this compound is essential to barrier function; therefore, an endothelial monolayer lacking clear expression of ZO-1 is expected to be lacking in barrier function. Second, the use of microscopy allows monitoring of morphological characteristics, such as cell shape and orientation. Cellular morphometry is particularly relevant as it relates to the response to shear stress [141].

2.5.4 Protein Expression Techniques

Direct assays of protein expression is useful for characterizing constituent cells used in the model. An analytical technique useful for monitoring the expression of specific proteins in a cell population is western blot. Total protein extracts from the population of cells are separated by gel electrophoresis according to size or charge, and are transferred to a nitrocellulose or polyvinylidene fluoride (PVDF) membrane, where they can be stained with specific antibodies [142]. The expression of this antibody is proportional to the total protein expressed, and can be quantitated using band densitometry. Any compound can be used for this technique, as long as there are antibodies available. Also, the expression, hence activity, of P-gp can be directly assayed using MDR biochemical assays [143]. These methods are particularly useful for

comprehensive BBB functional characterization, because TEER and permeability are focused on the paracellular pathway, while assays observing P-gp activity and expression focuses on the transcellular pathway, both of which are constituents of BBB function.

2.5.5 Microfluidics Simulations

Flow characteristics of the microfluidic structures used in this dissertation were elucidated early with the use of computational simulations. These simulations were conducted using Comsol 4.0, with the laminar flow multiphysics module. Drafted CAD files of the microfluidic structures can be exported into the Comsol model, or drawn within the software itself. 3D models with geometric meshes with approximately 3-5,000,000 element number were used to maximize model precision, while staying within the memory limits of the computers used (16 GB RAM). Assumptions made within these models include a Newtonian fluid with dynamic viscosity of 1.2 mPa·s (DMEM media with 5% fetal bovine serum), and with input conditions of flow-rate at the inlet, with 0 pressure at the outlets. Comsol's output is the flow velocity fields and the shear rate at all locations along the walls. From the shear rate, shear stress is calculated by multiplying the dynamic viscosity.

2.6 References

[1] Ehrlich, P. Das sauerstufbudurfnis des organismus. *Eine Farbenanalytische Studie Berlin, Germany: Hirschwald*. 1885.

[2] Lewandowsky, M. Zur lehre der cerebrospinalflussigkeit. *Z. klin. Med*. **40**(480):l900, 1900.

[3] Reese, T. and M. J. Karnovsky. Fine structural localization of a blood-brain barrier to exogenous peroxidase. *The Journal of cell biology*. **34**(1):207-217,

1967.

[4] Pardridge, W. M. Blood-brain barrier drug targeting: The future of brain drug development. *Molecular interventions*. **3**(2):90, 2003.

[5] Cardoso, F. L., D. Brites, and M. A. Brito. Looking at the blood–brain barrier: Molecular anatomy and possible investigation approaches. *Brain research reviews*. **64**(2):328-363, 2010.

[6] Sedlakova, R., R. Shivers, and R. Del Maestro. Ultrastructure of the blood-brain barrier in the rabbit. *Journal of submicroscopic cytology and pathology*. **31**(1):149-161, 1999.

[7] Fenstermacher, J., P. Gross, N. Sposito, V. Acuff, S. Pettersen, and K. Gruber. Structural and functional variations in capillary systems within the braina. *Annals of the New York Academy of Sciences*. **529**(1):21-30, 1988.

[8] Oldendorf, W. H., M. E. Cornford, and W. J. Brown. The large apparent work capability of the blood-brain barrier: A study of the mitochondrial content of capillary endothelial cells in brain and other tissues of the rat. *Annals of neurology*. **1**(5):409-417, 1977.

[9] Ohtsuki, S. and T. Terasaki. Contribution of carrier-mediated transport systems to the blood–brain barrier as a supporting and protecting interface for the brain; importance for cns drug discovery and development. *Pharmaceutical Research*. **24**(9):1745-1758, 2007.

[10] Pardridge, W. M. Blood-brain barrier biology and methodology. *Journal of neurovirology*. **5**(6):556-569, 1999.

[11] Persidsky, Y., S. H. Ramirez, J. Haorah, and G. D. Kanmogne. Blood–brain barrier: Structural components and function under physiologic and pathologic conditions. *Journal of Neuroimmune Pharmacology*. **1**(3):223-236, 2006.

[12] Fricker, G., *In vitro models to study blood-brain barrier function*, in *Drug absorption studies*. 2008, Springer. p. 397-417.

[13] Bernacki, J., A. Dobrowolska, K. Nierwinska, and A. Malecki. Physiology and pharmacological role of the blood-brain barrier. *Pharmacol Rep*. **60**(5):600-622, 2008.

[14] Wolburg, H., S. Noell, A. Mack, K. Wolburg-Buchholz, and P. Fallier-Becker. Brain endothelial cells and the glio-vascular complex. *Cell and tissue research*. **335**(1):75-96, 2009.

[15] Begley, D. J. and M. W. Brightman. Structural and functional aspects of the blood-brain barrier. *Prog Drug Res*. **61**(39-78, 2003.

[16] Wolburg, H., S. Noell, A. Mack, K. Wolburg-Buchholz, and P. Fallier-Becker. Brain endothelial cells and the glio-vascular complex. *Cell Tissue Res*. **335**(1):75-96, 2009.

[17] Citi, S. and M. Cordenonsi. Tight junction proteins. *Biochim Biophys Acta*. **1448**(1):1-11, 1998.

[18] Gonzalez-Mariscal, L., A. Betanzos, P. Nava, and B. E. Jaramillo. Tight junction proteins. *Prog Biophys Mol Biol*. **81**(1):1-44, 2003.

[19] Feldman, G. J., J. M. Mullin, and M. P. Ryan. Occludin: Structure, function and regulation. *Adv Drug Deliv Rev*. **57**(6):883-917, 2005.

[20] Matter, K. and M. S. Balda. Holey barrier: Claudins and the regulation of brain endothelial permeability. *J Cell Biol*. **161**(3):459-460, 2003.

[21] Hawkins, B. T. and T. P. Davis. The blood-brain barrier/neurovascular unit in health and disease. *Pharmacol Rev*. **57**(2):173-185, 2005.

[22] González-Mariscal, L., R. Tapia, and D. Chamorro. Crosstalk of tight junction components with signaling pathways. *Biochimica et Biophysica Acta (BBA)-Biomembranes*. **1778**(3):729-756, 2008.

[23] Terry, S., M. Nie, K. Matter, and M. S. Balda. Rho signaling and tight junction functions. *Physiology*. **25**(1):16-26, 2010.

[24] Kumar, P., Q. Shen, C. D. Pivetti, E. S. Lee, M. H. Wu, and S. Y. Yuan. Molecular mechanisms of endothelial hyperpermeability: Implications in inflammation. *Expert reviews in molecular medicine*. **11**(e19, 2009.

[25] Pardridge, W. M., P. L. Golden, Y. S. Kang, and U. Bickel. Brain microvascular and astrocyte localization of p-glycoprotein. *Journal of neurochemistry*. **68**(3):1278-1285, 1997.

[26] Choi, Y. K. and K.-W. Kim. Blood-neural barrier: Its diversity and coordinated cell-to-cell communication. *genesis*. **10**(11, 2008.

[27] Schinkel, A. H., E. Wagenaar, C. Mol, and L. van Deemter. P-glycoprotein in the blood-brain barrier of mice influences the brain penetration and pharmacological activity of many drugs. *Journal of Clinical Investigation*. **97**(11):2517, 1996.

[28] Pardridge, W. M., J. L. Buciak, and P. M. Friden. Selective transport of an anti-transferrin receptor antibody through the blood-brain barrier in vivo. *Journal of Pharmacology and Experimental Therapeutics*. **259**(1):66-70, 1991.

[29] Zlokovic, B. V. The blood-brain barrier in health and chronic neurodegenerative

disorders. *Neuron*. **57**(2):178-201, 2008.

[30] del Pino, M. M. S., D. R. Peterson, and R. A. Hawkins. Neutral amino acid transport characterization of isolated luminal and abluminal membranes of the blood-brain barrier. *Journal of Biological Chemistry*. **270**(25):14913-14918, 1995.

[31] Pardridge, W. M. Drug delivery to the brain. *J Cereb Blood Flow Metab*. **17**(7):713-731, 1997.

[32] Davson, H. and W. Oldendorf. Symposium on membrane transport. Transport in the central nervous system. *Proceedings of the Royal Society of Medicine*. **60**(4):326, 1967.

[33] Kacem, K., P. Lacombe, J. Seylaz, and G. Bonvento. Structural organization of the perivascular astrocyte endfeet and their relationship with the endothelial glucose transporter: A confocal microscopy study. *Glia*. **23**(1):1-10, 1998.

[34] Abbott, N. J., L. Rönnbäck, and E. Hansson. Astrocyte–endothelial interactions at the blood–brain barrier. *Nature Reviews Neuroscience*. **7**(1):41-53, 2006.

[35] Lee, S.-W., W. J. Kim, Y. K. Choi, H. S. Song, M. J. Son, I. H. Gelman, Y.-J. Kim, and K.-W. Kim. Ssecks regulates angiogenesis and tight junction formation in blood-brain barrier. *Nature medicine*. **9**(7):900-906, 2003.

[36] Hamm, S., B. Dehouck, J. Kraus, K. Wolburg-Buchholz, H. Wolburg, W. Risau, R. Cecchelli, B. Engelhardt, and M.-P. Dehouck. Astrocyte mediated modulation of blood-brain barrier permeability does not correlate with a loss of tight junction proteins from the cellular contacts. *Cell and tissue research*. **315**(2):157-166, 2004.

[37] Schinkel, A. H. P-glycoprotein, a gatekeeper in the blood–brain barrier. *Advanced drug delivery reviews*. **36**(2):179-194, 1999.

[38] Dehouck, B., M.-P. Dehouck, J.-C. Fruchart, and R. Cecchelli. Upregulation of the low density lipoprotein receptor at the blood-brain barrier: Intercommunications between brain capillary endothelial cells and astrocytes. *The Journal of cell biology*. **126**(2):465-473, 1994.

[39] Hurst, R. and I. Fritz. Properties of an immortalised vascular endothelial/glioma cell co-culture model of the blood-brain barrier. *Journal of cellular physiology*. **167**(1):81-88, 1996.

[40] Mi, H., H. Haeberle, and B. A. Barres. Induction of astrocyte differentiation by endothelial cells. *J Neurosci*. **21**(5):1538-1547, 2001.

[41] Ando, J. and K. Yamamoto. Vascular mechanobiology: Endothelial cell

responses to fluid shear stress. *Circulation journal: official journal of the Japanese Circulation Society*. **73**(11):1983, 2009.

[42] Ballermann, B. J., A. Dardik, E. Eng, and A. Liu. Shear stress and the endothelium. *Kidney International*. **54**(S100-S108, 1998.

[43] Ballermann, B. and M. Ott. Adhesion and differentiation of endothelial cells by exposure to chronic shear stress: A vascular graft model. *Blood purification*. **13**(3-4):125-134, 1995.

[44] Chen, J., B. Fabry, E. L. Schiffrin, and N. Wang. Twisting integrin receptors increases endothelin-1 gene expression in endothelial cells. *American Journal of Physiology-Cell Physiology*. **280**(6):C1475-C1484, 2001.

[45] Rizzo, V., C. Morton, N. DePaola, J. E. Schnitzer, and P. F. Davies. Recruitment of endothelial caveolae into mechanotransduction pathways by flow conditioning in vitro. *American Journal of Physiology-Heart and Circulatory Physiology*. **285**(4):H1720-H1729, 2003.

[46] Gudi, S. R., C. B. Clark, and J. A. Frangos. Fluid flow rapidly activates g proteins in human endothelial cells involvement of g proteins in mechanochemical signal transduction. *Circulation Research*. **79**(4):834-839, 1996.

[47] Olesen, S.-P., D. Claphamt, and P. Davies. Haemodynamic shear stress activates a k+ current in vascular endothelial cells. *Nature*. **331**(6152):168-170, 1988.

[48] Barakat, A., E. Leaver, P. Pappone, and P. Davies. A flow-activated chloride-selective membrane current in vascular endothelial cells. *Circulation research*. **85**(9):820-828, 1999.

[49] Chrétien, M. L., M. Zhang, M. R. Jackson, A. Kapus, and B. L. Langille. Mechanotransduction by endothelial cells is locally generated, direction-dependent, and ligand-specific. *Journal of cellular physiology*. **224**(2):352-361, 2010.

[50] Grabowski, E., E. Jaffe, and B. Weksler. Prostacyclin production by cultured endothelial cell monolayers exposed to step increases in shear stress. *J Lab Clin Med*. **105**(1):36-43, 1985.

[51] Ott, M. J. and B. J. Ballermann. Shear stress-conditioned, endothelial cell-seeded vascular grafts: Improved cell adherence in response to in vitro shear stress. *Surgery*. **117**(3):334-339, 1995.

[52] Colgan, O. C., G. Ferguson, N. T. Collins, R. P. Murphy, G. Meade, P. A. Cahill, and P. M. Cummins. Regulation of bovine brain microvascular endothelial tight junction assembly and barrier function by laminar shear stress.

American Journal of Physiology-Heart and Circulatory Physiology. **292**(6):H3190-H3197, 2007.

[53] Traub, O. and B. C. Berk. Laminar shear stress mechanisms by which endothelial cells transduce an atheroprotective force. *Arteriosclerosis, thrombosis, and vascular biology*. **18**(5):677-685, 1998.

[54] Frangos, J., L. McIntire, and S. Eskin. Shear stress induced stimulation of mammalian cell metabolism. *Biotechnology and bioengineering*. **32**(8):1053-1060, 1988.

[55] Abbott, N. J., D. E. Dolman, and A. K. Patabendige. Assays to predict drug permeation across the blood-brain barrier, and distribution to brain. *Curr Drug Metab*. **9**(9):901-910, 2008.

[56] Lundquist, S., M. Renftel, J. Brillault, L. Fenart, R. Cecchelli, and M.-P. Dehouck. Prediction of drug transport through the blood-brain barrier in vivo: A comparison between two in vitro cell models. *Pharmaceutical research*. **19**(7):976-981, 2002.

[57] Mensch, J., J. Oyarzabal, C. Mackie, and P. Augustijns. In vivo, in vitro and in silico methods for small molecule transfer across the bbb. *Journal of pharmaceutical sciences*. **98**(12):4429-4468, 2009.

[58] Hammarlund-Udenaes, M., M. Fridén, S. Syvänen, and A. Gupta. On the rate and extent of drug delivery to the brain. *Pharmaceutical research*. **25**(8):1737-1750, 2008.

[59] Liu, X., C. Chen, and B. J. Smith. Progress in brain penetration evaluation in drug discovery and development. *Journal of Pharmacology and Experimental Therapeutics*. **325**(2):349-356, 2008.

[60] Pardridge, W. M. Log (bb), ps products and in silico models of drug brain penetration. *Drug discovery today*. **9**(9):392-393, 2004.

[61] Löscher, W. and H. Potschka. Role of drug efflux transporters in the brain for drug disposition and treatment of brain diseases. *Progress in neurobiology*. **76**(1):22-76, 2005.

[62] Banks, W. A. Blood-brain barrier transport of cytokines: A mechanism for neuropathology. *Curr Pharm Des*. **11**(8):973-984, 2005.

[63] Hartz, A. M., B. Bauer, G. Fricker, and D. S. Miller. Rapid modulation of p-glycoprotein-mediated transport at the blood-brain barrier by tumor necrosis factor-alpha and lipopolysaccharide. *Mol Pharmacol*. **69**(2):462-470, 2006.

[64] Dehouck, M. P., P. Jolliet-Riant, F. Brée, J. C. Fruchart, R. Cecchelli, and J. P.

Tillement. Drug transfer across the blood-brain barrier: Correlation between in vitro and in vivo models. *Journal of neurochemistry*. **58**(5):1790-1797, 1992.

[65] Bendayan, R., G. Lee, and M. Bendayan. Functional expression and localization of p-glycoprotein at the blood brain barrier. *Microscopy research and technique*. **57**(5):365-380, 2002.

[66] Bicker, J., G. Alves, A. Fortuna, and A. Falcão. Blood–brain barrier models and their relevance for a successful development of cns drug delivery systems: A review. *European Journal of Pharmaceutics and Biopharmaceutics*. 2014.

[67] Yang, T., K. E. Roder, and T. J. Abbruscato. Evaluation of bend5 cell line as an in vitro model for the blood–brain barrier under normal and hypoxic/aglycemic conditions. *Journal of pharmaceutical sciences*. **96**(12):3196-3213, 2007.

[68] Cucullo, L., B. Aumayr, E. Rapp, and D. Janigro. Drug delivery and in vitro models of the blood-brain barrier. *Curr Opin Drug Discov Devel*. **8**(1):89-99, 2005.

[69] Cecchelli, R., B. Dehouck, L. Descamps, L. Fenart, V. Buée-Scherrer, C. Duhem, S. Lundquist, M. Rentfel, G. Torpier, and M.-P. Dehouck. In vitro model for evaluating drug transport across the blood–brain barrier. *Advanced drug delivery reviews*. **36**(2):165-178, 1999.

[70] Hatherell, K., P.-O. Couraud, I. A. Romero, B. Weksler, and G. J. Pilkington. Development of a three-dimensional, all-human< i> in vitro</i> model of the blood–brain barrier using mono-, co-, and tri-cultivation transwell models. *Journal of neuroscience methods*. **199**(2):223-229, 2011.

[71] Bussolari, S. R., C. F. Dewey Jr, and M. A. Gimbrone Jr. Apparatus for subjecting living cells to fluid shear stress. *Review of Scientific Instruments*. **53**(12):1851-1854, 1982.

[72] Dewey, C., M. Gimbrone, P. Davies, and S. Bussolari. The dynamic response of vascular endothelial cells to fluid shear stress. *Journal of biomechanical engineering*. **103**(3):177-185, 1981.

[73] Stanness, K. A., E. Guatteo, and D. Janigro. A dynamic model of the blood-brain barrier" in vitro". *Neurotoxicology*. **17**(2):481-496, 1995.

[74] Cucullo, L., M. Hossain, V. Puvenna, N. Marchi, and D. Janigro. The role of shear stress in blood-brain barrier endothelial physiology. *BMC neuroscience*. **12**(1):40, 2011.

[75] Santaguida, S., D. Janigro, M. Hossain, E. Oby, E. Rapp, and L. Cucullo. Side by side comparison between dynamic versus static models of blood–brain barrier in vitro: A permeability study. *Brain Research*. **1109**(1):1-13, 2006.

[76] Author, A. Microfluidics in commercial applications; an industry perspective. *Lab on a Chip*. **6**(9):1118-1121, 2006.

[77] Ziaie, B., A. Baldi, M. Lei, Y. Gu, and R. A. Siegel. Hard and soft micromachining for biomems: Review of techniques and examples of applications in microfluidics and drug delivery. *Advanced Drug Delivery Reviews*. **56**(2):145-172, 2004.

[78] Young, E. W. and C. A. Simmons. Macro- and microscale fluid flow systems for endothelial cell biology. *Lab Chip*. **10**(2):143-160, 2010.

[79] El-Ali, J., P. K. Sorger, and K. F. Jensen. Cells on chips. *Nature*. **442**(7101):403-411, 2006.

[80] Sivaraman, A., J. Leach, S. Townsend, T. Iida, B. Hogan, D. B. Stolz, R. Fry, L. Samson, S. Tannenbaum, and L. Griffith. A microscale in vitro physiological model of the liver: Predictive screens for drug metabolism and enzyme induction. *Current drug metabolism*. **6**(6):569-591, 2005.

[81] Powers, M. J., K. Domansky, M. R. Kaazempur-Mofrad, A. Kalezi, A. Capitano, A. Upadhyaya, P. Kurzawski, K. E. Wack, D. B. Stolz, and R. Kamm. A microfabricated array bioreactor for perfused 3d liver culture. *Biotechnology and Bioengineering*. **78**(3):257-269, 2002.

[82] Srigunapalan, S., C. Lam, A. R. Wheeler, and C. A. Simmons. A microfluidic membrane device to mimic critical components of the vascular microenvironment. *Biomicrofluidics*. **5**(1):13409, 2011.

[83] Gunther, A., S. Yasotharan, A. Vagaon, C. Lochovsky, S. Pinto, J. Yang, C. Lau, J. Voigtlaender-Bolz, and S. S. Bolz. A microfluidic platform for probing small artery structure and function. *Lab Chip*. **10**(18):2341-2349, 2010.

[84] Shevkoplyas, S. S., S. C. Gifford, T. Yoshida, and M. W. Bitensky. Prototype of an in vitro model of the microcirculation. *Microvascular research*. **65**(2):132-136, 2003.

[85] Douville, N. J., Y.-C. Tung, R. Li, J. D. Wang, M. E. El-Sayed, and S. Takayama. Fabrication of two-layered channel system with embedded electrodes to measure resistance across epithelial and endothelial barriers. *Analytical chemistry*. **82**(6):2505-2511, 2010.

[86] Barkefors, I., S. Thorslund, F. Nikolajeff, and J. Kreuger. A fluidic device to study directional angiogenesis in complex tissue and organ culture models. *Lab on a Chip*. **9**(4):529-535, 2009.

[87] Wong, K. H., J. M. Chan, R. D. Kamm, and J. Tien. Microfluidic models of vascular functions. *Annual review of biomedical engineering*. **14**(205-230, 2012.

[88] Booth, R. and H. Kim. Characterization of a microfluidic in vitro model of the blood-brain barrier ([small mu]bbb). *Lab on a Chip*. 2012.

[89] Xia, Y. and G. M. Whitesides. Soft lithography. *Annual review of materials science*. **28**(1):153-184, 1998.

[90] Wasa, K., *Handbook of sputter deposition technology: Fundamentals and applications for functional thin films, nano-materials and mems*. 2012: William Andrew.

[91] McDonald, J. C. and G. M. Whitesides. Poly (dimethylsiloxane) as a material for fabricating microfluidic devices. *Accounts of chemical research*. **35**(7):491-499, 2002.

[92] Thorsen, T., S. J. Maerkl, and S. R. Quake. Microfluidic large-scale integration. *Science*. **298**(5593):580-584, 2002.

[93] Chaudhury, M. K. and G. M. Whitesides. Direct measurement of interfacial interactions between semispherical lenses and flat sheets of poly (dimethylsiloxane) and their chemical derivatives. *Langmuir*. **7**(5):1013-1025, 1991.

[94] Charati, S. and S. Stern. Diffusion of gases in silicone polymers: Molecular dynamics simulations. *Macromolecules*. **31**(16):5529-5535, 1998.

[95] Lee, K., N. LaBianca, S. Rishton, S. Zolgharnain, J. Gelorme, J. Shaw, and T. P. Chang. Micromachining applications of a high resolution ultrathick photoresist. *Journal of Vacuum Science & Technology B*. **13**(6):3012-3016, 1995.

[96] Eddings, M. A., M. A. Johnson, and B. K. Gale. Determining the optimal pdms–pdms bonding technique for microfluidic devices. *Journal of Micromechanics and Microengineering*. **18**(6):067001, 2008.

[97] Duffy, D. C., J. C. McDonald, O. J. Schueller, and G. M. Whitesides. Rapid prototyping of microfluidic systems in poly (dimethylsiloxane). *Analytical chemistry*. **70**(23):4974-4984, 1998.

[98] Chueh, B.-h., D. Huh, C. R. Kyrtsos, T. Houssin, N. Futai, and S. Takayama. Leakage-free bonding of porous membranes into layered microfluidic array systems. *Analytical Chemistry*. **79**(9):3504-3508, 2007.

[99] Aran, K., L. A. Sasso, N. Kamdar, and J. D. Zahn. Irreversible, direct bonding of nanoporous polymer membranes to pdms or glass microdevices. *Lab on a Chip*. **10**(5):548-552, 2010.

[100] Nielsen, P. A., O. Andersson, S. H. Hansen, K. B. Simonsen, and G. Andersson. Models for predicting blood–brain barrier permeation. *Drug discovery today*.

16(11):472-475, 2011.

[101] Nicolazzo, J. A., S. A. Charman, and W. N. Charman. Methods to assess drug permeability across the blood-brain barrier. *Journal of pharmacy and pharmacology*. **58**(3):281-293, 2006.

[102] Dore-Duffy, P. Pericytes: Pluripotent cells of the blood brain barrier. *Current Pharmaceutical Design*. **14**(16):1581-1593, 2008.

[103] Garberg, P., M. Ball, N. Borg, R. Cecchelli, L. Fenart, R. Hurst, T. Lindmark, A. Mabondzo, J. Nilsson, and T. Raub. In vitro models for the blood–brain barrier. *Toxicology in vitro*. **19**(3):299-334, 2005.

[104] Roux, F., O. Durieu-Trautmann, N. Chaverot, M. Claire, P. Mailly, J. M. Bourre, A. Strosberg, and P. O. Couraud. Regulation of gamma-glutamyl transpeptidase and alkaline phosphatase activities in immortalized rat brain microvessel endothelial cells. *Journal of cellular physiology*. **159**(1):101-113, 1994.

[105] Poller, B., H. Gutmann, S. Krähenbühl, B. Weksler, I. Romero, P. O. Couraud, G. Tuffin, J. Drewe, and J. Huwyler. The human brain endothelial cell line hcmec/d3 as a human blood-brain barrier model for drug transport studies. *Journal of neurochemistry*. **107**(5):1358-1368, 2008.

[106] Hellinger, É., S. Veszelka, A. E. Tóth, F. Walter, Á. Kittel, M. L. Bakk, K. Tihanyi, V. Háda, S. Nakagawa, and T. Dinh Ha Duy. Comparison of brain capillary endothelial cell-based and epithelial (mdck-mdr1, caco-2, and vb-caco-2) cell-based surrogate blood–brain barrier penetration models. *European Journal of Pharmaceutics and Biopharmaceutics*. **82**(2):340-351, 2012.

[107] Ball, K., F. Bouzom, J. M. Scherrmann, B. Walther, and X. Declèves. Development of a physiologically based pharmacokinetic model for the rat central nervous system and determination of an in vitro–in vivo scaling methodology for the blood–brain barrier permeability of two transporter substrates, morphine and oxycodone. *Journal of pharmaceutical sciences*. **101**(11):4277-4292, 2012.

[108] HE Fang, Y. F., PENG Jing, LI Kong-Zhao, WU Li-Wen, DENG Xiao-Lu. Immortalized mouse brain endothelial cell line bend.3 displays the comparative barrier characteristics as the primary brain microvascular endothelial cells. *CJCP*. **12**(06):474-478, 2010.

[109] Watanabe, T., S. Dohgu, F. Takata, T. Nishioku, A. Nakashima, K. Futagami, A. Yamauchi, and Y. Kataoka. Paracellular barrier and tight junction protein expression in the immortalized brain endothelial cell lines bend.3, bend.5 and mouse brain endothelial cell 4. *Biological and Pharmaceutical Bulletin*.

36(3):492-495, 2013.

[110] Raub, T. J. Signal transduction and glial cell modulation of cultured brain microvessel endothelial cell tight junctions. *American Journal of Physiology-Cell Physiology*. **271**(2):C495-C503, 1996.

[111] Smith, M., Y. Omidi, and M. Gumbleton. Primary porcine brain microvascular endothelial cells: Biochemical and functional characterisation as a model for drug transport and targeting. *Journal of drug targeting*. **15**(4):253-268, 2007.

[112] Fu, C. T., J. F. Bechberger, M. A. Ozog, B. Perbal, and C. C. Naus. Ccn3 (nov) interacts with connexin43 in c6 glioma cells possible mechanism of connexin-mediated growth suppression. *Journal of Biological Chemistry*. **279**(35):36943-36950, 2004.

[113] Perrière, N., S. Yousif, S. Cazaubon, N. Chaverot, F. Bourasset, S. Cisternino, X. Declèves, S. Hori, T. Terasaki, and M. Deli. A functional in vitro model of rat blood–brain barrier for molecular analysis of efflux transporters. *Brain research*. **1150**(1-13, 2007.

[114] Wuest, D. M., A. M. Wing, and K. H. Lee. Membrane configuration optimization for a murine< i> in vitro</i> blood–brain barrier model. *Journal of neuroscience methods*. **212**(2):211-221, 2013.

[115] Ma, S. H., L. A. Lepak, R. J. Hussain, W. Shain, and M. L. Shuler. An endothelial and astrocyte co-culture model of the blood–brain barrier utilizing an ultra-thin, nanofabricated silicon nitride membrane. *Lab on a Chip*. **5**(1):74-85, 2005.

[116] Demeuse, P., A. Kerkhofs, C. Struys-Ponsar, B. Knoops, C. Remacle, and P. van den Bosch de Aguilar. Compartmentalized coculture of rat brain endothelial cells and astrocytes: A syngenic model to study the blood–brain barrier. *Journal of neuroscience methods*. **121**(1):21-31, 2002.

[117] Hurwitz, A., J. Berman, W. Rashbaum, and W. Lyman. Human fetal astrocytes induce the expression of blood-brain barrier specific proteins by autologous endothelial cells. *Brain research*. **625**(2):238-243, 1993.

[118] Tilling, T., D. Korte, D. Hoheisel, and H. J. Galla. Basement membrane proteins influence brain capillary endothelial barrier function in vitro. *Journal of neurochemistry*. **71**(3):1151-1157, 1998.

[119] Tilling, T., C. Engelbertz, S. Decker, D. Korte, S. Hüwel, and H.-J. Galla. Expression and adhesive properties of basement membrane proteins in cerebral capillary endothelial cell cultures. *Cell and tissue research*. **310**(1):19-29, 2002.

[120] Li, G., M. J. Simon, L. M. Cancel, Z.-D. Shi, X. Ji, J. M. Tarbell, B. Morrison

III, and B. M. Fu. Permeability of endothelial and astrocyte cocultures: In vitro blood–brain barrier models for drug delivery studies. *Annals of biomedical engineering*. **38**(8):2499-2511, 2010.

[121] Haseloff, R., I. Blasig, H.-C. Bauer, and H. Bauer. In search of the astrocytic factor (s) modulating blood–brain barrier functions in brain capillary endothelial cells in vitro. *Cellular and molecular neurobiology*. **25**(1):25-39, 2005.

[122] Siddharthan, V., Y. V. Kim, S. Liu, and K. S. Kim. Human astrocytes/astrocyte-conditioned medium and shear stress enhance the barrier properties of human brain microvascular endothelial cells. *Brain research*. **1147**(39-50, 2007.

[123] Kuo, Y.-C. and C.-H. Lu. Effect of human astrocytes on the characteristics of human brain-microvascular endothelial cells in the blood–brain barrier. *Colloids and Surfaces B: Biointerfaces*. **86**(1):225-231, 2011.

[124] Förster, C., M. Burek, I. A. Romero, B. Weksler, P. O. Couraud, and D. Drenckhahn. Differential effects of hydrocortisone and tnfα on tight junction proteins in an in vitro model of the human blood–brain barrier. *The Journal of physiology*. **586**(7):1937-1949, 2008.

[125] Perriere, N., P. Demeuse, E. Garcia, A. Regina, M. Debray, J. P. Andreux, P. Couvreur, J. M. Scherrmann, J. Temsamani, and P. O. Couraud. Puromycin-based purification of rat brain capillary endothelial cell cultures. Effect on the expression of blood–brain barrier-specific properties. *Journal of neurochemistry*. **93**(2):279-289, 2005.

[126] Zhang, J., K. Tan, and H. Gong. Characterization of the polymerization of su-8 photoresist and its applications in micro-electro-mechanical systems (mems). *Polymer testing*. **20**(6):693-701, 2001.

[127] Papautsky, I., B. K. Gale, S. Mohanty, T. A. Ameel, and A. B. Frazier. Effects of rectangular microchannel aspect ratio on laminar friction constant. *Proceedings of SPIE-The International Society for Optical Engineering, Proceedings of the 1999 Microfluidic Devices and Systems II, Santa Clara*. **3877**(147-158, 1999.

[128] Ehret, R., W. Baumann, M. Brischwein, A. Schwinde, K. Stegbauer, and B. Wolf. Monitoring of cellular behaviour by impedance measurements on interdigitated electrode structures. *Biosensors and Bioelectronics*. **12**(1):29-41, 1997.

[129] Deli, M. A., C. S. Ábrahám, Y. Kataoka, and M. Niwa. Permeability studies on in vitro blood–brain barrier models: Physiology, pathology, and pharmacology. *Cellular and molecular neurobiology*. **25**(1):59-127, 2005.

[130] Reichel, A., D. J. Begley, and N. J. Abbott, *An overview of in vitro techniques*

for blood-brain barrier studies, in *The blood-brain barrier*. 2003, Springer. p. 307-324.

[131] Toth, A., S. Veszelka, S. Nakagawa, M. Niwa, and M. A Deli. Patented in vitro blood-brain barrier models in cns drug discovery. *Recent patents on CNS drug discovery*. **6**(2):107-118, 2011.

[132] Butt, A. M. Effect of inflammatory agents on electrical resistance across the blood-brain barrier in pial microvessels of anaesthetized rats. *Brain Res*. **696**(1-2):145-150, 1995.

[133] Franke, H., H.-J. Galla, and C. T. Beuckmann. An improved low-permeability in vitro-model of the blood–brain barrier: Transport studies on retinoids, sucrose, haloperidol, caffeine and mannitol. *Brain research*. **818**(1):65-71, 1999.

[134] Hoheisel, D., T. Nitz, H. Franke, J. Wegener, A. Hakvoort, T. Tilling, and H.-J. Galla. Hydrocortisone reinforces the blood–brain barrier properties in a serum free cell culture system. *Biochemical and biophysical research communications*. **244**(1):312-316, 1998.

[135] Madara, J. L. Regulation of the movement of solutes across tight junctions. *Annual review of physiology*. **60**(1):143-159, 1998.

[136] Gumbleton, M. and K. L. Audus. Progress and limitations in the use of in vitro cell cultures to serve as a permeability screen for the blood-brain barrier. *Journal of pharmaceutical sciences*. **90**(11):1681-1698, 2001.

[137] Wuest, D. M. and K. H. Lee. Optimization of endothelial cell growth in a murine in vitro blood–brain barrier model. *Biotechnology journal*. **7**(3):409-417, 2012.

[138] Cantrill, C. A., R. A. Skinner, N. J. Rothwell, and J. I. Penny. An immortalised astrocyte cell line maintains the in vivo phenotype of a primary porcine in vitro blood–brain barrier model. *Brain Research*. **1479**(0):17-30, 2012.

[139] Perrière, N., S. Yousif, S. Cazaubon, N. Chaverot, F. Bourasset, S. Cisternino, X. Declèves, S. Hori, T. Terasaki, M. Deli, J.-M. Scherrmann, J. Temsamani, F. Roux, and P.-O. Couraud. A functional in vitro model of rat blood–brain barrier for molecular analysis of efflux transporters. *Brain Research*. **1150**(0):1-13, 2007.

[140] Kumar, A. Convective diffusion process of blood vessels in the presence of porous effects. *Academic of Open Internet Journal Vol*. 21):1-21, 2005.

[141] Levesque, M. and R. Nerem. The elongation and orientation of cultured endothelial cells in response to shear stress. *Journal of biomechanical engineering*. **107**(4):341-347, 1985.

[142] Towbin, H., T. Staehelin, and J. Gordon. Electrophoretic transfer of proteins from polyacrylamide gels to nitrocellulose sheets: Procedure and some applications. *Proceedings of the National Academy of Sciences*. **76**(9):4350-4354, 1979.

[143] Fruttero, R., M. Crosetti, K. Chegaev, S. Guglielmo, A. Gasco, F. Berardi, M. Niso, R. Perrone, M. A. Panaro, and N. A. Colabufo. Phenylsulfonylfuroxans as modulators of multidrug-resistance-associated protein-1 and p-glycoprotein. *Journal of medicinal chemistry*. **53**(15):5467-5475, 2010.

CHAPTER 3

CHARACTERIZATION OF A MICROFLUIDIC *IN VITRO* MODEL OF THE BLOOD-BRAIN BARRIER (μBBB)[1]

3.1 Abstract

The blood-brain barrier (BBB), a unique selective barrier for the central nervous system (CNS), hinders the passage of most compounds to the CNS, complicating drug development. Innovative *in vitro* models of the BBB can provide useful insights into its role in CNS disease progression and drug delivery. Static transwell models lack fluidic shear stress, while the conventional dynamic *in vitro* BBB lacks a thin dual cell layer interface. To address both limitations, we developed a microfluidic blood-brain barrier (μBBB) which closely mimics the *in vivo* BBB with a dynamic environment and a comparatively thin culture membrane (10μm). To test validity of the fabricated BBB model, μBBBs were cultured with b.End3 endothelial cells, both with and without co-cultured C8-D1A astrocytes, and their key properties were tested with optical imaging, trans-endothelial electrical resistance (TEER), and permeability assays. The resultant imaging of ZO-1 revealed clearly expressed tight junctions in b.End3 cells, Live/Dead assays indicated high cell viability, and astrocytic morphology of C8-D1A cells were confirmed by ESEM and GFAP immunostains. By day 3 of endothelial culture, TEER

[1] Reproduced by permission of The Royal Society of Chemistry. Published: Lab on a Chip, 2012, Vol 12, p 1784-1792. http://pubs.rsc.org/en/content/articlelanding/2012/lc/c2lc40094d

levels typically exceeded 250Ωcm^2 in μBBB co-cultures, and 25Ωcm^2 for transwell co-cultures. Instantaneous transient drop in TEER in response to histamine exposure was observed in real-time, followed by recovery, implying stability of the fabricated μBBB model. Resultant permeability coefficients were comparable to previous BBB models, and were significantly increased at higher pH (>10). These results demonstrate that the developed μBBB system is a valid model for some studies of BBB function and drug delivery.

3.2 Introduction

Diseases of the central nervous system (CNS) present a prevalent and ever-increasing burden for the world healthcare industry. For example, Alzheimer's disease is diagnosed in an estimated 24 million people, a number projected to double every 20 years [1]. Despite such emerging demands for treatment of CNS diseases, only 7% of CNS drugs in clinical development reach the marketplace (Figure 3.1A), compared to the 12% average across all therapeutic areas, or 20% for cardiovascular drugs [2,3].

This low success rate is attributed primarily to a unique CNS structure coined as the blood-brain barrier (BBB) [3], which introduces a pharmacokinetic hurdle by blocking compounds from entering brain tissues from capillaries [4]. Only compounds smaller than about 500Da easily cross the BBB, but few CNS diseases consistently respond to this category of molecules [5].

Because the BBB blocks nearly all polar or large compounds, new drug treatments for the CNS of higher molecular weight must take BBB function into account, requiring more extensive preclinical studies. The use of *in vitro* models of the BBB would augment

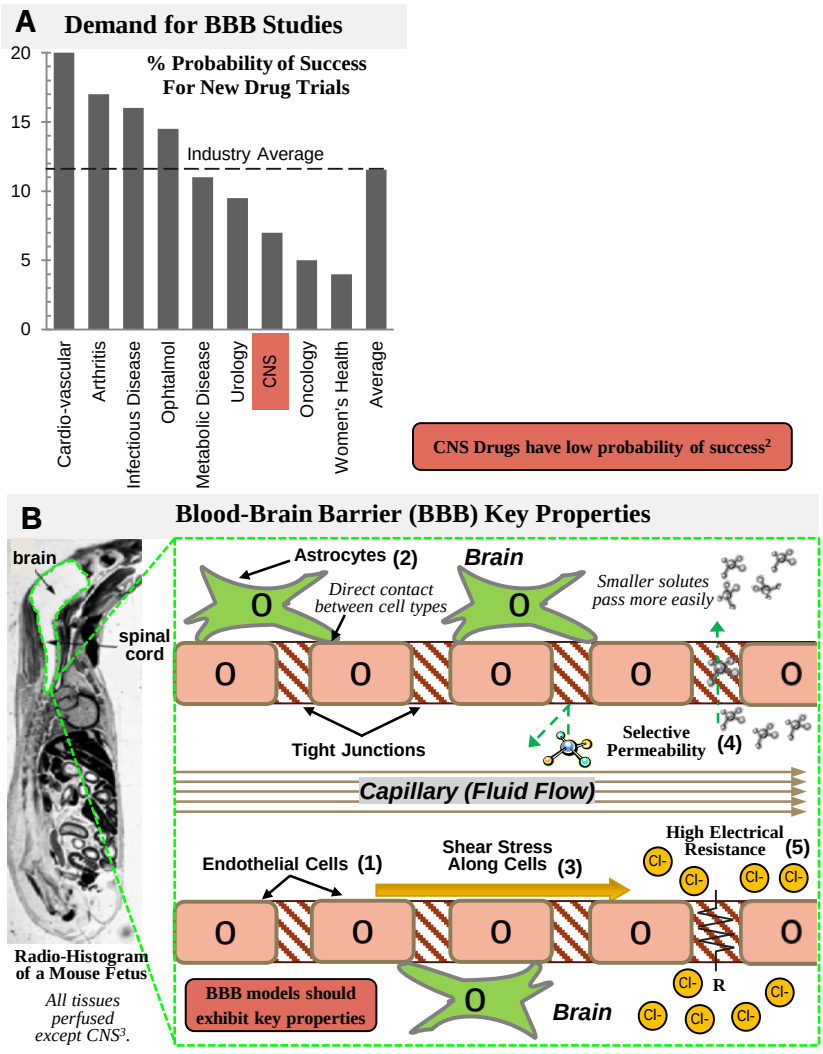

Figure 3.1 Motivation and background for μBBB development. (A) Probability of success is lower for new CNS drugs than those in other healthcare areas due to the unique architecture of brain capillaries [2]. (B) The CNS is unique due to the extraordinary selectivity of the BBB [3]. Better model systems of the BBB will contribute to development of CNS disease treatments. Effective *in vitro* BBB models should successfully include key properties: (1) endothelial cells with tight junction expression; (2) co-culture with astrocytes; (3) presence of shear stress; (4) selective permeability to compounds; (5) high electrical resistance across tight junctions.

the conventional pharmaceutical approach focusing on drug design, help predict the penetration of drug candidates across the BBB [24], and allow prescreening and optimization of new treatments prior to animal and clinical studies [25]. BBB models can also be used to study the role of barrier function on CNS disease progression [26], and test innovative methods of delivery [27].

BBB studies have been performed largely in two platforms: *in vivo* and *in vitro* models (Table 3.1). *In vivo* models directly utilize entire living organisms, typically rats or mice, while *in vitro* models construct artificial environments with cultured cells to mimic *in vivo* structures. *In vitro* models are a valuable precursor to animal models due to lower cost, time, and ethical constraints. More specific to the BBB, unlike in animal studies, *in vitro* models enable controlled, repeatable, and noninvasive tests: permeability assays, resistance measurements, and microscopy.

Table 3.1 Qualitative comparison of standard BBB models with the μBBB proposed in this article.

Experimental system	***In vivo* models**	***In vitro* models**		
System type [Citations]	Animals [6-8]	Transwells [9-18]	DIV-BBB [19-22]	μBBB [23]
Relative cost	High	Very Low	Low	Low
Massively-parallel, controlled, and repeatedly identical	No	Yes	Yes	Yes
Shear stress/dynamic flow (Quantitative analysis)	Yes (No)	No -	Yes (Yes)	Yes (Yes)
Space between co-cultures	Immediate	<10 μm	>150 μm	<10 μm
Functional media volumes	N/A	0.5-2 ml	1.4 ml	12 μl
Time to steady-state TEER	N/A	3-4 days	9-12 days	3-4 days
TEER electrodes – Ion flow profile (Gap size) (Fixed position)	Invasive	Uniform (<2mm) (No)	Non-uniform (>1cm) (Yes)	Uniform (<400μm) (Yes)
Nondestructive microscopy	No	Yes	No	Yes
Fabrication	N/A	Simple	Complex	Moderate

Although traditional *in vivo* models provide environments closer to the human phenotype, they cannot provide massively-parallel, controlled, and repeatedly identical environments for reliable and quantitative studies (Table 3.1). More importantly in terms of practicality, *in vivo* models require extraordinary amounts of cost, time, and man-hours per test, while increasingly facing ethical issues as well.

In vitro models are able to significantly reduce such issues by offering identical environments in numerous arrays, as well as lower cost, time, and ethical constraints. Thus, the development of valid *in vitro* models can facilitate the overall drug development process by acting as a precursor, or even a replacement, for animal studies.

The validity of an *in vitro* model is dependent on how well it reproduces the key physiological and biological characteristics of its *in vivo* archetype (Figure 3.1B). The key characteristics of the BBB include: (1) the primary structure, consisting of strongly expressed tight junctions between endothelial cells which directly control compound permeability [28]; (2) co-culture of endothelial cells with astrocytes including endfoot contact, which plays an important role in modulating barrier function through cell-cell signaling [29]; (3) mechanotransductive effects of shear stress from fluid flow on endothelial cells, which is known to critically influence cell differentiation and tight junction formation [30,31]; (4) selective permeability from the constituted structures to dissolved compounds; (5) maintenance of high electrical resistance representing the maturity and soundness of the structures.

To mimic such key characteristics, various *in vitro* models have been developed to date [9-22] and can be mainly divided into two groups: static and dynamic models, defined by the inclusion of fluid flow, resulting in shear stress over the surface of the

cells. Static models have been the most widely used since the first transwell setup in 1991 [11]. Recently, dynamic *in vitro* BBB (DIV-BBB) [20-22] models have been developed which utilize hollow fibers to mimic the BBB architecture and flow conditions, providing adequate shear stress. However, wall thickness (150μm) is significantly higher than transwell thickness (10μm), discouraging cell-cell interaction, and DIV-BBBs take significantly longer to reach steady-state TEER values [20,32] than static transwell models. To our knowledge, no existing BBB systems have addressed each of these shortcomings yet.

In order to address the issue, we have developed a microfluidic BBB (μBBB) [23] that includes each of the following advantages over existing *in vivo* and *in vitro* static and dynamic BBB Models (Table 1): (1) significantly lower costs and timescales than *in vivo* studies; (2) massively-parallel, controlled, and repeated environments not available in *in* vivo models; (3) dynamic microenvironment providing shear stress stimulation to the cells, and allowing the improved analysis of test compounds and controlled delivery compared to static models; (4) much thinner culture membrane, decreasing the distance between co-cultured cells from DIV-BBB models. In addition, the developed μBBB model uses smaller functional volumes for quicker media exchange and material conservation. Shorter times to steady-state TEER levels allow a more rapid turn-around time, shortening experiments and allowing a more high-throughput approach to experimentation. The developed μBBB also enables installation of high-density electrodes with tiny (200 μm) gaps between either electrode and the cell layers, with uniform ion flow density, minimizing background resistance and error. Nondestructive microscopy of the system is possible by carefully designing electrode locations, due to

transparency of the substrate. Finally, the developed μBBB is polymer-based, allowing comparatively rapid and low-cost fabrication.

This paper reports the detailed design, fabrication, and characterization of the developed *in vitro* dynamic thin-membrane μBBB system, including multilayered polymer fabrication, cell culturing procedure, validation of the developed models through optical imaging, static and transient permeability tests, and TEER measurements under different concentrations of various tracers.

3.3 Structure and Fabrication

3.3.1 Structure

The developed μBBB is a multilayered microfluidic device comprising four PDMS substrates, two glass layers, and a porous polycarbonate membrane sandwiched at the center between the PDMS layers (Figure 3.2A). The assembled device houses two perpendicularly-crossing channels to introduce dynamic flows, a porous membrane at the intersection of the flow channels for cell culture, and multiple embedded electrodes to monitor TEER across the barrier. The channels are 200μm high, and 2mm (luminal) or 5mm (abluminal) wide at the cell culture interface ensuring laminar flows. The porous membrane is located at the channel junction has an area of $10mm^2$ (Figure 3.2B-C). The abluminal channel has a high aspect ratio (10:1) to promote uniform shear stress distribution across endothelial cells, and the luminal channel is significantly wider to minimize shear stresses on the astrocytes. Opposite the membrane on each side are two sets of two AgCl thin-film TEER electrode pairs forming a four-point sensing structure. The areas of the current electrodes are designed to be proportional (75%) to the cell

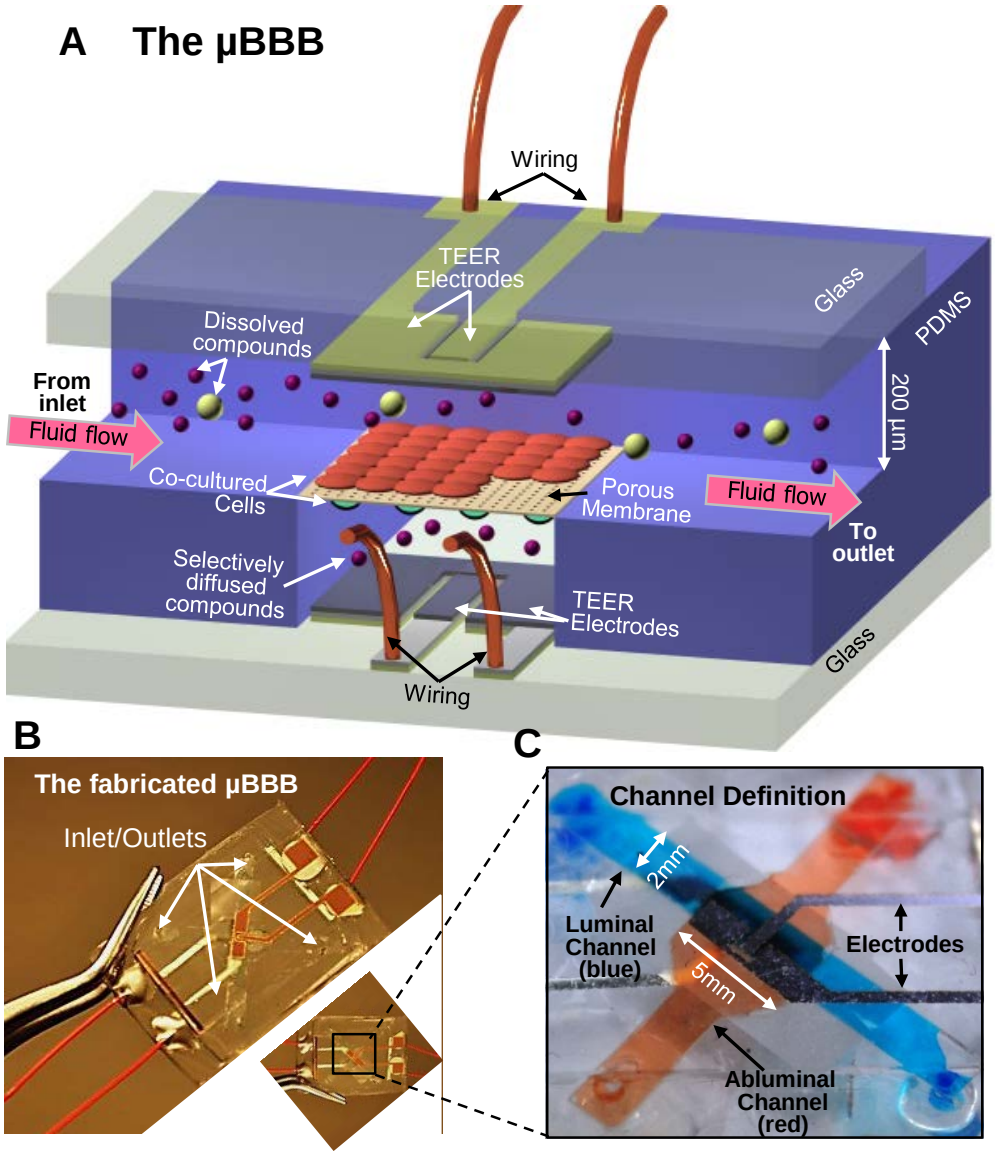

Figure 3.2 Structure and design of the developed μBBB. (A) The μBBB system comprises two perpendicular flow channels. (B) The fully fabricated μBBB chip. (C) Close-up view. Channels model the lumenal (blue) and ablumenal (red) sides of the neurovascular unit. Endothelial cells and astrocytes are respectively cultured on the lumenal and ablumenal sides of the enclosed porous membrane. Channel heights are 200 μm, and channel widths are 2mm (lumen) and 5mm (albumen).

culture area in order to encourage uniformly distributed ion flow. For interconnection, there are two pairs of fluidic and electrical I/Os, respectively.

3.3.2 Fabrication

The μBBB was fabricated by sequentially bonding the four patterned PDMS sub-layers, two embedded electrode layers, and the sandwiched polycarbonate membrane, resulting in a fully integrated device (Figure 3.3). First, electrode layers were produced by cleaning 1mm glass slides with piranha etch, and sputter depositing (Denton Discovery 18) thin-film electrodes with 20nm Cr, 150nm Au, and 800nm Ag. Instachange marking film (3M) was patterned with a laser patterning system (Universal) to be used as a sputter

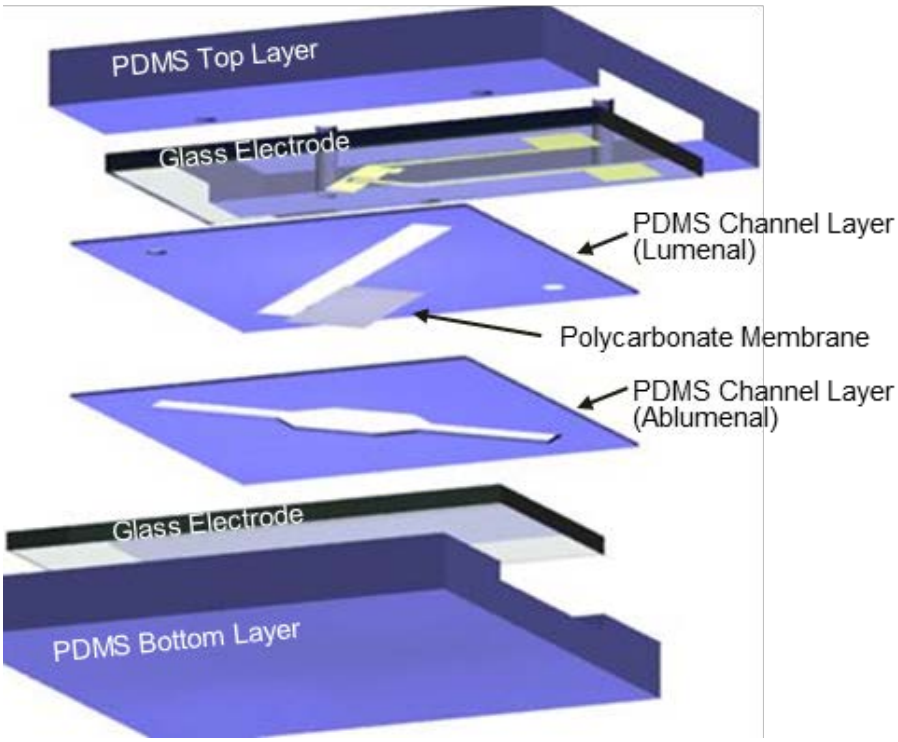

Figure 3.3 Components of the μBBB. The μBBB consists of four PDMS layers, two embedded glass electrode layers, and a piece of polycarbonate membrane.

mask. Silver surface was chlorinated chemically with $FeCl_3$ for 60s at room temperature to generate an electrochemically active AgCl surface. Glass slides were diced (Disco DAD641) to 18mm by 25mm and embedded in 3mm thick PDMS and cured at 65° for 2h. Four I/O holes (0.5mm) were cored in the top layers by punching.

To produce the channel feature layers, PDMS prepolymer was spin-coated at 288 RPM for 1m and cured at 65°C for 2 hours to produce 200µm sheets, and features were laser-patterned. Polycarbonate sheets (400nm pores, 10µm thick) were cut from transwells (Corning) to 5x10mm rectangles. The top and bottom PDMS layers, the polycarbonate sheets, and the PDMS channel layers were bonded using spin-coated and stamped 50:50 ratio PDMS pre-polymer:toluene as previously described [33]. Copper wire was bonded to bond-pads with silver epoxy for electrical connections.

3.4 Cell Culture

In order to form a dual-layer BBB on the chip, co-culture of endothelial and astrocytic cells was performed by seeding on both sides of the porous membrane in the fabricated device by flowing cell suspensions. Specifically, b.End3 (endothelial) and C8D1A (astrocyte) cell lines were employed utilizing standard mammalian tissue culture methods for their ease of use.

The fabricated µBBB platform was sterilized and adhesion-seeded by steadily perfusing for up to seven days. Gas-permeable manifold tubing (0.25mm ID) was attached to 22½ gauge needles and 10µl pipet tips. Tips were sealed to theinlet holes with silicone sealant (DC734), and chips were connected to a 205S peristaltic cartridge pump (Watson-Marlow) for fluid manipulation (Figure 3.4). 250 µl 8-well strips were used as

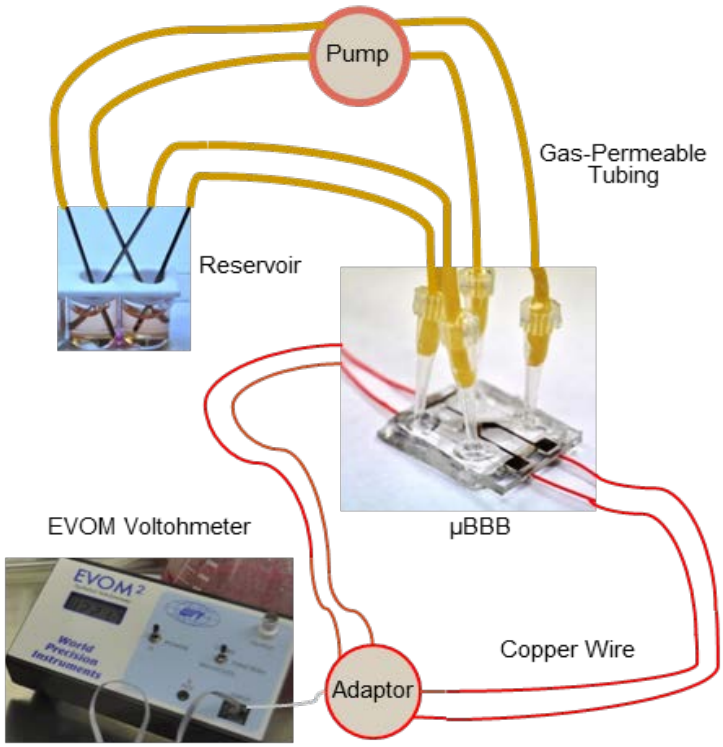

Figure 3.4 Testing setup for validating the µBBB. Fully assembled µBBB includes gas-permeable tubing run through a peristaltic pump to a plugged reservoir for each channel. Electrode wiring is connected through an electrode adaptor to an EVOM Epithelial Voltohmeter for TEER measurement.

reservoirs, covered with gas-permeable TFE/silicone plugs (BioTech Solutions). Chips were perfused with 70% ethanol to prevent contamination. To facilitate cell adhesion, the membrane was coated with 10µg/ml fibronectin for two hours, then filled with growth medium and fully cleared of bubbles prior to cell seeding.

Next, the platforms were first seeded on the abluminal side with astrocytes at the concentration of $6e^4/cm^2$ by flooding concentrated cell suspension ($3e^6$/ml) in the abluminal chamber and inverting the devices at zero flow for two hours. Before seeding endothelial cells, the µBBB was perfused with medium at 1.3 µl/min for two days.

Then, b.End3 [34] cells were secondly seeded at the concentration of $6e^4/cm^2$ in the luminal channel and allowed to adhere for two hours before rinsing with medium perfused at 1.3µl/min for twelve hours, followed by 2.6µl/min subsequently.

Note that cells used for seeding BBB models were taken from confluent cultures (after D3 after passage) only. Static BBB models were tested by seeding astrocytes at $6e^4/cm^2$ on the underside of transwells (Corning) pretreated with 10µg/ml human fibronectin (Cultrex) in PBS for two hours and allowed to adhere for two hours, then cultured for two days prior to endothelial cell seeding on the topside at $6e^4/cm^2$.

All cell cultivation and BBB experiments, including the devices and pump assembly, were carried out in a Nu-Aire Autoflow 4750 incubator which maintains a constant interior environment at 5% CO_2 and 37°C, as indicated by internal temperature and CO_2 sensors in the incubator, with certified accuracies of $\pm$0.0125°C and $\pm$0.1%, respectively. Cell suspensions were centrifuged in an Eppendorf 5810, and sterile work was done in a class II biosafety cabinet (Thermo Fisher). Media used for all procedures was DMEM:F12 (CellGro), supplemented with 10% FBS (Hyclone), 1% Penicillin/Streptomycin, and 1% Fungizone (EMD). Media was buffered (NaOh or HCl buffers) to 7.4pH (VWR sympHony) and sterile-filtered for all experiments, except for experiments in which media was buffered to 10pH. All media was supplemented with 1.2 g/L sodium bicarbonate to minimize changes in pH, though any changes in pH over the course of µBBB experiments were not measured due to volume limitations of the pH meter. The endothelial cell line b.End3 and astrocytic cell line C8-D1A were received from ATCC.

3.5 Testing Methodology

To validate the fabricated μBBB system, the three most common methods were employed [35]: (1) *cell imaging* to observe structure and morphology, (2) *TEER levels* to evaluate cell confluence and tight junction integrity, and (3) *permeability assays* to evaluate barrier selectivity. Cells were imaged with a Live/Dead assay to verify cell viability, and immunostained to look at expression of astrocyte marker GFAP and tight junction component zonal occluding-1 (ZO-1). TEER was measured as an indicator of cell confluence and tight junction integrity, with time to maximum TEER being indicative of BBB development time. Fluxes of fluorescent-labeled tracer molecules were measured to assess permeability to larger solutes. To observe the system's response to environmental changes, cells were exposed to histamine during TEER measurement and high pH during permeability assays. Real-time TEER was measured in co-cultured μBBB models during exposure to histamine (Calbiochem) at 100 μM and 150 μM concentrations. Permeability was measured in μBBB models exposed to DMEM:F12 media with elevated pH (>10) for four hours.

3.5.1 Imaging

Light-phase and ESEM imaging were used for morphological observations, Live/Dead assay was used to assess viability, and immunostaining was used to look at expression of glial and tight junction marker proteins GFAP and ZO-1. To assess viability of cultured cells, Live/Dead (MGT) solution was incubated for ninety minutes and imaged using a Nikon fluorescence microscope. For immunostaining of both cell types, cells were fixed with 4% paraformaldehyde (Avantor) for ten minutes at room

temperature. Cells were permabilized with 0.1% Triton X-100 in PBS for 10m and blocked with 5% goat serum (Rockland) and 1% unconjugated goat anti-mouse IgG F(ab')$_2$ fragment (ImmunoPure) in permeabilization buffer for one hour. Cultures were incubated with primary antibody in blocking solution overnight at 4ºC. Cultures were rinsed with blocking solution and left in secondary antibody for one hour, counter-stained with DAPI (Enzo) for five minutes, and imaged with a Nikon fluorescence microscope. Mouse anti-ZO-1 (Invitrogen) was used in conjunction with Alexa Fluor 488 goat anti-mouse secondary antibody (Invitrogen). Rabbit anti-GFAP (Invitrogen) was used in conjunction with Alexa Fluor 488 goat anti-rabbitt secondary antibody (Invitrogen). For imaging with environmental SEM (FEI Quanta 600 FEG), astrocyte cultures were rinsed and fixed in 4% paraformaldehyde solution for twenty-four hours at 4°C.

3.5.2 TEER Measurement

Over the course of BBB experiments, TEER was measured twice a day to monitor cell confluence and development of tight junctions. For measurement of TEER, voltage and current electrode wires were connected via an electrode adaptor (WPI) to an EVOM2 epithelial voltohmeter (WPI). The EVOM2 passes a constant 10μA AC current at 12.5Hz while measuring resistance. To calculate TEER, initial D0 Background resistances R_b were subtracted from total resistance R_C at each time point and normalized for area, giving TEER values in Ωcm^2 as in the following equation.

$$TEER = (R_C - R_b)A \tag{3.1}$$

For real-time data collection during histamine exposure, the EVOM2 was connected to LabView on a PC via a data acquisition device (Texas Instruments). TEER of transwell

cultures were measured daily by placing them in an Endohm chamber (WPI) and connecting it to the EVOM2.

3.5.3 Permeability

To assess barrier permeabilities to large compounds, fluxes of fluorescent tracers over a wide range of sizes were measured after steady-state TEER has been reached under each variant condition: monolayer, co-culture, and co-culture with elevated pH. The permeability of the system to dissolved compounds is detected by measuring the rate of diffusion across the membrane. After D3 of endothelial culture, FITC-Dextrans 4k, 20k, 70k (Sigma), and propidium iodide (Biotium) were passed at a concentration 500µg/ml in media through the luminal channel of each device, and blank media was passed through the abluminal channel. The level of fluorescence in the media collected from the abluminal channels were measured using a BioRad Synergy Plate Reader, and converted to concentration according to prepared standards. Solute flux J_s was calculated by dividing concentration change by assay time. Permeability coefficients were calculated using the conventional equation for permeability [36]

$$P = \frac{J_s}{A \cdot C_L} \tag{3.2}$$

where P is the permeability coefficient, J_s is solute flux across the membrane, A is membrane area, and C_L is concentration on the luminal (source) side of the membrane. Epithelial coefficients P_e were calculated by subtracting the inverse of the overall P value by the inverse of coefficient P_b from a blank membrane, as in the following equation for permeability normalization [37].

$$\frac{1}{P_e} = \frac{1}{P} - \frac{1}{P_b} \tag{3.3}$$

All permeability assays were conducted after day 3 of endothelial culture. Assays were conducted for both monolayer and co-cultured devices. To evaluate the effect of pH elevation on permeability, assay was repeated with cultures exposed to media containing pH>10 for four hours.

3.6 Results and Discussion

The measurements indicated the validity of the developed μBBB model as an effective *in vitro* model system for studies of barrier function and drug delivery. The generally recognized characteristics of a valid *in vitro* BBB model include practicality and ease of use, *in vivo*-like cell morphology, functional expression of BBB-specific proteins, and a restricted paracellular pathway as indicated by high TEER and low permeability to compounds [38]. The b.End3 cell line has been previously characterized as having acceptably high functionality of P-glycoprotein transporter, as well as expression of numerous transporters [34]. Finally, the restrictive paracellular pathway was demonstrated by TEER levels over 250 Ωcm^2 and tracer permeabilities comparable to previous BBB models [37].

3.6.1 Imaging

Imaging results were indicative of *in vivo*-like morphologies for both cell types, validating structural requirements for BBB. Results from Live/Dead assays conducted on D3 of endothelial culture on μBBB membranes indicated high cell viability (>90%) of

endothelial cells cultured in the system (Figure 3.5A) Similar cell survival was seen for astrocytes cultured in the system. Immunostains of b.End3 cells cultured in the system revealed distinct expression of tight junction component ZO-1 by day 3 of culture (Figure 3.5B). Immunostains on D2 typically lacked as clearly distinct expression of ZO-1 as seen on day 3-4, suggesting a three-day minimum for full barrier development, consistent with the TEER results. Evaluation of the endothelial monolayer structure of b.End3 cells confirmed previous analysis on the cell line as valid for BBB models [34], that tight junctions were readily expressed by day 3 of culture in the system, even without astrocyte co-culture.

Morphological analysis of the C8-D1A cell line was necessary due to a lack of described previous models using the cell line. The C8D1A cell line regularly expressed an astrocytic morphology with distinct neurites. Immunostains of C8D1A cells revealed expression of GFAP, which is a marker specific to astrocytes (Figure 3.5C). ESEM of astrocytes cultured on polycarbonate membrane revealed good adhesion to the substrate (Figure 3.5D), though the neurites were typically wider (>1μm) than the pore diameter (0.4μm), so it is unlikely that endfeet were able to migrate through the pores. Further study should be performed to find a feasible membrane with large enough pores to encourage direct cell-cell contact between cell types, while not large enough to introduce problems with adhesion or cell migration through the membrane.

Note that the experimental setup was small enough for the entire pump system to be placed in the incubator at 37°C, and up to 4 devices could be run simultaneously with our 8-channel pumphead. Imaging indicated that both cell types exhibited characteristics desirable for BBB study, and cells are co-cultured in close contact.

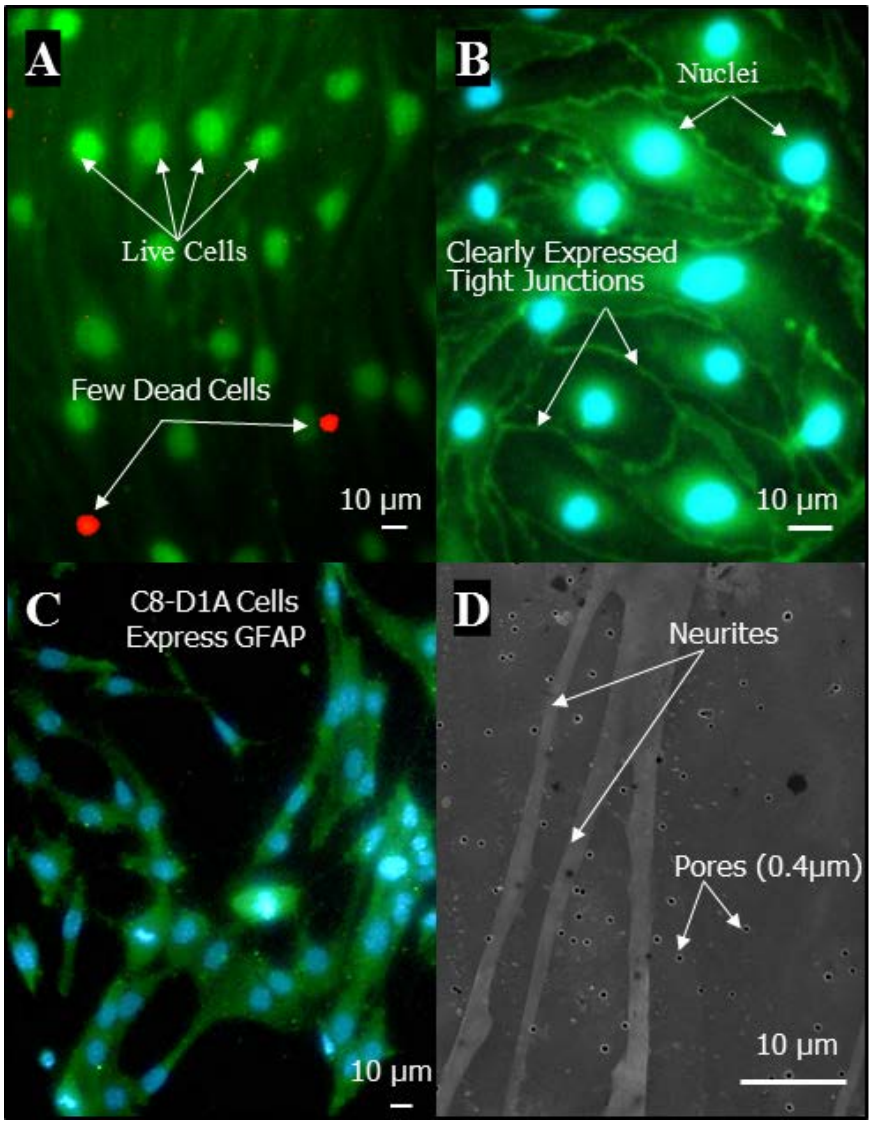

Figure 3.5 Representative images of cells in µBBB. (A) Live/Dead stain (green:live, red:dead) of bEnd.3 cells on day 3 of culture on µBBB membrane indicates high cell viability. (B) Immunostains of tight junction component ZO-1 (green) in bEnd.3 cells on day 3 indicate distinct tight junction expression. Nuclei counter-stained with DAPI (blue). (C) Immunostains of GFAP (green) in C8-D1A cells reveal astrocytic morphology on polycarbonate membrane. Nuclei counter-stained with DAPI (blue). (D) ESEM of C8-D1A neurites on porous polycarbonate membrane.

3.6.2 TEER

TEER results indicated acceptably high [39] electrical resistance for BBB models, with conveniently short time to steady-state TEER levels, and effectively demonstrated a transient response to histamine. For both static transwell experiments and dynamic µBBB cultures, cultures typically reached steady-state levels by day 3-4 of endothelial cell culture (Figure 3.6). This is indicative of full tight junction development, in congruence with the ZO-1 imaging data, so day 3 was the minimum threshold for endpoint testing such as permeability assays, immunostains, and TEER response assays. For both systems, co-culturing endothelial cells with astrocytes significantly increased the steady-state TEER levels, as indicated by the arithmetic means over several runs shown in Figure 3.6.

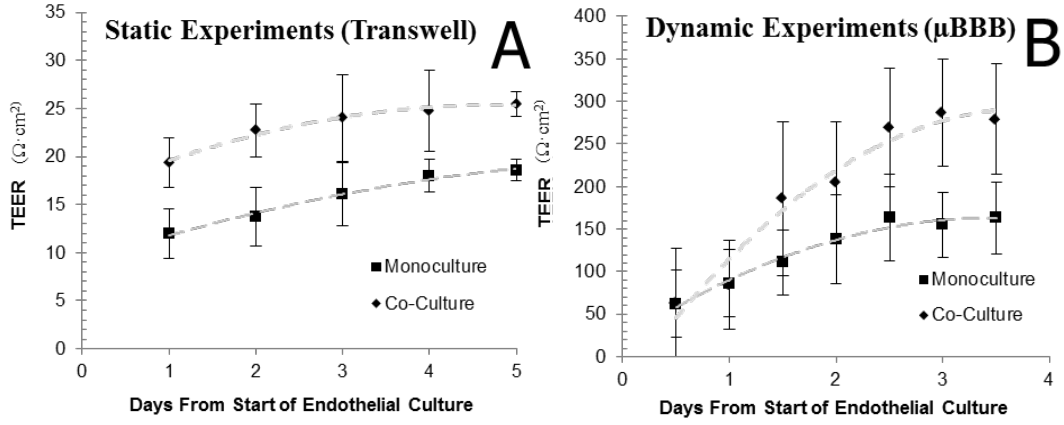

Figure 3.6 TEER levels of static and dynamic experiments over time, beginning on D0 of endothelial culture. (A) TEER development of transwells seeded with b.End3 cells in monoculture and in co-culture with astrocytes. (B) TEER development of µBBB devices seeded with b.End3 cells in monoculture and in co-culture with astrocytes. Both systems typically reached steady-state TEER by D3 of culture. All $n \geq 3$.

3.6.2.1 Steady-State TEER Measurements

The steady-state TEER values in dynamic μBBB chips were significantly higher than our static transwell controls (Figure 3.7) using the same cell lines, media formulations, and voltohmeter. TEER levels of μBBB co-cultures regularly exceeded 250Ωcm^2, compared to only 25Ωcm^2 in transwell co-cultures. Supported by previous studies reporting shear stress effects on endothelial cells [31,40-48] we reasonably hypothesize that this significant increase in TEER may be due to the effects of shear stress on endothelial cells. Shear stress has a known mechano-transductive effect on endothelial molecular pathways [44,45,48], and has been seen to up-regulate expression of tight junction proteins [47] and increase RNA levels of BBB transporter proteins [30] in

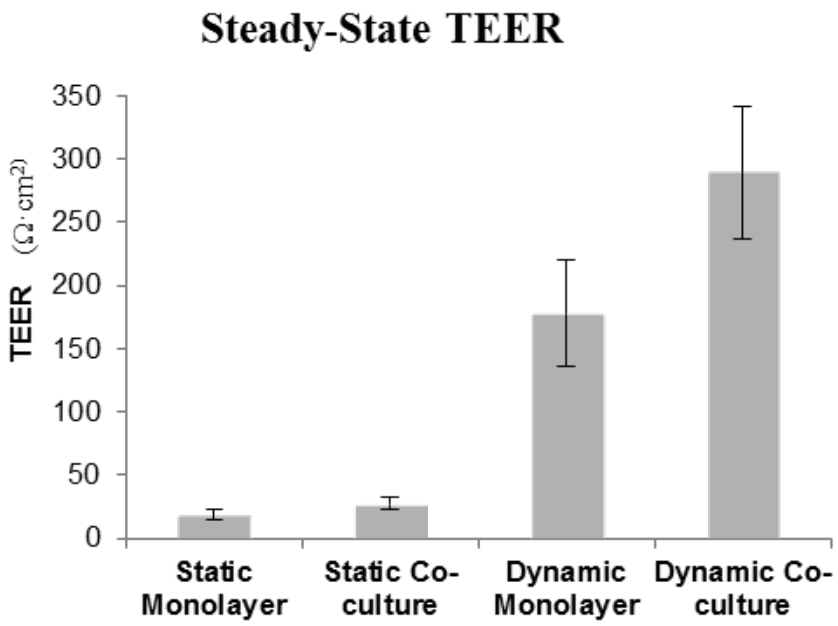

Figure 3.7 Steady-state TEER levels of each base condition. Dynamic cultures reached significantly higher TEER levels than static cultures. For both systems, co-cultures developed higher TEER levels than endothelial monolayers alone.

vascular endothelial cells, modulate cytoskeletal structure [31,42], and shows less inflammatory effects with definitive directional flow [46] than disturbed flow [49].

However, other differences exist between the μBBB system and our transwell controls which may factor into differences in results, such as total cell numbers and media volumes, culture surface/volume ratios, ratio between endothelial cells and astroctyes, and TEER electrode characteristics such as size, gap, and orientation.

Though *in vivo* TEER levels are greater than 1000 Ωcm^2, a consensus has been reached that for a system showing sufficiently high TEER levels over 150 Ωcm^2, reasonably representative data can be obtained [39], while our system typically exceeded 250 Ωcm^2.

3.6.2.2 Dynamic TEER Measurements

A transient drop and recovery to the original levels in TEER was observed as a result of exposure to histamine (Figure 3.8), indicating the robustness of the model for repeated at long-term testing purposes. The drop occurred very rapidly upon exposure to histamine, and TEER returned to initial levels within six minutes at 100μM histamine concentration, and fifteen minutes for 150μM concentrations. Maximum TEER drop was approximately 30% for 100μM histamine, and 50% for 150μM histamine. A similar transient response of endothelial cells to histamine has been reported in previous studies [50-54]. This effect has been attributed to brief formation of trans-endothelial gap formation [55], and has also been suggested to be due to increased trans-cytosis [56]. The ability to observe real-time transient changes in TEER without disturbing the system is a significant practical advantage of our system.

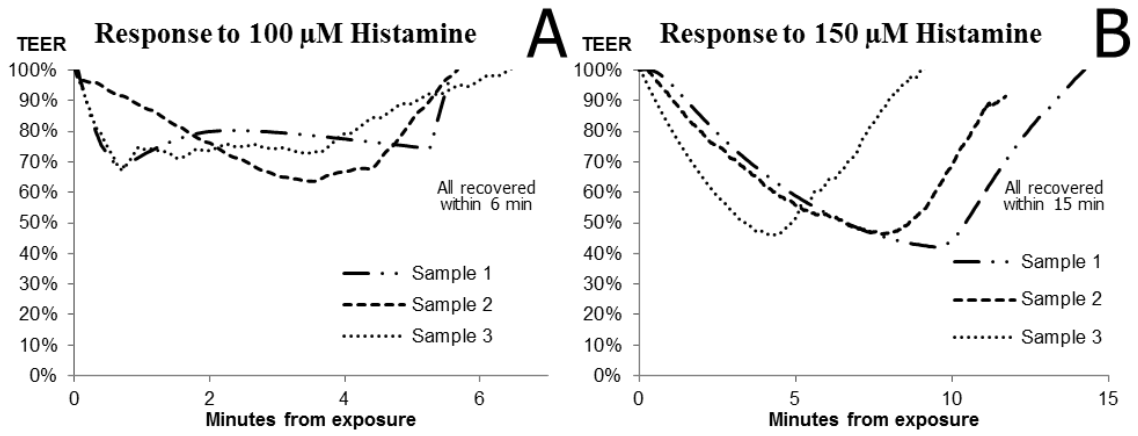

Figure 3.8 Continuous response to histamine exposure in three samples at each concentration. Co-cultured µBBB on D4 were perfused with histamine at two concentrations. (A) Three samples perfused with 100µM histamine saw a transient drop of up to 30% over a period of five-seven minutes. (B) Three samples perfused with 150µM histamine saw a transient drop of up to 50% over a period of eight-fifteen minutes.

3.6.3 Permeability

Permeabilities of µBBB cultures to large molecules were shown to be selective according to size, and seen to be slightly lower for co-cultures than endothelial cells alone, and found to be higher when pH is significantly elevated. The µBBB system is advantageous for permeability assays, because Equation 3.2 assumes tracer concentrations are kept constant, which is not necessarily true for static models in which concentrations in both chambers change with time. This is a valid assumption for flow-based BBB models, because fresh media at constant concentration is continuously delivered to the chamber. Permeability coefficients of Dextrans 4kD, 20kD, and 70kD, and propidium iodide were calculated and plotted according to stokes radius, or the radius of a sphere with the same diffusive properties (Figure 3.9). Results for all conditions showed higher permeability to tracers of lower stokes radius, indicating that smaller

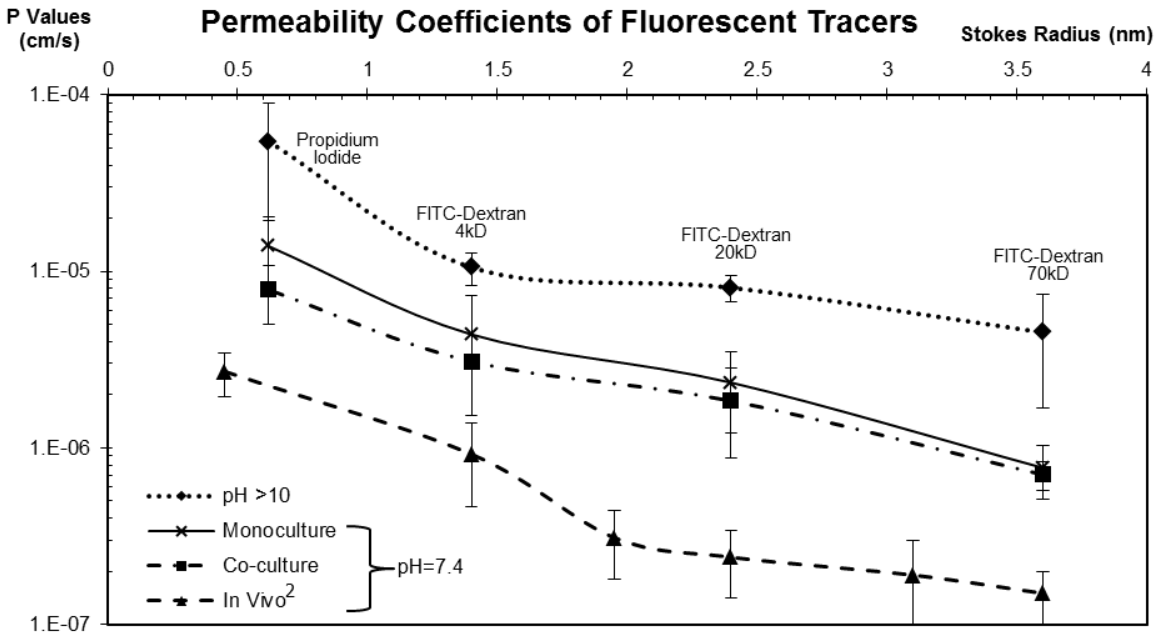

Figure 3.9 Permeabilities of cultured μBBB under different conditions. Tracer molecules FITC-Dextrans 4k, 20k, 70k, and propidium idodide reveal selectivity according to size. Also plotted for reference is *in vivo* data from a previous study[7], which showed a lower permeability curve than all *in vitro* models. Co-cultures showed lower permeability than monocultured b.End3 cells alone. Increasing pH to 10 for four hours resulted in significantly increased permeabilities. All $n \geq 3$.

compounds pass through junctions easier. Co-cultured systems showed lower permeability than for monoculture of endothelial cells alone, consistent with the higher TEER levels. Exposing μBBB co-cultures to significantly higher pH levels (>10) for four hours led to significantly higher permeabilities to all tracers, indicating loss of barrier function. This increase in permeability due to heightened pH has been observed in previous BBB models [57,58], and is indicative of a drop in barrier function. However, permeabilities for both co-cultures and endothelial monoculture were higher than those previously reported from *in vivo* studies [7]. To our knowledge, results from a BBB model with permeability levels as low as *in vivo* have yet to be achieved.

3.7 Conclusions

We have developed a μBBB that effectively mimics the dynamic cerebrovascular environment with fluid shear stress, and the results from this characterization study indicate that the model expresses sufficient key characteristics of a BBB model. Tight junction expression in the b.End3 cells and GFAP expression were characteristic of *in vivo*. The μBBB showed significantly higher TEER levels than in static models, with a comparatively short time to steady-state TEER to the DIV-BBB system. Real-time TEER response was shown to be feasible through measurement of transient effects histamine testing. Permeability assays were demonstrated in the system, with a selective permeability over a wide range of tracer sizes. These characteristics indicate that the μBBB system is a useful and enabling tool for further studies of BBB function and delivery. It can be used to monitor changes in barrier function in response to various environmental stimuli, such as barrier-enhancing or barrier-opening drugs. Finally, through permeability assays the system can be used to predict the rate of delivery of new drugs across the BBB. Thus, we believe use of the fabricated μBBB is a valid option for preclinical studies.

3.8 Acknowledgements

This research was supported by the Utah Science Technology and Research Initiative (USTAR) and the DARPA Young Faculty Award 2011 (N66001-11-14149). Microfabrication was performed at the state-of-the-art University of Utah Nano Fabrication Facility located in the Sorenson Molecular Biotechnology Building.

3.9 References

[1] Ferri, C. P., M. Prince, C. Brayne, H. Brodaty, L. Fratiglioni, M. Ganguli, K. Hall, K. Hasegawa, H. Hendrie, and Y. Huang. Global prevalence of dementia: A delphi consensus study. *The Lancet*. **366**(9503):2112-2117, 2006.

[2] Pangalos, M. N., L. E. Schechter, and O. Hurko. Drug development for cns disorders: Strategies for balancing risk and reducing attrition. *Nat Rev Drug Discov*. **6**(7):521-532, 2007.

[3] Pardridge, W. M., W. H. Oldendorf, P. Cancilla, and H. J. Frank. Blood-brain barrier: Interface between internal medicine and the brain. *Ann Intern Med*. **105**(1):82-95, 1986.

[4] Cardoso, F. L., D. Brites, and M. A. Brito. Looking at the blood-brain barrier: Molecular anatomy and possible investigation approaches. *Brain Res Rev*. **64**(2):328-363, 2010.

[5] Pardridge, W. M. Blood-brain barrier drug targeting: The future of brain drug development. *Mol Interv*. **3**(2):90-105, 151, 2003.

[6] Soni, S., A. K. Babbar, R. K. Sharma, and A. Maitra. Delivery of hydrophobised 5-fluorouracil derivative to brain tissue through intravenous route using surface modified nanogels. *J Drug Target*. **14**(2):87-95, 2006.

[7] Yuan, W., Y. Lv, M. Zeng, and B. M. Fu. Non-invasive measurement of solute permeability in cerebral microvessels of the rat. *Microvasc Res*. **77**(2):166-173, 2009.

[8] Preston, E., J. Slinn, I. Vinokourov, and D. Stanimirovic. Graded reversible opening of the rat blood-brain barrier by intracarotid infusion of sodium caprate. *J Neurosci Methods*. **168**(2):443-449, 2008.

[9] Weidenfeller, C., C. N. Svendsen, and E. V. Shusta. Differentiating embryonic neural progenitor cells induce blood-brain barrier properties. *J Neurochem*. **101**(2):555-565, 2007.

[10] Nakagawa, S., M. A. Deli, H. Kawaguchi, T. Shimizudani, T. Shimono, A. Kittel, K. Tanaka, and M. Niwa. A new blood-brain barrier model using primary rat brain endothelial cells, pericytes and astrocytes. *Neurochem Int*. **54**(3-4):253-263, 2009.

[11] Rubin, L. L., D. E. Hall, S. Porter, K. Barbu, C. Cannon, H. C. Horner, M. Janatpour, C. W. Liaw, K. Manning, J. Morales, and et al. A cell culture model of the blood-brain barrier. *J Cell Biol*. **115**(6):1725-1735, 1991.

[12] Wegener, J., A. Hakvoort, and H. J. Galla. Barrier function of porcine choroid

plexus epithelial cells is modulated by camp-dependent pathways in vitro. *Brain Res*. **853**(1):115-124, 2000.

[13] Raub, T. J. Signal transduction and glial cell modulation of cultured brain microvessel endothelial cell tight junctions. *Am J Physiol*. **271**(2 Pt 1):C495-503, 1996.

[14] Bruckener, K. E., A. el Baya, H. J. Galla, and M. A. Schmidt. Permeabilization in a cerebral endothelial barrier model by pertussis toxin involves the pkc effector pathway and is abolished by elevated levels of camp. *J Cell Sci*. **116**(Pt 9):1837-1846, 2003.

[15] Neuhaus, W., V. E. Plattner, M. Wirth, B. Germann, B. Lachmann, F. Gabor, and C. R. Noe. Validation of in vitro cell culture models of the blood-brain barrier: Tightness characterization of two promising cell lines. *J Pharm Sci*. **97**(12):5158-5175, 2008.

[16] Schiera, G., S. Sala, A. Gallo, M. P. Raffa, G. L. Pitarresi, G. Savettieri, and I. Di Liegro. Permeability properties of a three-cell type in vitro model of blood-brain barrier. *J Cell Mol Med*. **9**(2):373-379, 2005.

[17] Cohen-Kashi Malina, K., I. Cooper, and V. I. Teichberg. Closing the gap between the in-vivo and in-vitro blood-brain barrier tightness. *Brain Res*. **1284**(12-21, 2009.

[18] Li, G., M. J. Simon, L. M. Cancel, Z. D. Shi, X. Ji, J. M. Tarbell, B. Morrison, 3rd, and B. M. Fu. Permeability of endothelial and astrocyte cocultures: In vitro blood-brain barrier models for drug delivery studies. *Ann Biomed Eng*. 2010.

[19] Cucullo, L., P. O. Couraud, B. Weksler, I. A. Romero, M. Hossain, E. Rapp, and D. Janigro. Immortalized human brain endothelial cells and flow-based vascular modeling: A marriage of convenience for rational neurovascular studies. *J Cereb Blood Flow Metab*. **28**(2):312-328, 2008.

[20] Santaguida, S., D. Janigro, M. Hossain, E. Oby, E. Rapp, and L. Cucullo. Side by side comparison between dynamic versus static models of blood-brain barrier in vitro: A permeability study. *Brain Res*. **1109**(1):1-13, 2006.

[21] Cucullo, L., M. S. McAllister, K. Kight, L. Krizanac-Bengez, M. Marroni, M. R. Mayberg, K. A. Stanness, and D. Janigro. A new dynamic in vitro model for the multidimensional study of astrocyte-endothelial cell interactions at the blood-brain barrier. *Brain Res*. **951**(2):243-254, 2002.

[22] Neuhaus, W., R. Lauer, S. Oelzant, U. P. Fringeli, G. F. Ecker, and C. R. Noe. A novel flow based hollow-fiber blood-brain barrier in vitro model with immortalised cell line pbmec/c1-2. *J Biotechnol*. **125**(1):127-141, 2006.

[23] Booth, R. and H. Kim. A multi-layered microfluidic device for in vitro blood-brain barrier permeability studies. *International Conference on Miniaturized Systems for Chemistry and Life Sciences*. **15**(1388-1390, 2011.

[24] Reichel, A. Addressing central nervous system (cns) penetration in drug discovery: Basics and implications of the evolving new concept. *Chem Biodivers*. **6**(11):2030-2049, 2009.

[25] Cucullo, L., B. Aumayr, E. Rapp, and D. Janigro. Drug delivery and in vitro models of the blood-brain barrier. *Curr Opin Drug Discov Devel*. **8**(1):89-99, 2005.

[26] Hawkins, B. T. and T. P. Davis. The blood-brain barrier/neurovascular unit in health and disease. *Pharmacol Rev*. **57**(2):173-185, 2005.

[27] Pathan, S. A., Z. Iqbal, S. M. Zaidi, S. Talegaonkar, D. Vohra, G. K. Jain, A. Azeem, N. Jain, J. R. Lalani, R. K. Khar, and F. J. Ahmad. Cns drug delivery systems: Novel approaches. *Recent Pat Drug Deliv Formul*. **3**(1):71-89, 2009.

[28] Wolburg, H. and A. Lippoldt. Tight junctions of the blood-brain barrier: Development, composition and regulation. *Vascul Pharmacol*. **38**(6):323-337, 2002.

[29] Haseloff, R. F., I. E. Blasig, H. C. Bauer, and H. Bauer. In search of the astrocytic factor(s) modulating blood-brain barrier functions in brain capillary endothelial cells in vitro. *Cell Mol Neurobiol*. **25**(1):25-39, 2005.

[30] Cucullo, L., M. Hossain, V. Puvenna, N. Marchi, and D. Janigro. The role of shear stress in blood-brain barrier endothelial physiology. *BMC Neurosci*. **12**(40, 2011.

[31] Galbraith, C. G., R. Skalak, and S. Chien. Shear stress induces spatial reorganization of the endothelial cell cytoskeleton. *Cell Motil Cytoskeleton*. **40**(4):317-330, 1998.

[32] Frampton, J. P., M. L. Shuler, W. Shain, and M. R. Hynd. Biomedical technologies for in vitro screening and controlled delivery of neuroactive compounds. *Cent Nerv Syst Agents Med Chem*. **8**(3):203-219, 2008.

[33] Chueh, B. H., D. Huh, C. R. Kyrtsos, T. Houssin, N. Futai, and S. Takayama. Leakage-free bonding of porous membranes into layered microfluidic array systems. *Anal Chem*. **79**(9):3504-3508, 2007.

[34] Omidi, Y., L. Campbell, J. Barar, D. Connell, S. Akhtar, and M. Gumbleton. Evaluation of the immortalised mouse brain capillary endothelial cell line, b.End3, as an in vitro blood-brain barrier model for drug uptake and transport studies. *Brain Res*. **990**(1-2):95-112, 2003.

[35] Deli, M. A., C. S. Abraham, Y. Kataoka, and M. Niwa. Permeability studies on in vitro blood-brain barrier models: Physiology, pathology, and pharmacology. *Cell Mol Neurobiol*. **25**(1):59-127, 2005.

[36] Pardridge, W. M., D. Triguero, J. Yang, and P. A. Cancilla. Comparison of in vitro and in vivo models of drug transcytosis through the blood-brain barrier. *J Pharmacol Exp Ther*. **253**(2):884-891, 1990.

[37] Li, G., M. J. Simon, L. M. Cancel, Z. D. Shi, X. Ji, J. M. Tarbell, B. Morrison, 3rd, and B. M. Fu. Permeability of endothelial and astrocyte cocultures: In vitro blood-brain barrier models for drug delivery studies. *Ann Biomed Eng*. **38**(8):2499-2511, 2010.

[38] Nicolazzo, J. A., S. A. Charman, and W. N. Charman. Methods to assess drug permeability across the blood-brain barrier. *J Pharm Pharmacol*. **58**(3):281-293, 2006.

[39] Vastag, M. and G. M. Keseru. Current in vitro and in silico models of blood-brain barrier penetration: A practical view. *Curr Opin Drug Discov Devel*. **12**(1):115-124, 2009.

[40] Thoumine, O., R. M. Nerem, and P. R. Girard. Oscillatory shear stress and hydrostatic pressure modulate cell-matrix attachment proteins in cultured endothelial cells. *In Vitro Cell Dev Biol Anim*. **31**(1):45-54, 1995.

[41] Nerem, R. M., R. W. Alexander, D. C. Chappell, R. M. Medford, S. E. Varner, and W. R. Taylor. The study of the influence of flow on vascular endothelial biology. *Am J Med Sci*. **316**(3):169-175, 1998.

[42] Ookawa, K., M. Sato, and N. Ohshima. Time course changes in cytoskeletal structures of cultured endothelial cells exposed to shear stress. *Front Med Biol Eng*. **5**(2):121-125, 1993.

[43] Desai, S. Y., M. Marroni, L. Cucullo, L. Krizanac-Bengez, M. R. Mayberg, M. T. Hossain, G. G. Grant, and D. Janigro. Mechanisms of endothelial survival under shear stress. *Endothelium*. **9**(2):89-102, 2002.

[44] Tzima, E., M. Irani-Tehrani, W. B. Kiosses, E. Dejana, D. A. Schultz, B. Engelhardt, G. Cao, H. DeLisser, and M. A. Schwartz. A mechanosensory complex that mediates the endothelial cell response to fluid shear stress. *Nature*. **437**(7057):426-431, 2005.

[45] Li, Y. S., J. H. Haga, and S. Chien. Molecular basis of the effects of shear stress on vascular endothelial cells. *J Biomech*. **38**(10):1949-1971, 2005.

[46] Chien, S. Molecular basis of rheological modulation of endothelial functions: Importance of stress direction. *Biorheology*. **43**(2):95-116, 2006.

[47] Siddharthan, V., Y. V. Kim, S. Liu, and K. S. Kim. Human astrocytes/astrocyte-conditioned medium and shear stress enhance the barrier properties of human brain microvascular endothelial cells. *Brain Res*. **1147**(39-50, 2007.

[48] Chien, S. Mechanotransduction and endothelial cell homeostasis: The wisdom of the cell. *Am J Physiol Heart Circ Physiol*. **292**(3):H1209-1224, 2007.

[49] Chien, S. Effects of disturbed flow on endothelial cells. *Ann Biomed Eng*. **36**(4):554-562, 2008.

[50] van Nieuw Amerongen, G. P., R. Draijer, M. A. Vermeer, and V. W. van Hinsbergh. Transient and prolonged increase in endothelial permeability induced by histamine and thrombin: Role of protein kinases, calcium, and rhoa. *Circ Res*. **83**(11):1115-1123, 1998.

[51] Schilling, L. and M. Wahl. Opening of the blood-brain barrier during cortical superfusion with histamine. *Brain Res*. **653**(1-2):289-296, 1994.

[52] Gulati, A., K. N. Dhawan, R. Shukla, R. C. Srimal, and B. N. Dhawan. Evidence for the involvement of histamine in the regulation of blood-brain barrier permeability. *Pharmacol Res Commun*. **17**(4):395-404, 1985.

[53] Takeda, T., Y. Yamashita, S. Shimazaki, and Y. Mitsui. Histamine decreases the permeability of an endothelial cell monolayer by stimulating cyclic amp production through the h2-receptor. *J Cell Sci*. **101 (Pt 4)**(745-750, 1992.

[54] Abbott, N. J. Inflammatory mediators and modulation of blood-brain barrier permeability. *Cell Mol Neurobiol*. **20**(2):131-147, 2000.

[55] Wu, N. Z. and A. L. Baldwin. Transient venular permeability increase and endothelial gap formation induced by histamine. *Am J Physiol*. **262**(4 Pt 2):H1238-1247, 1992.

[56] Deli, M. A., M. P. Dehouck, R. Cecchelli, C. S. Abraham, and F. Joo. Histamine induces a selective albumin permeation through the blood-brain barrier in vitro. *Inflamm Res*. **44 Suppl 1**(S56-57, 1995.

[57] Nielsen, H. M. and M. R. Rassing. Nicotine permeability across the buccal tr146 cell culture model and porcine buccal mucosa in vitro: Effect of ph and concentration. *Eur J Pharm Sci*. **16**(3):151-157, 2002.

[58] Nielsen, H. M. and M. R. Rassing. Tr146 cells grown on filters as a model of human buccal epithelium: Iii. Permeability enhancement by different ph values, different osmolality values, and bile salts. *Int J Pharm*. **185**(2):215-225, 1999.

CHAPTER 4

A MULTIPLE-CHANNEL, MULTIPLE-ASSAY PLATFORM FOR CHARACTERIZATION OF FULL-RANGE SHEAR STRESS EFFECTS ON VASCULAR ENDOTHELIAL CELLS[2]

4.1 Abstract

Vascular endothelial cells (VECs), which line blood vessels and are key to understanding pathologies and treatments of various diseases, experience highly variable wall shear stress (WSS) *in vivo* (1-60dyn/cm^2), imposing numerous effects on physiological and morphological functions. Previous flow-based systems for studying these effects have been limited in range, and comprehensive information on VEC functions at the full spectrum of WSS has not been available yet. To allow rapid characterization of WSS effects, we developed the first multiple channel microfluidic platform that enables a wide range (~x15) of homogeneous WSS conditions while simultaneously allowing trans-monolayer assays, such as permeability and trans-endothelial electrical resistance (TEER), as well as cell morphometry and protein expression. Flow velocity/WSS distributions between channels were predicted with COMSOL simulation and verified by measurement with an integrated micro-flow sensor array. Biomechanical responses of the brain microvascular endothelial cell line bEnd.3 to

[2] Reproduced by permission of The Royal Society of Chemistry. Published: Lab on a Chip, 2014, Vol 14, p 1880-1890. http://pubs.rsc.org/en/Content/ArticleLanding/2014/LC/c3lc51304a

the full natural spectrum of WSS were investigated with the platform. Under increasing WSS conditions ranging from 0-86 dyn/cm^2, (1) permeabilities of FITC-conjugated dextran and propidium iodide decreased respectively at rates of 4.06e^{-8} and 6.04e^{-8}cm/s per dyn/cm^2; (2) TEER increased at a rate of 0.8 Ωcm^2 per dyn/cm^2; (3) cells increased alignment along the flow direction under increasing WSS; and finally (4) increased protein expression of both tight junction component ZO-1 (~5x) and efflux transporter P-gp (~6x) were observed at 86 dyn/cm^2 compared to static controls via western blot. We conclude that the presented microfluidic platform is a valid approach for comprehensively assaying cell responses to fluidic WSS.

4.2 Introduction

Vascular endothelial cells (VECs), which line all blood vessels and comprise the interface between blood and surrounding tissue, are a key to understanding pathologies and treatments of vascular systems, dictating numerous vascular functions critical to homeostasis and drug delivery thoughout the body [1,2]. Their governing functions [3] include permeability [4], angiogenesis [5], cell migration, proliferation, and apoptosis [6], impacting processes involved in inflammation [7], thrombosis [8], metastasis [9], and drug pharmacokinetics, all of which play critical roles in pathology and treatment of the two leading causes of death in the US [10]: cancer [11] and cardiovascular disease [12], as an example.

VECs have been found to delicately regulate such functions in response to dynamic microenvironments, and one major environmental parameter is the shear stress experienced at the vessel wall, or wall shear stress (WSS), induced by the flow of blood

through the vasculature. VECs are reported to experience **mechontransductive effects on cell phenotype** when exposed to WSS via membrane-bound mechanosensors [13-15] (Figure 4.1A). Such effects include the induced modulation of a myriad of biomolecular pathways leading to various physiological responses [16], such as resistance to apoptosis [17,18], upregulation of tight junction proteins (ZO-1, occludin) [19], extracellular matrix components (fibronectin, laminin) [20], membrane-bound efflux transporters (P-gp) [21] and integrins [22], as well as cytoskeletal restructuring and cell reorientation in relation to the flow direction [23-28]. The effects caused by WSS impact VEC functions relevant to pathology. For example, atherosclerosis, the leading cause of heart attack and stroke [29], has been correlated with low stress regions [30], while atheroprotective responses have been observed in high-stress regions [31], and WSS as high as 300 dyn/cm^2 has been measured in cases of vessel stenosis [32]. This variability in cell microenvironment indicates the need for comprehensive understanding of the adaptive responses of VECs to the WSS applied by the highly dynamic, highly variable microenvironment of the *in vivo* vasculature, and for delineating the practical limitations of dynamic *in vitro* culture conditions.

The study of VECs' responses to WSS has remained quite challenging both *in vivo* and *in vitro,* due to the difficulty in realizing the wide range of WSS conditions (**1-60dyn/cm^2)** [33] *in vivo*, and utilizing it for comprehensive assays. Such a large WSS range is mainly caused by significant variations of vessel sizes (8μm-2.5cm) and their differently localized pressure [34] (Figure 4.1B). *In vivo* investigation does not provide reproducible and controllable testing conditions due to natural variations in tissue complexity and structural contiguity, forbidding precisely defined correlations between

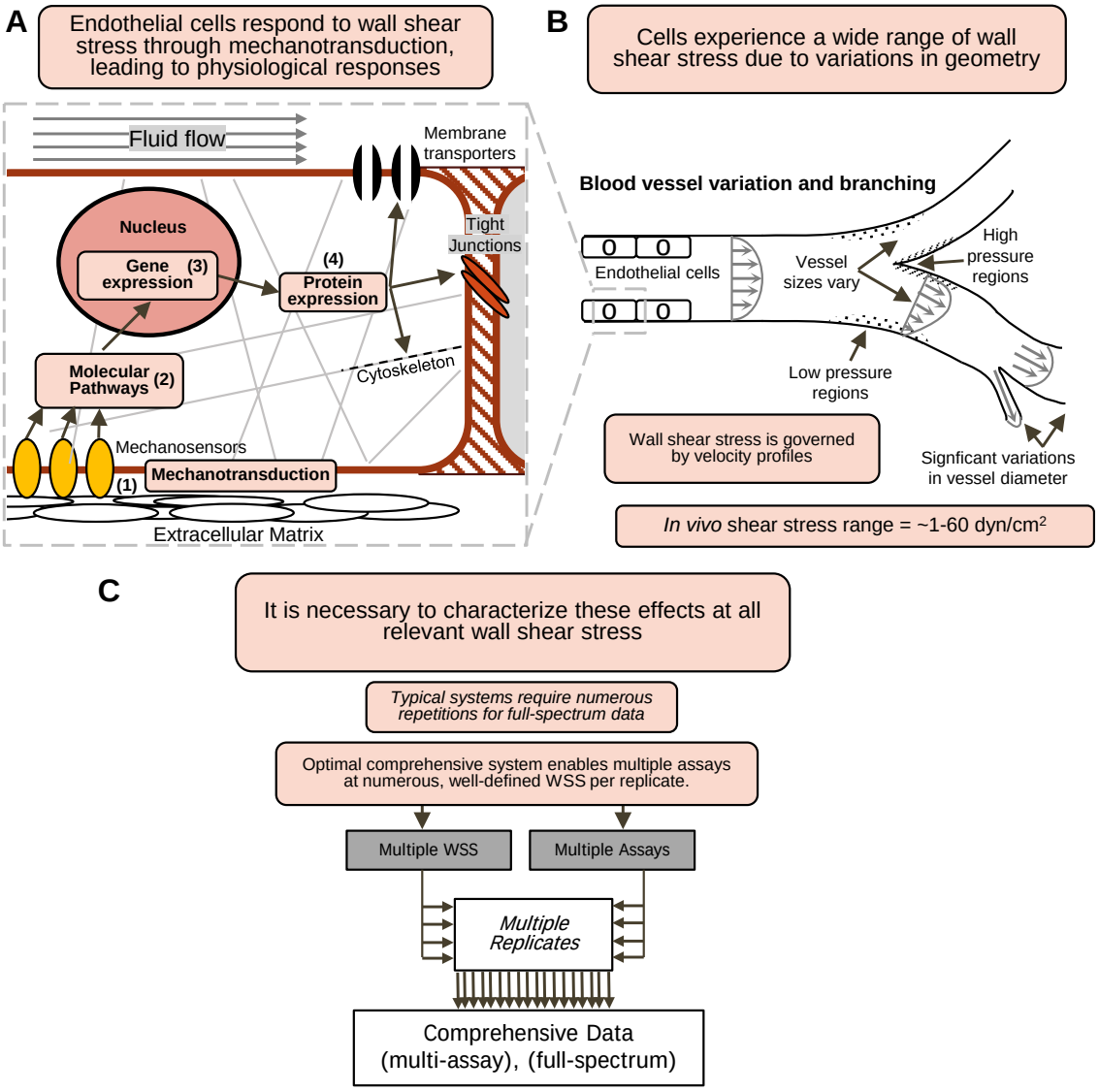

Figure 4.1 Studying the relationship between vascular wall shear stress (WSS) and endothelial cell (EC) physiology. (A) VECs respond through mechano-transduction via mechanosensors (integrins and kinases), ultimately leading to significant changes in protein expression, such as in membrane transport, tight junctions, and cytoskeletal re-organization. (B) The WSS experienced by vascular endothelial cells varies significantly (1-60 dyn/cm^2) at different geometric locations *in vivo*. (C) An optimal, fully comprehensive approach to testing the relationship between WSS and VEC responses requires multiple well-defined, discrete WSS, and extraction of data via multiple assays, including trans-membrane testing, per replicate chip.

and repeatability of flow conditions [35], have failed thus far to effectively provide characterization spanning the physiologically relevant full spectrum of WSS. This is because all previous VEC cultures systems for assaying WSS effects (Table 4.1) are either limited to a single WSS condition per unit [13,23,26,27,36-45], or are limited in the types of feasible assays, due either to a lack of an integrated membrane [46] (preventing assays of barrier properties), or to non-uniformity in applied WSS among a cell population under assay [47-52] (preventing reliable correlation of assay results with discrete WSS). Though recently a closed-loop braille-display device has applied distinctly different WSS to three parallel channels [24], it covered only a limited shear stress range of <12dyn/cm^2 due to the limited flow rates from the integrated micro pumps and did not allow trans-monolayer assay. In summary, no VEC culture system has simultaneously achieved (1) multiple on-chip WSS conditions for isolated cell populations, while (2) allowing trans-membrane assays yet.

To address such issues, we have developed a **multichannel and multiassay platform** (Figure 4.1C) where a single fluidic input produces multiple distinct WSS magnitudes homogenously applied to isolated VEC populations cultured on membranes, allowing multiple types of assays in a reproducible and controllable manner. To allow rapid characterization spanning the full *in vivo* WSS range (1-60dyn/cm^2), the platform employed four parallel channels producing distinct WSS with ~15x range of magnitude. In practice, by compounding the on-chip WSS variance with varying input flow-rates, useful quantitative data spanning the full spectrum of WSS can be efficiently gathered from a single experimental pump setup (16-channel peristaltic pump), and seeded from a single standard plate (75cm^2) of VECs (Figure 4.2). For example, 8 chips in parallel in a

Table 4.1 Comparison of flow-based *in vitro* systems for characterizing WSS effects on vascular endothelial cells.

Dynamic *in vitro* platforms for characterization of wall shear stress effects on vascular endothelial cells			
System type	**Multiple WSS conditions per unit**	**Isolated cell populations with homogenously applied WSS**	**Trans-monolayer assays**
Presented microfluidic system	***Yes***	***Yes***	***Yes***
Microfluidic (braille closed-loop) [24]	Yes	Yes	No
Rotational systems [47-49]	Yes	No	Yes
Microfluidic (geometric variation) [50-52]	Yes	No	No
Hollow fiber / capillary systems [21,49]	No	Yes	Yes
Microfluidic (constant-width channels) [26,36-41]	No	Yes	Yes
Parallel-plate flow chambers [13,23,27,42-45]	No	Yes	Yes

standard 16-cartridge pump, useful quantitative data spanning the full spectrum of WSS can be efficiently gathered from a single experimental pump setup, and seeded from a single standard plate (75cm^2) compounded by varying input flow rates to each chip, will result in 32 distinct WSS. Furthermore, the designed ~15x magnitude range allows a single test to cover the full span of WSS experienced in brain capillaries (3-20dyn/cm^2) [53], which is the origin of the cell line used in this characterization study. Thus, the presented approach massively reduces required cells/reagents and turn-around time, while allowing unprecedented high-throughput, comprehensive WSS characterization assays. To allow trans-membrane assays, including trans-endothelial electrical resistance (TEER) and permeability, this platform employs the cross-junction structure used in our

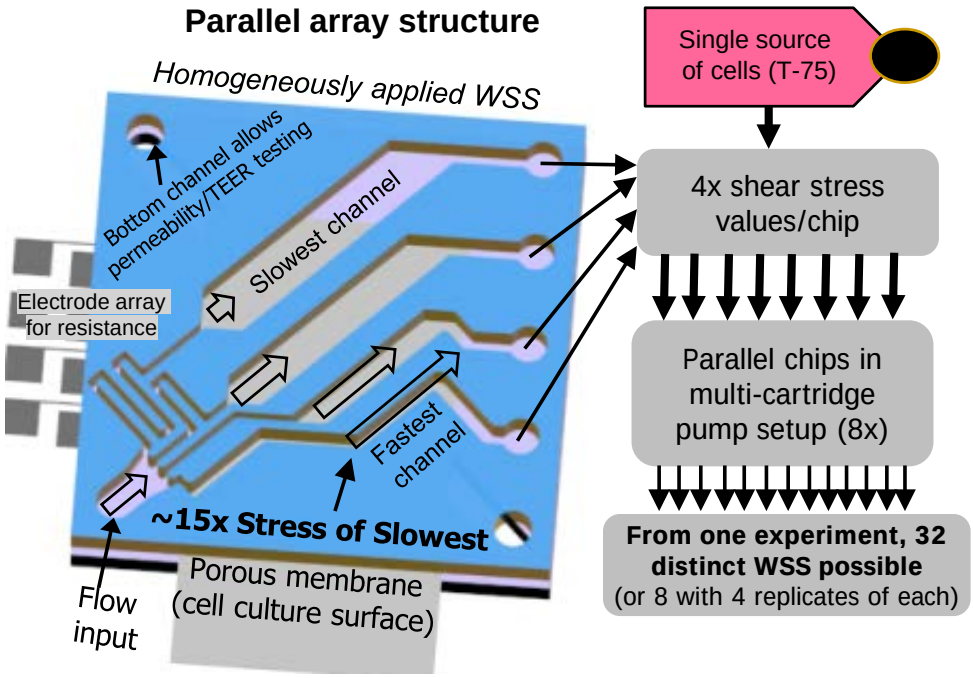

Figure 4.2 The presented parallel channel array allows multiple high-throughput characterization assays of WSS effects on cultured endothelial cells. Four channels subject independent populations of endothelial cells to homogeneous WSS level at a ~15x range. Thus, from a single culture plate source with 8 chips in parallel in a single peristaltic pump setup, 32 quantitative shear stress assay datapoints can be achieved per experiment, spanning the full physiological WSS range (1-60dyn/cm^2) with replicates.

previously reported microfluidic BBB model [41].

This paper reports the design, fabrication, and testing results of the developed multichannel, multiassay WSS platform. To evaluate the effectiveness of the platform to produce a wide range of WSS, quantitative testing results are discussed, including velocity discretization into parallel channels (1) by COMSOL simulation and (2) by experimental measurements with an integrated micro-flow sensor array. Next, the validity of the platform as a high-throughput tool to correlate full-spectrum WSS effects with VEC properties of a particular cell line was quantitatively verified on the brain

microvascular endothelial cell line bEnd.3 by measuring (3) cell morphology (cell elongation and orientation), (4) trans-monolayer permeability, (5) monolayer TEER, and (6) protein expression of tight junctions (ZO-1) and membrane-bound efflux transporters (P-gp).

4.3 Structures and Fabrication

To produce high-variance WSS distributions, a parallel array microfluidic structure of four channels was fabricated utilizing standard PDMS processing techniques to have significant differences in fluidic resistance among the channels, causing variations in the flow velocities and thus the resultant WSS.

4.3.1 Microfluidic Parallel-Channel Structure

The parallel array platform consists of four top (luminal) channels and one bottom (abluminal) channel that cross perpendicularly, all of which were constructed from multiple stacked poly-dimethylsiloxane (PDMS) layers (Figure 4.3A). The four luminal channels branch from one common inlet and have independent outlets to simplify fluidic control and enable high-throughput parallel permeability assays. The four luminal channels have discrete widths (0.73, 1.53, 2.33, 3.13 mm) with varying geometries at the branching region, subsequently causing different fluidic resistances, flow velocities and uniform WSS in each channel. When these channels were constructed in multiple layers by stacking PDMS substrates, a porous polycarbonate (PC) membrane was inserted to be free-standing at the channel junction, providing a monolayer cell culture surface allowing

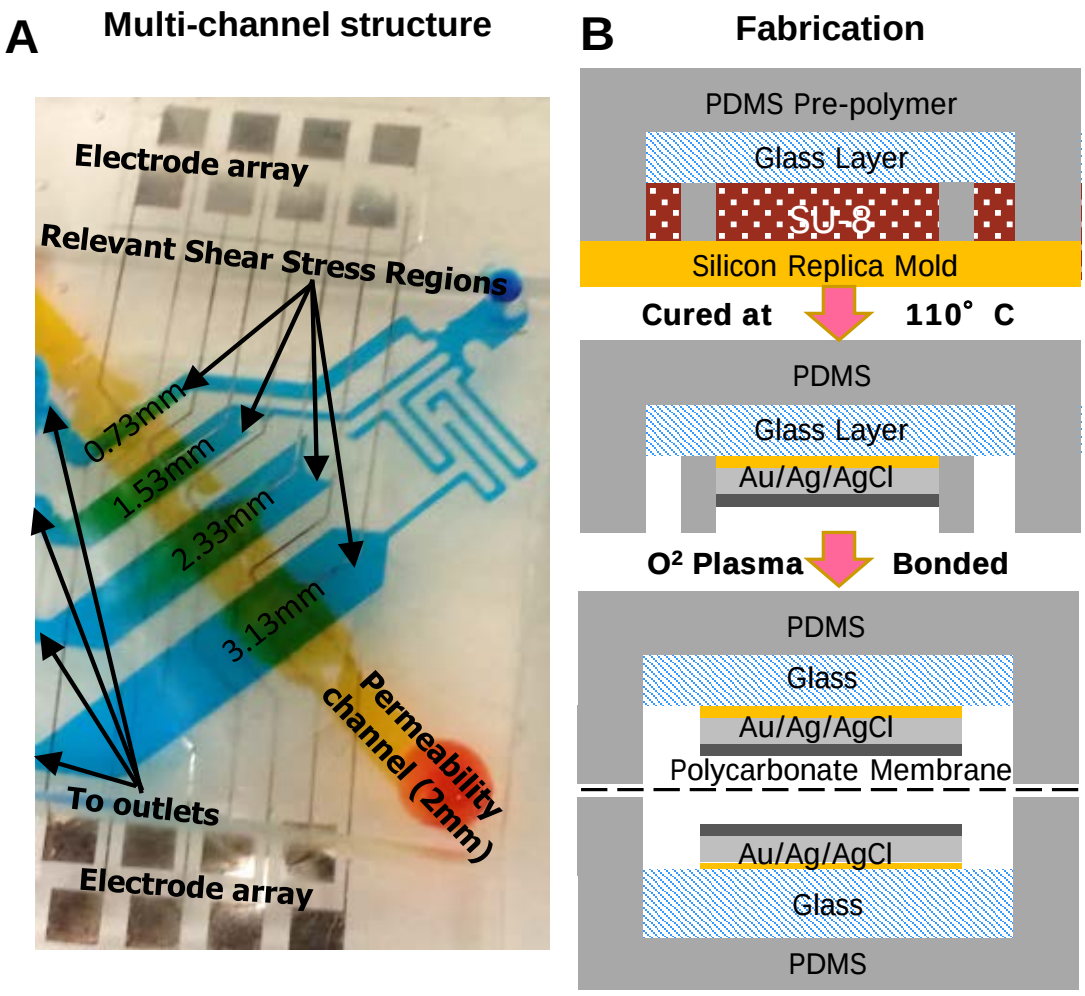

Figure 4.3 Multichannel device structure and fabrication. (A) Multichannel structure comprises 4 channels branched from a common inlet, exerting homogenous WSS at 4 distinct values to VECs cultured in the channel. A 2mm channel is fixed below, with a free-standing porous polycarbonate membrane as the culture surface. (B) To fabricate the multilayered microfluidic devices, sputter-deposited glass electrode layers were embedded in PDMS pre-polymer (10:1) over a lithographically defined SU-8 mold and cured at 110°C. Channel layers and an APTES-treated polycarbonate membrane were bonded together with O^2 plasma activation.

trans-monolayer assays (permeability/TEER) at each junction, as in the previously described μBBB system [41]. Flanking both sides of each PC culture surface, a set of thin-film AgCL electrodes were located to monitor TEER in the standard four-point sensing configuration minimizing error from parasitic resistance from external wires and contacts. The channel heights were initially set at 200μm, ensuring laminar flow and maxim izing aspect ratio of the channels for WSS uniformity.

The platform structure was fabricated (Figure 4.3B) similarly to the previously described μBBB system [41] with some modifications. First, embedded electrodes for TEER measurement were fabricated on a glass wafer by sputtering Cr/Au/Ag (20/80/800nm) and patterning layers using liftoff lithography (LOR-10B photoresist). The silver (Ag) surface was chlorinated with 30mM $FeCl_3$ for 50s to convert it into AgCl for corrosion resistant electrodes. Next, the channels were constructed among multiple PDMS layers. Channel molds were lithographically constructed from SU-8 2075 (200μm thick) on a silicon substrate, and silanized overnight with tridecafluoro-1,1,2,2-tetrahydrooctyl trichlorosilane in a vacuum chamber to minimize stiction and ease the separation during the molding process. On top of the SU-8 mold, PDMS layers were sequentially cast (10:1 elastomer:curing agent) and heat-cured (110ºC, 30m). Following thirty minutes pretreatment of the PC membrane with 5% 3-aminopropyltriethoxysilane (APTES) at 80°C [54], a reliable bond between the membrane and PDMS channel layers was generated with O^2 plasma (125W, 20s) at 25°C. Residual APTES on the membrane was dissolved in ethanol. This bond method significantly decreased occurrences of leaks under high flow compared with the standard method using spin-coated PDMS pre-polymer [55], with no observed losses of cell adhesion. To generate the minimum total

protein required for western blot (>25 μg), a large 5mm-wide, 175mm-long microfluidic channel was separately constructed.

4.3.2 Integrated Micro-Flow Sensor Array

In order to directly measure the WSS distributions in each microchannel and confirm the simulation results, a micro-flow sensor array was fabricated and integrated into the channel (Figure 4.4A). The flow sensor utilized a standard suspended thermal conductivity detector (TCD) configuration [56]. An identical free-standing flow sensor was suspended in each channel at 70μm above the bottom wall. Each flow sensor consists of a meander-shaped 10μm wide electrode suspended over an area of 1160μm by 490μm above a channel. The interval between adjacent electrode crossings was 120μm, while the total length of the meander sensor was 7.8mm.

The micro-flow sensor was fabricated with standard microfabrication techniques (Figure 4.4B). First, LPCVD (1μm) silicon nitride was deposited on a Si substrate, followed by sputter deposition of Pt/Ti layers (200nm/10nm), which was patterned to form 10μm wide sensor signal feed-through lines to the electrical pads. The Pt/Ti layer was then electrically passivated by another layer of patterned PECVD silicon nitride (450nm). Then the passivation layer was etched by RIE defining the sensor structure. Utilizing the same mask, anisotropic DRIE and isotropic Xactive XeF_2 etching were combined to etch the silicon substrate and partially suspend (with columns) the sensor structure at 70μm from the channel surface. Finally, the fabricated substrate was bonded to a 130μm PDMS channel structure, completing the structure of the final platform.

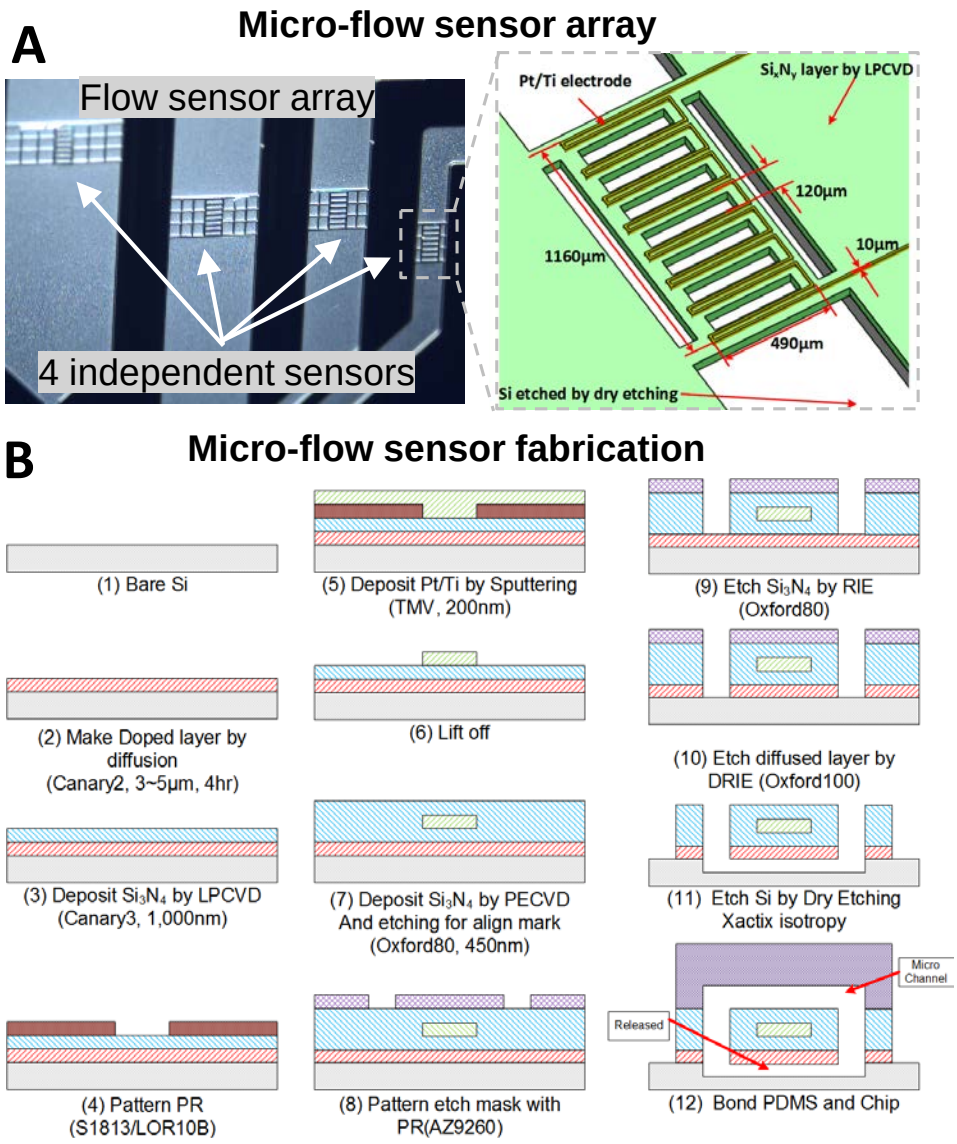

Figure 4.4 Micro-flow sensor array structure and fabrication. (A) Fabricated micro-flow sensor array to measure WSS distributions in the parallel array structure. The micro-flow sensor structure is the same for all four channels, except the connecting bridge structure. (B) Fabrication process for the integrated micro-flow sensor in each microchannel. The sensor was fabricated on a N-doped silicon substrate by depositing LPCVD nitride, lift-off patterning 10μm wide Pt/Ti electrodes, depositing PECVD nitride, then layer and bulk etching the sensor structure with RIE, DRIE, and Xactix to generate the partially suspended structure.

4.4 Cell Culture

The cell line tested in this study was the brain endothelial cell line bEnd.3 [57]. The cells were grown with DMEM/F12 (Lonza), and was supplemented with 10% fetal bovine serum (Hyclone), 1% Penicillin/Streptomycin and amphotericin B (EMD). Media pH was buffered to ~7.35 for all experiments. All cells used for experiments were taken from confluent cultures only, within two days after confluence was reached. All cell cultivation and shear stress experiments were carried out in a humid incubator (Nu-Aire Autoflow 4750) with 5% CO_2 kept at a constant 37°C. Cell suspensions were centrifuged in an Eppendorf 5810, and all sterile work was performed in a class II biosafety cabinet (Thermo Fisher). Sterilization of microfluidic devices and tubing was carried out with 70% ethanol and UV radiation prior to use. A single T-75 flask was sufficient for seeding a parallel array of microfluidic cell culture models for shear stress experiments. Antibodies used in this study were: Primary rabbit anti-ZO-1 (GeneTex GTX108592), primary rabbit anti-MDR-1 (Santa Cruz sc-8313), primary rabbit β-actin (Abcam ab8227), secondary HRP-conjugated goat anti-rabbit (Abcam ab6721), and secondary Alexa Fluor 488 goat anti-rabbit (Molecular Probes A-11008).

4.5 Testing Methodology

First, the fabricated platform was evaluated on its capability of producing a wide range of WSS by (1) predictions based on analytical calculation and simulations and (2) direct flow velocity measurement from the integrated micro-flow sensor array. Next, the validity of the platform as the high-throughput tool to correlate full-spectrum WSS effects with VEC properties was evaluated by monitoring the (3) cell morphology (shape and

orientation angle), (4) trans-monolayer permeability, (5) TEER, and (6) protein expression of tight junctions and efflux transporters of the bEnd.3 cell line.

4.5.1 Prediction of the Wall Shear Stress by Simulation

In order to predict the resultant WSS levels that cells experience at the channel wall, (1) fine-mesh 3D COMSOL simulations were performed to obtain velocity profiles at different heights from the wall; (2) shear rate *dU/dz* at the wall was calculated by COMSOL based on the velocity gradient right above the wall; (3) shear rate was multiplied with the proportionality constant μ, or viscosity, as in the following equation (Figure 4.5A) [58]:

$$\tau = \frac{dU}{dz}\mu \tag{4.1}$$

COMSOL simulation utilized the laminar flow module that derives velocity fields from the Navier-Stokes Equations. Assumptions used in the model were Newtonian fluid (μ=1.2mPa·s for media with serum), the no-slip condition, with equal pressure at all outlets. Note that the COMSOL simulations and analytical calculations also assumed that all flow in each of the described devices at all relevant flow-rates is completely laminar, with a Reynolds number several orders of magnitude lower than the turbulent threshold (2300), which is a reasonable assumption in microfluidics [59]. It was assumed that the effects of flow-induced deformation of the channel walls [60] was negligible at all relevant flow-rates for the study, and that the channel walls remained rigid for the purpose of WSS calculation and measurement in this study.

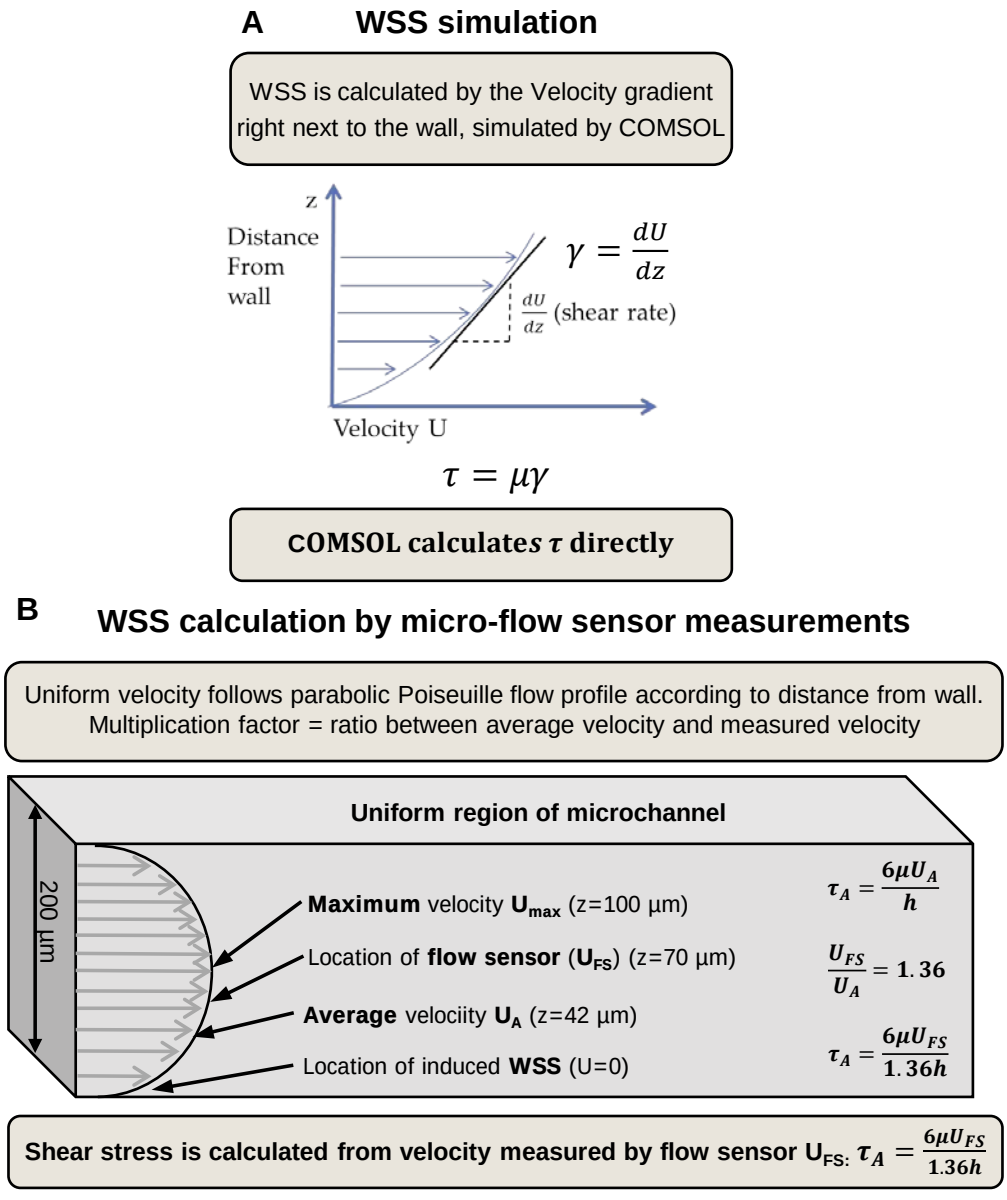

Figure 4.5 Shear stress calculation methods. All channels are 200 μm high. (A) WSS was simulated by COMSOL based on the vertical velocity gradient *dU/dz* multiplied by the dynamic viscosity μ. (B) Uniform velocity (70 μm height) measured by the micro-flow sensor was used to calculate the average shear stress τ_A based on the standard equation for shear stress in a rectangular microchannel based on the average velocity U_A. The ratio between U_A and U_{FS} is 1.36, so this multiplication factor was used to derive the average wall shear stress equation for micro-flow sensor measurements.

4.5.2 Shear Stress Measurement with Integrated Micro-Flow Sensors

In parallel to COMSOL simulation, the average WSS (τ_A) at the wall was calculated from the velocity measurement by the fabricated micro-flow sensor (U_{FS}) in each channel (Figure 4.5B). Since the fabricated microsensor was located at 70μm above the wall, the measurement does not directly represent the average velocity (located at 42μm height for our device), necessitating an adjustment process in order to utilize the well-established relationship between the average velocity (U_A) and τ_A in a rectangular channel [58]. For this adjustment, the ratio between U_{FS} and U_A, as obtained from the Poiseuille flow velocity profile in the vertical direction of the channel, was found to be ~1.36, and was applied as a multiplication constant to the denominator of the standard equation for average WSS in a rectangular channel [58], allowing calculation of τ_A from U_{FS}:

$$\tau_A = \frac{6\mu U_{FS}}{1.36h} \tag{4.2}$$

where h is channel height and μ is the dynamic viscosity.

To prepare for the induction of WSS into the parallel channels, fluidic interconnection was established by sealing marprene or silicone tubing (0.25, 0.38, 0.76, 1.0, 1.59mm) to the inlet ports (DC734 adhesive) with 22 or 18 gauge needles and 200μl pipet tips. Through the ports, fluid was manipulated with a 16-cartridge peristaltic pump (Watson-Marlow 205S). Then, measurement utilizing the fabricated micro-flow sensor was performed, while certain flow rates were supplied through the platform. The terminals of the micro-flow sensors were connected to a Wheatstone Bridge circuit to measure voltage offsets resulting from differential thermal dissipation. Defined flows of

DI water from a steady-flow syringe pump (KDS210) were injected in reverse through the outlets to generate calibration curves for each sensor. Electrical measurements were made with a power supply (GW Instek PSP603) and an NI DAQ. After 10s continuous flow, thus when flow is stable, 5V was applied and output voltage was recorded (10s, 1kHz) through the DAQ. Following brief cooldown, the process was repeated at least three times. To measure the velocity distributions under forward flow, known flow rates were injected through the inlet, and the measured voltage outputs in each channel were fitted to their calibration curves to calculate uniform velocity.

For further comparison, volumetric flow measurements (at least 3 replicates) at the outlet of each chip were fit to the standard equation for average WSS:

$$\tau_A = \frac{6Q\mu}{h^2 w} \tag{4.3}$$

4.5.3 Application of Shear Stress to Cultured Endothelial Cells

To analyse physiological effects of WSS on confluent cultures, the platforms were prepared by sealing marprene or silicone tubing to inlet ports in connection to a 16-cartridge peristaltic pump. Permeability/TEER measurement required two dedicated cartridges, and imaging & western blot measurement required one dedicated cartridge. Depending on tubing volume, 8-well strips (300 μL) with poly-tetrafluoroethylene plugs or centrifuge tubes lined with parafilm were used as media reservoirs. The entire experimental setup (pump, platforms, and reservoirs) was placed in a CO_2 incubator. Though flow-rates differed among the four parallel channels, they were appropriate for simultaneous cell seeding and channel flushing to be practical. To culture cells in the

fabricated platform, the platform was sterilized first with 70% ethanol and coated overnight with fibronectin and collagen IV (100µg/mL each) to facilitate cell adhesion. After sterilization, b.End3 cells were seeded in the devices at a density of $6e^4/cm^2$ and allowed to adhere in a static condition (no flows) for two hours. Then the platforms were flushed with sterile DMEM/F12 media and perfused at very low flows (uncharacterized minimum pump setting) for 3 days to allow cell confluence and optimal cell anchorage. Media reservoirs were changed daily. Experimental WSS was applied for twenty-four hours prior to quantitative assays to characterize the WSS effects on bEnd.3 physiology.

4.5.4 Morphometric Analysis

In order to evaluate the shear stress effects on cell morphology, VECs were imaged on-chip and both shape and orientation angle of the cells were analyzed with CellProfiler software, while various WSS was applied to each channel. For cell imaging preparation, monolayers of b.End3 cells were fixed with 4% paraformaldehyde (Avantor) for twenty minutes at room temperature. Cell membranes were permeabilized with 0.1% Triton X-100 in PBS for twenty minutes. Cells were then blocked for one hour under gentle rotation with 5% bovine serum albumin in permeabilization buffer, and cells were incubated overnight at 4°C with anti-ZO-1 primary antibody. Cells were then incubated with Alexa-fluor 488-conjugated secondary antibody for one hour under gentle rotation. To visualize the cells, they were imaged with a fluorescent Nikon microscope. To quantitatively assess changes in cell morphology under various WSS, images were processed with CellProfiler to measure cell dimensions and positions (Figure 4.6A), modeling cells as ellipses.

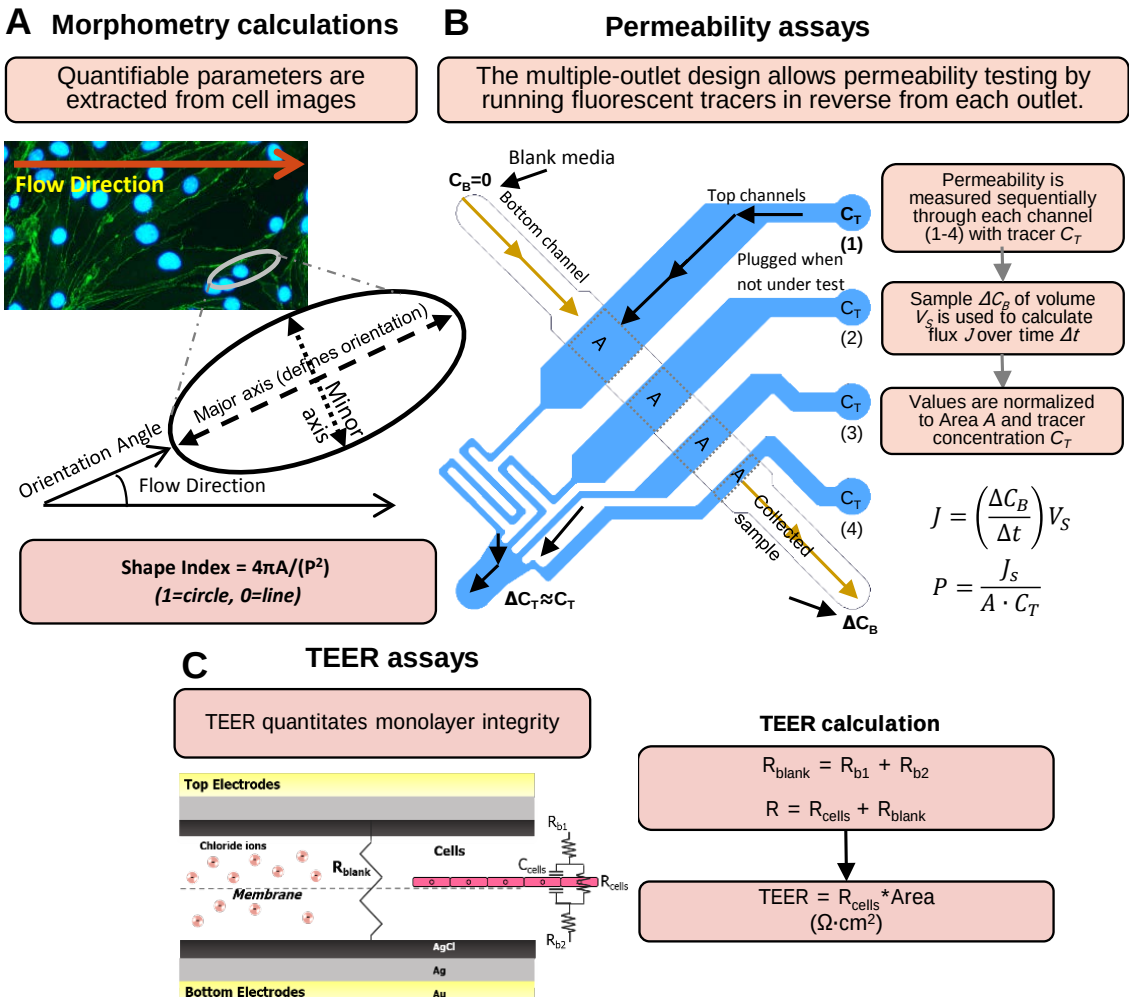

Figure 4.6 Testing methodology. (A) Morphometry calculations. To quantify ZO-1-tagged images taken at different WSS, dimensions, and orientations were analyzed with CellProfiler software, providing orientation angle away from flow direction, and shape index, defining properties of each cell. (B) Permeability assays. Fluorescent tracers of concentration C_T were sequentially flowed in reverse through each channel outlet (with the other three outlets plugged) and flux was calculated by measuring tracer concentration in the bottom channel perfusate, and was normalized to channel junction area and top concentration to give permeability coefficients. (C) TEER assays. To measure monolayer integrity, TEER was measured by connecting electrode terminals to an EVOM epithelial voltohmeter, and cell resistance was found by subtracting readings by blank membrane measurements, and transformed by area to give TEER values.

To quantify cell elongation, we used shape index *(SI)*

$$SI = \frac{4\pi A}{P^2} \tag{4.4}$$

where *A*=area and *P*=perimeter. An object with *SI* of 1 is a circle, and *SI* of 0 is a straight line. To quantify cell alignment, the orientation angle (OA) is defined as the angle (0-90°) between the cell's major axis and direction of flow. Negative orientation angles were inverted to their positive values.

4.5.5 Permeability Assay

In order to evaluate the shear stress effects on the cross-membrane transfer of molecules, the permeability of two commonly used fluorescent tracers, fluorescein isothiocyanate (FITC)-dextran (4kD size) and propidium iodide, was monitored in each channel in reference to the corresponding WSS values. Fluorescent tracer concentrations were measured with a BioRad Synergy plate reader for FITC-Dextran 4k (490/525nm excitation/emission) and propidium iodide (536/617nm), and fitted to known standards to calculate the concentration values. Then, the concentration values were utilized to calculate the corresponding permeability (Figure 4.6B). The tracer flux *J* through the cell layer was measured with the following flux equation

$$J = \left(\frac{\Delta C_B}{\Delta t}\right) V_S \tag{4.5}$$

where ΔC_B is bottom perfusate concentration change, Δt is assay time, and V_S is bottom perfusate sample volume. Permeability coefficients were calculated [61,62] for each tracer with the conventional equation for permeability

$$P = \frac{J_s}{A \cdot C_T} \tag{4.6}$$

where P is the permeability coefficient, A is culture area, and C_T is the concentration being flowed through the top channel. To normalize values for blank membrane flux, endothelial coefficients P_e were calculated by subtracting the inverse of the measured P value by the inverse of coefficient P_b through a blank membrane (no cells), as in the following equation [63].

$$\frac{1}{P_e} = \frac{1}{P} - \frac{1}{P_b} \tag{4.7}$$

4.5.6 TEER Assay

TEER values were measured under various WSS levels to evaluate the changes in confluence and integrity of tight junctions. For measurement of TEER (Figure 4.6C), voltage and current electrode pads were connected through 30-gauge wires with conductive silver epoxy via an electrode adaptor (WPI) to an EVOM2 epithelial voltohmeter (WPI). The EVOM2 passes a constant 10μA AC current at 12.5Hz while measuring resistance changes. To calculate TEER, initial D0 Background resistances R_{blank} were subtracted from measured resistance following twenty-four hour WSS R, and normalized for the cell culture area for that particular channel, giving TEER values in Ωcm^2 from:

$$TEER = (R - R_{blank})A \tag{4.8}$$

4.5.7 Western Blot

Protein expression assays were performed to affirm the causes of physiological responses under various shear stress levels. Particularly, two proteins were monitored, tight junction component ZO-1 and membrane efflux transporter p-glycoprotein (P-gp), at multiple WSS because these proteins correlate with monolayer tightness and membrane transport activity. Cells were scraped from the channel substrate surface, or 6-well static controls, with a cell scraper and lysed. Following 10s sonication, total protein was centrifuged (12000RPM, 15m) and separated from pellet. Protein was quantified with BCA total protein assay, and 25μg protein was loaded in 4-12% Bis-Tris gels (Novex) and run at 200V for ~one hour, or until sufficiently separated. Following the one hour transfer to nitrocellulose membrane at 30V, membranes were blocked with 5% skim milk (one hour) in TBS-Tween-20. Rabbit primary antibodies for ZO-1, MDR-1 (P-gp), and β-actin as a loading control, were incubated overnight at 4°C. Goat anti-rabbit horseradish peroxidase secondary antibody was incubated for one hour, and chemiGlow (AlphaInnotech) was applied to the membrane, and imaged for band analysis with a FluorChem FC2 imaging system.

4.6 Results and Discussion

4.6.1 Shear Stress Simulation and Measurement

COMSOL simulation results indicated that the horizontal profile of velocity and WSS within a channel is largely uniform except the high-drag regions near the side-walls within a distance of ~200 μm (Figure 4.7A). This uniformity helps optimize the homogeneity of the discrete WSS experienced by the cells in the channel, as it is desired

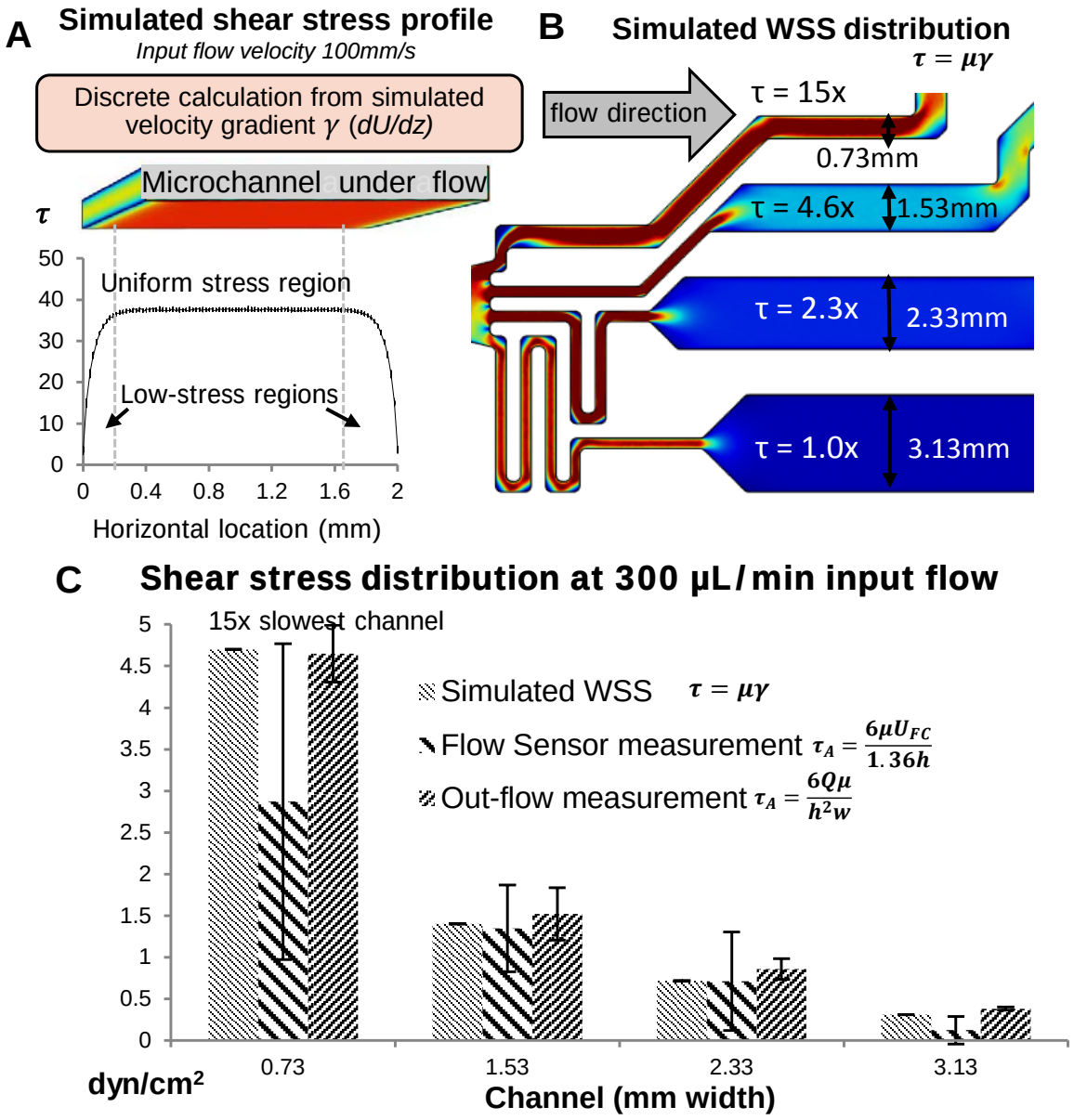

Figure 4.7 WSS characterization results. (A) Horizontal WSS profile in the channel is largely uniform, between the high-drag regions (~200 µm) by either sidewall of the channel. (B) WSS distributions were found by COMSOL simulation to be 15, 4.6, and 2.3 times the minimum value for the parallel array, based on the vertical velocity gradient *dU/dz* adjacent to the wall in each channel. (C) Shear stress distributions between the four channels at 300 µL/min were compared between simulation results, micro-flow sensor measurements, and volumetric measurements of channel out-flows following timed perfusion. Values for the middle two channels were sufficiently equivalent, but there were discrepancies with the fastest and slowest channels for the flow-sensor results. Standard deviation error bars displayed, all test replicates were $n \geq 3$.

to achieve as uniform an environment for all cells in a particular population. Due to the high-drag region, which is independent of channel width and only related to channel height, the proportion of cells experiencing lower shear stress is smaller for the wider channels, so the wider channels have a more homogenous profile, indicating the need for a high aspect ratio to optimize accuracy of WSS measurements. Though the high-drag regions in the smallest channel make up a slightly larger surface area than the uniform region (~330), its lower aspect ratio was necessary to achieve high WSS variance between channels.

COMSOL simulation results also showed that uniform WSS distribution among four channels were repeatedly achieved with the span ratio of ~15x relative magnitude between the fastest and slowest channels regardless of input flow-rate (Figure 4.7B). Thus, the simulation results indicated that the full *in vivo* shear stress spectrum of 1-60dyn/cm^2 is achievable in as few as two parallel chips with two different input flow-rates of at least ~4x difference, allowing very rapid application and testing of the full physiological spectrum.

Figure 4.7C shows the COMSOL simulation results (eq. 4.1) in comparison to the micro-flow sensor measurements (eq. 4.2) and estimation from the volumetric measurements (eq. 4.3) at an example input flow-rate of 300 μL/min. The comparison revealed that all three values matched within 10% error for the two center channels, indicating the validity of both prediction and measurement methods. The WSS values from the micro-flow sensors showed that the discrepancy becomes larger for the smallest (0.73mm) and largest (3.13mm) channel sizes by 22% and 66% of the simulated values, respectively.

4.6.2 Morphometric Analysis

Image analysis data from optical measurements showed that the bEnd.3 cells did not exhibit any notable change in shape index, a measure of cell elongation, with increases in WSS (Figure 4.8A). It is known that the tested cell line in this study (bEnd.3) holds a characteristic highly-elongated morphology under static conditions [57], and we hypothesize that this trait makes the cell line less susceptible to changes in *SI* than other cell types with a rounder, more "cobble-stone" morphology under static conditions. For example, human aortic endothelial cells with a static *SI* of 0.7 have exhibited a decrease to 0.4 at 12 dyn/cm^2 WSS [64], and bovine aortic endothelial cells with a static *SI* of 0.76 have also shown a decrease to 0.31 at 20 dyn/cm^2 WSS [65], while the utilized bEnd.3 cell line has initially low *SI* of 0.13 or 0.1 (mean) or 0.1 (median) at static condition.

Optical measurement data also showed that the cell lines adjusted their orientation with the flow direction under increasing WSS (Figure 4.8B). The mean orientation angles respectively decreased from 45.3° to 18.1° under the WSS range from 0 (static) to the highest tested at 86 dyn/cm^2, while the overall trend of the mean values formed a linear correlation (R^2 of 0.61), suggesting an increase in cell alignment with increasing WSS. Residual analysis of the linear regression of the orientation angle data (R^2 of 0.05) indicated a right (positive) skew as indicated by the distribution of the residuals (Figure 4.8C) and the normal probability plot (Figure 4.8D). In congruence, the median values were consistently higher than the mean values, resulting in discrete mean and median values in Figure 4.8. Median values also showed a linear decrease along with WSS, ranging from 47.6 to 14.6 for static control and 86 dyn/cm^2, respectively.

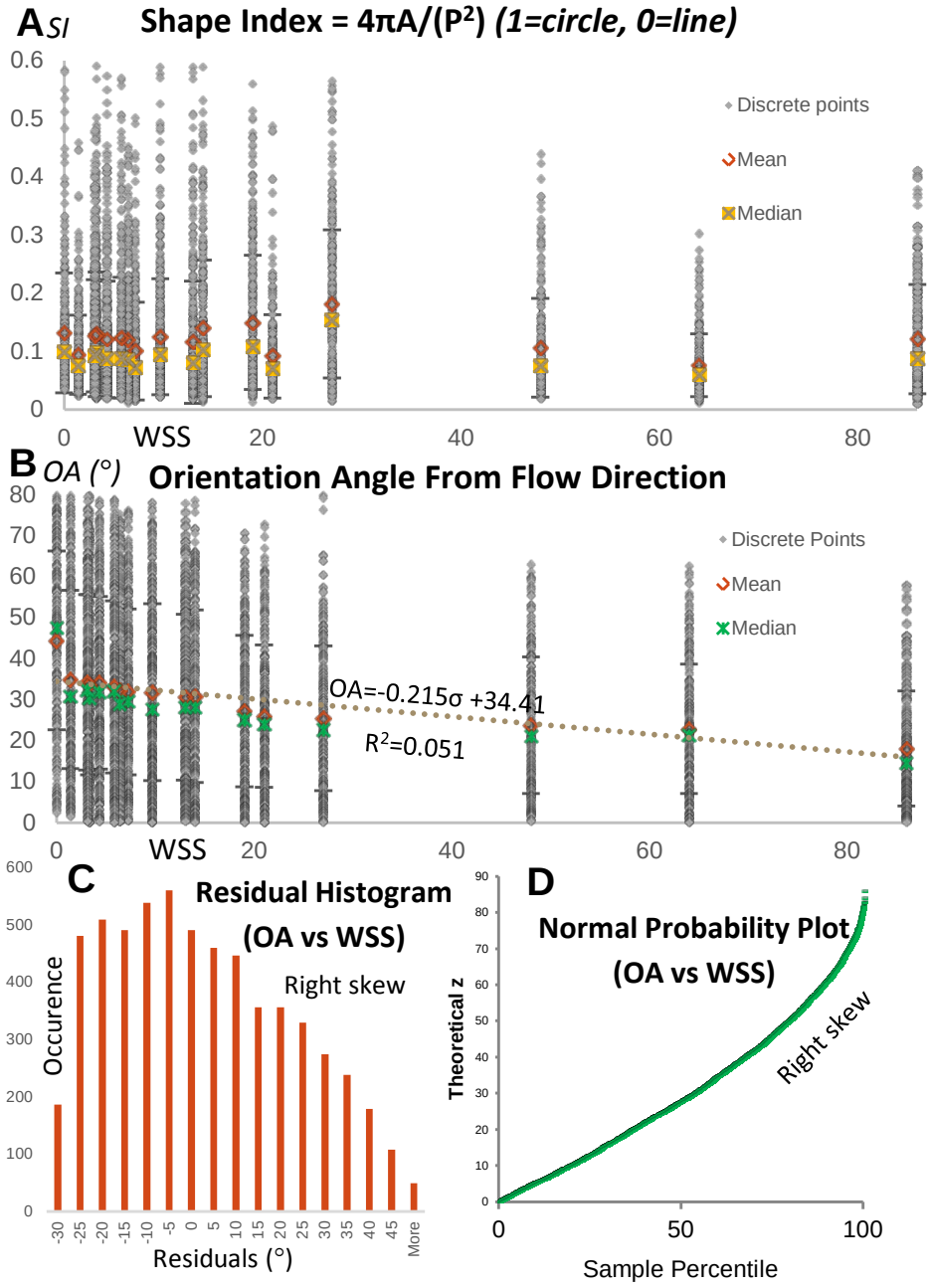

Figure 4.8 Morphometry results. Each data-point represents measurements from an individual cell. Also displayed are mean and median values. (A) bEnd.3 cell shape index measurements with increased WSS. No trend was evident. (B) Linear regression analysis of orientation angle data suggested increased alignment, with an R^2 of 0.051. Orientation angle showed a slight alignment along with WSS. The higher mean values than median values are expected, given the right (positive) skew indicated by the (C) residual histogram and (D) normal probability plot for the orientation angle regression analysis.

4.6.3 Permeability

Experimental measurement results demonstrated that the permeability of chemical compounds decreased with increasing WSS. Figure 4.9 shows the resultant permeability coefficients of fluorescent tracers FITC-Dextran 4kD (Figure 4.9A) and propidium iodide (Figure 4.9B). The permeabilities of FITC-dextran and propidium iodide decreased from averages of $7.4e^{-6}$cm/s and $2.3e^{-5}$cm/s to $4.0e^{-6}$cm/s and $1.9e^{-5}$cm/s, respectively, with increasing WSS from 0.35 to 86 dyn/cm^2. The decreasing rates for the permeability of the fluorescent tracers were $4.06e^{-8}$cm/s and $6.04e^{-8}$cm/s per dyn/cm^2 for FITC-Dextran and PI, respectively. Minimum and maximum average values ranged from $7.4e^{-6}$cm/s and $2.3e^{-5}$cm/s (0.35dyn/cm^2) to $4.0e^{-6}$cm/s and $1.9e^{-5}$cm/s (86dyn/cm^2) for FITC-Dextran 4kD and PI, respectively. A reduction in standard deviation was observed at WSS above 20 dyn/cm^2. Though FITC-Dextran's mean value increased slightly from 64 to 86 dyn/cm^2, the mean values fall within a standard error of each other. For all conditions, the tests were repeated at least 8 times ($n>8$).

Permeability was consistently higher for propidium iodide than for FITC-Dextran. This agrees with the expectation based on the lower molecular weight (668D) than FITC-Dextran (~4kD), making diffusion more rapid. Note that for FITC-Dextran at higher WSS (near 86dyn/cm^2) the increased mean permeability may indicate a slight loss of cell adhesion, but the increase is not significant, and was not observed in the propidium iodide permeability data, nor was a decrease in TEER observed. Potential issues with cell adhesion are cell line-specific, so testing of other cell types with reduced anchorage strength may potentially indicate losses in anchorage with the presence of "pinholes", or missing cells in the monolayer, increasing permeability at higher WSS. The bEnd.3 cell

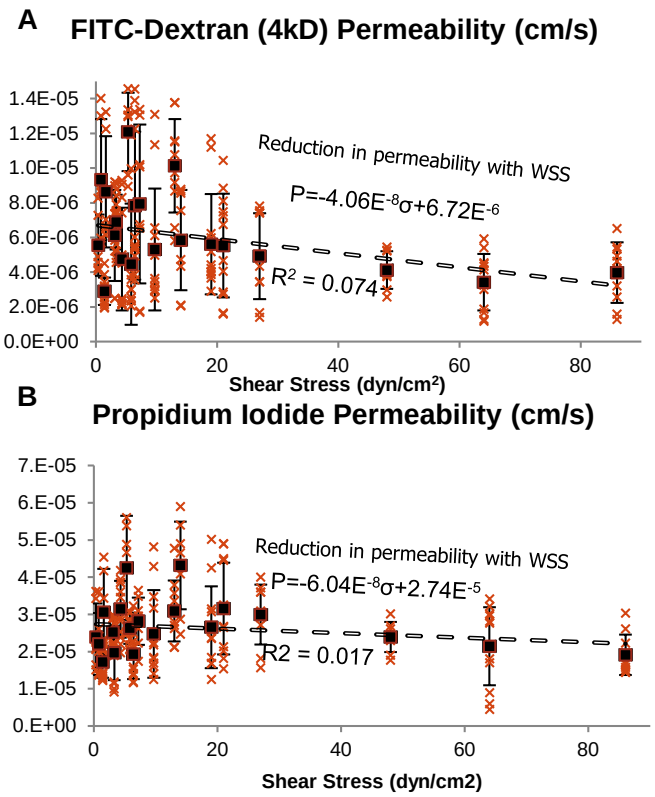

Figure 4.9 Permeability of FITC-conjugated Dextran 4kD (A) and propidium iodide (B) at WSS magnitudes ranging from 0.35-84dyn/cm^2 indicated a decrease in permeability with increasing WSS, at -4.06e-8 and -6.04e-8 unit permeability/unit WSS, respectively. Standard deviation was notably reduced at WSS higher than ~20 dyn/cm^2. All sample replicates n>8.

line was selected for the testing due to their characteristic high surface adherence.

4.6.4 TEER

TEER was measured with the independent electrode sets to evaluate monolayer integrity under varying flow conditions. In correlation with the permeability results in Figure 4.10, the measurement data showed that there was an increase in TEER with increasing WSS at a rate of 0.8Ωcm^2 per dyn/cm^2, ranging from 183Ωcm^2 at near-static 1.4dyn/cm^2 to 230Ωcm^2 at 86dyn/cm^2. As with the previously discussed permeability

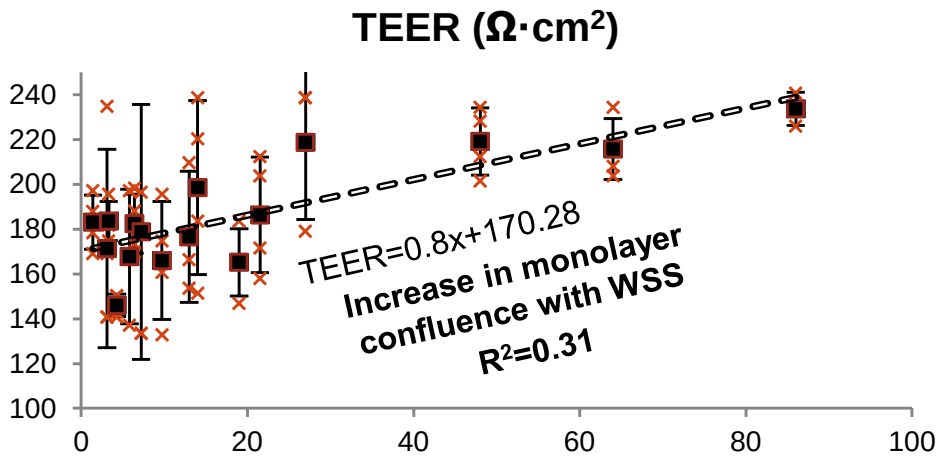

Figure 4.10 TEER measured following high shear stress was increased at about 0.8 unit resistance/unit WSS. These data indicate increased barrier tightness with higher WSS, in correlation with permeability results. All replicate n>3.

results, apparent anchorage losses resulting in reduced TEER was not observed at high WSS.

It is noteworthy to mention that a consensus exists for BBB models that TEER levels must exceed 150Ωcm^2 for reasonably representative permeability data to be obtained [66] in comparison to typical *in vivo* TEER levels (>1000Ωcm^2). The measured TEER values in this paper exceeded 150Ωcm^2 at all tested values of WSS. This also supports the use of the bEnd.3 cell line under the described culture conditions for use in BBB testing studies at high WSS of 60 dyn/cm^2, at the high end of the shear stress seen *in vivo*.

4.6.4 Western Blot Analysis

The protein expression analysis data provided by western blot analysis (Figure 4.11) showed significant increases in expression of both tight junction component ZO-1 and efflux transporter P-gp under three distinct WSS, relative to static control derived from 6-well plates. The protein expression relatively increased ~5x for ZO-1 and ~6x for P-gp at 58 dyn/cm^2 compared to the static condition (0 dyn/cm^2). Notably, a larger relative increase in ZO-1 was observed at 14 dyn/cm^2 (~5x), while P-gp expression increased significantly (~4x) at 4.7dyn/cm^2.

Both proteins are known to influence trans-monolayer properties, such as permeability and TEER; thus the increase in the measured value in protein expression under increasing WSS matches well to the results obtained in aforementioned methods: reduction in permeability and increase in TEER with increases in WSS conditions.

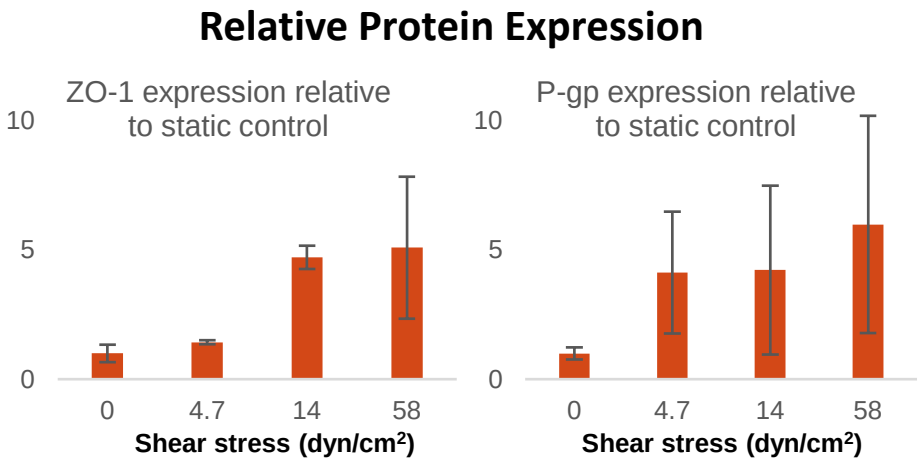

Figure 4.11 Densitometric relative band analysis for western blots from cell lysates of brain endothelial cells grown to confluence and exposed to twenty-four hours of WSS were compared with static controls grown in 6-wells. Results are weighted to β-actin as a gel loading control. Static control was derived from 6-wells plates. These data indicate significant increases in tight junction and efflux transporter expression under WSS at up to an average of ~5x and ~6x for ZO-1 and P-gp, respectively, at 58 dyn/cm^2 WSS. All replicate n>3.

4.7 Conclusions

This paper reported the design, fabrication, and testing results of the microfluidic platform that enables application of the WSS range (1-60dyn/cm^2) of the full physiologically relevant spectrum on vascular endothelial cells (VECs), while allowing multiple physiological, biochemical, and trans-membrane assays in a high throughput manner on a chip. To allow rapid full-spectrum characterization of WSS effects, we developed the four channel microfluidic platform that simultaneously produces shear stresses spanning ~15x in magnitude. Flow distributions were predicted with COMSOL simulation and verified by the direct measurement with a micro-flow sensor array and volume measurement. Multiple assays were performed, including cell morphometry, protein expression, permeability and TEER, on the brain microvascular endothelial cell line bEnd.3.

Morphometric image analysis showed increased alignment with flow direction with increases in WSS. Permeability measurement exhibited decreasing permeability with increasing WSS at rates of 4.06e^{-8} and 6.04e^{-8}cm/s per dyn/cm^2 for FITC-conjugated Dextran and propidium iodide, respectively. TEER measurement data showed an increase with increasing WSS by a rate of 0.8 Ωcm^2 per dyn/cm^2. Finally, the western blot results demonstrated notable increase in expression of a tight junction component ZO-1 and an efflux transporter P-gp by ~500% and 600%, respectively, compared to static controls. These results indicate that the bEnd.3 cell line responds to WSS *in vitro* in a magnitude-dependent manner, providing insights for optimal flow conditions for dynamic VEC culture models.

Based on the results, we also conclude that the presented microfluidic approach

is a valid protocol for rapidly assaying physiological responses to the full spectrum of WSS, as well as elucidating limitations of practical flow conditions, for a particular combination of VEC cell line or primary cell type and culture conditions.

4.8 Acknowledgments

This research was supported by the Utah Science Technology and Research Initiative (USTAR). Microfabrication was performed at the University of Utah Nano Fabrication Facility located in the Sorenson Molecular Biotechnology Building. Western blot and microscopy was performed at the Furgeson Research Group in the Pharmaceutics Department at the University of Utah, with special thanks to Ms. Pilju Youn and Prof. Darin Furgeson.

4.9 References

[1] Bazzoni, G. and E. Dejana. Endothelial cell-to-cell junctions: Molecular organization and role in vascular homeostasis. *Physiological Reviews*. **84**(3):869-901, 2004.

[2] Rajendran, P., T. Rengarajan, J. Thangavel, Y. Nishigaki, D. Sakthisekaran, G. Sethi, and I. Nishigaki. The vascular endothelium and human diseases. *International Journal of Biological Sciences*. **9**(10):1057-1069, 2013.

[3] Michiels, C. Endothelial cell functions. *Journal of cellular physiology*. **196**(3):430-443, 2003.

[4] Rubin, L. L. and J. M. Staddon. The cell biology of the blood-brain barrier. *Annu Rev Neurosci*. **22**(11-28, 1999.

[5] Angiogenesis, M. E. C.-s. and P. Factor. Endothelial receptor tyrosine kinases involved in angiogenesis. *The Journal of cell biology*. **129**(4):895-898, 1995.

[6] Chien, S. Mechanotransduction and endothelial cell homeostasis: The wisdom of the cell. *Am J Physiol Heart Circ Physiol*. **292**(3):H1209-1224, 2007.

[7] Mantovani, A., F. Bussolino, and E. Dejana. Cytokine regulation of endothelial cell function. *The FASEB journal*. **6**(8):2591-2599, 1992.

[8] Pearson, J. D. Endothelial cell function and thrombosis. *Best Practice & Research Clinical Haematology*. **12**(3):329-341, 1999.

[9] Gasic, G. J. Role of plasma, platelets, and endothelial cells in tumor metastasis. *Cancer and Metastasis Reviews*. **3**(2):99-114, 1984.

[10] Miniño, A. M. and S. L. Murphy. Death in the united states, 2010. *NCHS data brief*. **99**(10):1-8, 2012.

[11] Moss, M. A., S. Zimmer, and K. W. Anderson. Role of metastatic potential in the adhesion of human breast cancer cells to endothelial monolayers. *Anticancer research*. **20**(3A):1425-1433, 2000.

[12] Quyyumi, A. A. Endothelial function in health and disease: New insights into the genesis of cardiovascular disease. *The American journal of medicine*. **105**(1):32S-39S, 1998.

[13] Tzima, E., M. Irani-Tehrani, W. B. Kiosses, E. Dejana, D. A. Schultz, B. Engelhardt, G. Cao, H. DeLisser, and M. A. Schwartz. A mechanosensory complex that mediates the endothelial cell response to fluid shear stress. *Nature*. **437**(7057):426-431, 2005.

[14] Chien, S., S. Li, and Y. J. Shyy. Effects of mechanical forces on signal transduction and gene expression in endothelial cells. *Hypertension*. **31**(1 Pt 2):162-169, 1998.

[15] Chien, S. Molecular basis of rheological modulation of endothelial functions: Importance of stress direction. *Biorheology*. **43**(2):95-116, 2006.

[16] Acevedo, A. D., S. S. Bowser, M. E. Gerritsen, and R. Bizios. Morphological and proliferative responses of endothelial cells to hydrostatic pressure: Role of fibroblast growth factor. *J Cell Physiol*. **157**(3):603-614, 1993.

[17] Dimmeler, S., J. Haendeler, V. Rippmann, M. Nehls, and A. M. Zeiher. Shear stress inhibits apoptosis of human endothelial cells. *FEBS letters*. **399**(1):71-74, 1996.

[18] Wu, C. C., Y. S. Li, J. H. Haga, R. Kaunas, J. J. Chiu, F. C. Su, S. Usami, and S. Chien. Directional shear flow and rho activation prevent the endothelial cell apoptosis induced by micropatterned anisotropic geometry. *Proc Natl Acad Sci U S A*. **104**(4):1254-1259, 2007.

[19] Siddharthan, V., Y. V. Kim, S. Liu, and K. S. Kim. Human astrocytes/astrocyte-conditioned medium and shear stress enhance the barrier properties of human

brain microvascular endothelial cells. *Brain Res*. **1147**(39-50, 2007.

[20] Thoumine, O., R. M. Nerem, and F. R. Girard. Oscillatory shear stress and hydrostatic pressure modulate cell-matrix attachment proteins in cultured endothelial cells. *In Vitro Cellular & Developmental Biology-Animal*. **31**(1):45-54, 1995.

[21] Cucullo, L., M. Hossain, V. Puvenna, N. Marchi, and D. Janigro. The role of shear stress in blood-brain barrier endothelial physiology. *BMC Neurosci*. **12**(40, 2011.

[22] Urbich, C., D. H. Walter, A. M. Zeiher, and S. Dimmeler. Laminar shear stress upregulates integrin expression: Role in endothelial cell adhesion and apoptosis. *Circ Res*. **87**(8):683-689, 2000.

[23] Galbraith, C. G., R. Skalak, and S. Chien. Shear stress induces spatial reorganization of the endothelial cell cytoskeleton. *Cell Motil Cytoskeleton*. **40**(4):317-330, 1998.

[24] Song, J. W., W. Gu, N. Futai, K. A. Warner, J. E. Nor, and S. Takayama. Computer-controlled microcirculatory support system for endothelial cell culture and shearing. *Anal Chem*. **77**(13):3993-3999, 2005.

[25] Nakadate, H., H. Minamitani, and S. Aomura. Combinations of hydrostatic pressure and shear stress influence morphology and adhesion molecules in cultured endothelial cells. *Conf Proc IEEE Eng Med Biol Soc*. **2010**(3812-3815, 2010.

[26] van der Meer, A. D., A. A. Poot, J. Feijen, and I. Vermes. Analyzing shear stress-induced alignment of actin filaments in endothelial cells with a microfluidic assay. *Biomicrofluidics*. **4**(1):11103, 2010.

[27] Braddon, L. G., D. Karoyli, D. G. Harrison, and R. M. Nerem. Maintenance of a functional endothelial cell monolayer on a fibroblast/polymer substrate under physiologically relevant shear stress conditions. *Tissue Eng*. **8**(4):695-708, 2002.

[28] Chien, S. Effects of disturbed flow on endothelial cells. *Ann Biomed Eng*. **36**(4):554-562, 2008.

[29] Poredoš, P. State-of-the-art review: Endothelial dysfunction in the pathogenesis of atherosclerosis. *Clinical and Applied Thrombosis/Hemostasis*. **7**(4):276-280, 2001.

[30] Malek, A. M., S. L. Alper, and S. Izumo. Hemodynamic shear stress and its role in atherosclerosis. *JAMA: the journal of the American Medical Association*. **282**(21):2035-2042, 1999.

[31] Reneman, R. S., T. Arts, and A. P. G. Hoeks. Wall shear stress – an important determinant of endothelial cell function and structure – in the arterial system in vivo. *Journal of Vascular Research*. **43**(3):251-269, 2006.

[32] Dolan, J., J. Kolega, and H. Meng. High wall shear stress and spatial gradients in vascular pathology: A review. *Annals of Biomedical Engineering*. **41**(7):1411-1427, 2013.

[33] Loscalzo, J. and A. I. Schafer, *Thrombosis and hemorrhage*. 2003: Lippincott Williams & Wilkins.

[34] Koutsiaris, A. G., S. V. Tachmitzi, N. Batis, M. G. Kotoula, C. H. Karabatsas, E. Tsironi, and D. Z. Chatzoulis. Volume flow and wall shear stress quantification in the human conjunctival capillaries and post-capillary venules in vivo. *Biorheology*. **44**(5-6):375-386, 2007.

[35] Young, E. W. and C. A. Simmons. Macro- and microscale fluid flow systems for endothelial cell biology. *Lab Chip*. **10**(2):143-160, 2010.

[36] Chen, H., J. Cornwell, H. Zhang, T. A. Lim, R. Resurreccion, T. Port, G. Rosengarten, and R. Nordon. Cardiac-like flow generator for long-term imaging of endothelial cell responses to circulatory pulsatile flow at microscale. *Lab Chip*. 2013.

[37] Young, E. W., A. R. Wheeler, and C. A. Simmons. Matrix-dependent adhesion of vascular and valvular endothelial cells in microfluidic channels. *Lab Chip*. **7**(12):1759-1766, 2007.

[38] Hsu, S., R. Thakar, D. Liepmann, and S. Li. Effects of shear stress on endothelial cell haptotaxis on micropatterned surfaces. *Biochem Biophys Res Commun*. **337**(1):401-409, 2005.

[39] Shao, J., L. Wu, J. Wu, Y. Zheng, H. Zhao, Q. Jin, and J. Zhao. Integrated microfluidic chip for endothelial cells culture and analysis exposed to a pulsatile and oscillatory shear stress. *Lab Chip*. **9**(21):3118-3125, 2009.

[40] Estrada, R., G. A. Giridharan, M. D. Nguyen, T. J. Roussel, M. Shakeri, V. Parichehreh, S. D. Prabhu, and P. Sethu. Endothelial cell culture model for replication of physiological profiles of pressure, flow, stretch, and shear stress in vitro. *Anal Chem*. **83**(8):3170-3177, 2011.

[41] Booth, R. and H. Kim. Characterization of a microfluidic in vitro model of the blood-brain barrier (μbbb). *Lab on a Chip*. **12**(10):1784-1792, 2012.

[42] Dangaria, J. H. and P. J. Butler. Macrorheology and adaptive microrheology of endothelial cells subjected to fluid shear stress. *Am J Physiol Cell Physiol*. **293**(5):C1568-1575, 2007.

[43] Fernandez, P., C. Bourget, R. Bareille, R. Daculsi, and L. Bordenave. Gene response in endothelial cells cultured on engineered surfaces is regulated by shear stress. *Tissue Eng*. **13**(7):1607-1614, 2007.

[44] Thoumine, O., R. M. Nerem, and P. R. Girard. Oscillatory shear stress and hydrostatic pressure modulate cell-matrix attachment proteins in cultured endothelial cells. *In Vitro Cell Dev Biol Anim*. **31**(1):45-54, 1995.

[45] Miao, H., Y. L. Hu, Y. T. Shiu, S. Yuan, Y. Zhao, R. Kaunas, Y. Wang, G. Jin, S. Usami, and S. Chien. Effects of flow patterns on the localization and expression of ve-cadherin at vascular endothelial cell junctions: In vivo and in vitro investigations. *J Vasc Res*. **42**(1):77-89, 2005.

[46] Chueh, B.-h., D. Huh, C. R. Kyrtsos, T. Houssin, N. Futai, and S. Takayama. Leakage-free bonding of porous membranes into layered microfluidic array systems. *Analytical chemistry*. **79**(9):3504-3508, 2007.

[47] Noris, M., M. Morigi, R. Donadelli, S. Aiello, M. Foppolo, M. Todeschini, S. Orisio, G. Remuzzi, and A. Remuzzi. Nitric oxide synthesis by cultured endothelial cells is modulated by flow conditions. *Circulation research*. **76**(4):536-543, 1995.

[48] Seebach, J., P. Dieterich, F. Luo, H. Schillers, D. Vestweber, H. Oberleithner, H. J. Galla, and H. J. Schnittler. Endothelial barrier function under laminar fluid shear stress. *Lab Invest*. **80**(12):1819-1831, 2000.

[49] Colgan, O. C., G. Ferguson, N. T. Collins, R. P. Murphy, G. Meade, P. A. Cahill, and P. M. Cummins. Regulation of bovine brain microvascular endothelial tight junction assembly and barrier function by laminar shear stress. *Am J Physiol Heart Circ Physiol*. **292**(6):H3190-3197, 2007.

[50] Rossi, M., R. Lindken, B. P. Hierck, and J. Westerweel. Tapered microfluidic chip for the study of biochemical and mechanical response at subcellular level of endothelial cells to shear flow. *Lab Chip*. **9**(10):1403-1411, 2009.

[51] Wang, J., J. Heo, and S. Z. Hua. Spatially resolved shear distribution in microfluidic chip for studying force transduction mechanisms in cells. *Lab Chip*. **10**(2):235-239, 2010.

[52] Wang, L., Z. L. Zhang, J. Wdzieczak-Bakala, D. W. Pang, J. Liu, and Y. Chen. Patterning cells and shear flow conditions: Convenient observation of endothelial cell remoulding, enhanced production of angiogenesis factors and drug response. *Lab Chip*. **11**(24):4235-4240, 2011.

[53] Desai, S. Y., M. Marroni, L. Cucullo, L. Krizanac-Bengez, M. R. Mayberg, M. T. Hossain, G. G. Grant, and D. Janigro. Mechanisms of endothelial survival under shear stress. *Endothelium*. **9**(2):89-102, 2002.

[54] Aran, K., L. A. Sasso, N. Kamdar, and J. D. Zahn. Irreversible, direct bonding of nanoporous polymer membranes to pdms or glass microdevices. *Lab Chip*. **10**(5):548-552, 2010.

[55] Chueh, B. H., D. Huh, C. R. Kyrtsos, T. Houssin, N. Futai, and S. Takayama. Leakage-free bonding of porous membranes into layered microfluidic array systems. *Anal Chem*. **79**(9):3504-3508, 2007.

[56] Kuo, J. T., L.-Y. Chang, P.-Y. Li, T. Hoang, and E. Meng. A microfluidic platform with integrated flow sensing for focal chemical stimulation of cells and tissue. *Sensors and Actuators B: Chemical*. **152**(2):267-276, 2011.

[57] Omidi, Y., L. Campbell, J. Barar, D. Connell, S. Akhtar, and M. Gumbleton. Evaluation of the immortalised mouse brain capillary endothelial cell line, b.End3, as an in vitro blood-brain barrier model for drug uptake and transport studies. *Brain Res*. **990**(1-2):95-112, 2003.

[58] White, F. M., *Fluid mechanics*. 4 ed. 1999: McGraw-Hill International.

[59] Papautsky, I., B. K. Gale, S. Mohanty, T. A. Ameel, and A. B. Frazier. Effects of rectangular microchannel aspect ratio on laminar friction constant. *Proceedings of SPIE-The International Society for Optical Engineering, Proceedings of the 1999 Microfluidic Devices and Systems II, Santa Clara*. **3877**(147-158, 1999.

[60] Gervais, T., J. El-Ali, A. Gunther, and K. F. Jensen. Flow-induced deformation of shallow microfluidic channels. *Lab Chip*. **6**(4):500-507, 2006.

[61] Yuan, W., G. Li, E. S. Gil, T. L. Lowe, and B. M. Fu. Effect of surface charge of immortalized mouse cerebral endothelial cell monolayer on transport of charged solutes. *Ann Biomed Eng*. **38**(4):1463-1472, 2010.

[62] Pardridge, W. M., D. Triguero, J. Yang, and P. A. Cancilla. Comparison of in vitro and in vivo models of drug transcytosis through the blood-brain barrier. *J Pharmacol Exp Ther*. **253**(2):884-891, 1990.

[63] Li, G., M. J. Simon, L. M. Cancel, Z. D. Shi, X. Ji, J. M. Tarbell, B. Morrison, 3rd, and B. M. Fu. Permeability of endothelial and astrocyte cocultures: In vitro blood-brain barrier models for drug delivery studies. *Ann Biomed Eng*. **38**(8):2499-2511, 2010.

[64] Nakadate, H., H. Minamitani, and S. Aomura. *Combinations of hydrostatic pressure and shear stress influence morphology and adhesion molecules in cultured endothelial cells*. in *Engineering in Medicine and Biology Society (EMBC), 2010 Annual International Conference of the IEEE*. 2010: IEEE.

[65] Gray, B. L., D. K. Lieu, S. D. Collins, R. L. Smith, and A. I. Barakat.

Microchannel platform for the study of endothelial cell shape and function. *Biomedical Microdevices*. **4**(1):9-16, 2002.

[66] Vastag, M. and G. M. Keseru. Current in vitro and in silico models of blood-brain barrier penetration: A practical view. *Curr Opin Drug Discov Devel*. **12**(1):115-124, 2009.

CHAPTER 5

PERMEABILITY ANALYSIS OF NEUROACTIVE DRUGS THROUGH A DYNAMIC MICROFLUIDIC *IN VITRO* BLOOD-BRAIN BARRIER MODEL[3]

5.1 Abstract

This paper presents the permeability analysis of neuroactive drugs and correlation with *in vivo* brain/plasma ratios in a dynamic microfluidic blood-brain barrier (BBB) model. Permeability of seven neuroactive drugs (Ethosuximide, Gabapentin, Sertraline, Sunitinib, Traxoprodil, Varenicline, PF-304014) and trans-endothelial electrical resistance (TEER) were quantified in both dynamic (microfluidic) and static (transwell) BBB models, either with brain endothelial cells (bEnd.3) in monoculture, or in co-culture with glial cells (C6). Dynamic cultures were exposed to 15dyn/cm^2 shear stress to mimic the *in vivo* environment. Dynamic models resulted in significantly higher average TEER (respective 5.9-fold and 8.9-fold increase for co-culture and monoculture models) and lower drug permeabilities (average respective decrease of 0.050 and 0.052 log(cm/s) for co-culture and monoculture) than static models; and co-culture models demonstrated higher average TEER (respective 90% and 25% increase for static and dynamic models) and lower drug permeability (average respective decrease of 0.063 and 0.061 log(cm/s)

[3] Reproduced by permission of Springer Publishing. Annals of Biomedical Engineering, 2014. Ahead of print. DOI 10.1007/s10439-014-1086-5

for static and dynamic models) than monoculture models. Correlation of the resultant logP_e values (ranging from -4.06 to -3.63 log(cm/s)) with *in vivo* brain/plasma ratios (ranging from 0.42 to 26.8) showed highly linear correlation (R^2>0.85) for all model conditions, indicating the feasibility of the dynamic microfluidic BBB model for prediction of BBB clearance of pharmaceuticals.

5.2 Introduction

Despite increasing demands for new treatments of disorders of the central nervous system (CNS) such as Alzheimer's Disease (AD) [1], CNS drug research progress has been significantly hindered by the prohibitive barrier from capillaries to brain tissue, the blood-brain barrier (BBB). Recent studies reported that AD was diagnosed in 1/3rd of senior deaths in the US [2], while a new case of AD is developed every 67 seconds [3]. However, the clinical success rates for new CNS compounds (7%) remain lower than other healthcare areas such as cardiovascular disease (20%) [4], while the average cost to develop a drug exceeded $1 billion [5]. Such low success rates have been attributed partially to limited prediction capability in preclinical models to assess the passage of drugs across the BBB [6]. The BBB, mainly comprised of the capillary's brain endothelial cells, is the key barrier restricting perfusion of nearly 100% of large (>500 Da) molecules and 98% of small molecules [7], complicating determination of effective dose concentrations of drugs targeting the CNS.

To potentially accelerate the development of new CNS-targeting pharmaceuticals, the high-throughput evaluation of trans-BBB properties can be achieved by developing massively-parallel, low-cost predictive models of BBB clearance [8] either *in vivo* or *in*

vitro. The BBB preclinical models allow the discovery of rejected compounds earlier and enable the reduction of attrition rates in clinical trials [9]. They are capable of predicting whether a compound's interaction with the BBB will compromise its functionality or whether it reaches the CNS in significant amounts to have a pharmacodynamic effect [10]. *In vivo* models provide similarly complex environments to human physiological conditions; however, they are subject to high cost, time, and ethical constraints. *In vitro* models, within the scope of cellular physiology, resolve such issues and enable feasible isolation and observation of individual physiological mechanisms in repeatable and controllable manners, resultantly emerging as a promising alternative or augmenting model for early drug screening (Figure 5.1A).

In vitro BBB models recently incorporated dynamic flows, replicating more realistic *in vivo* conditions for higher prediction capability. The flow-based dynamic *in vitro* BBB models have exploited the mechanotransductive response of endothelial cells to wall shear stress (WSS) and its effect on BBB functions [11-14]. For example, the authors' previous dynamic models reported higher trans-endothelial electrical resistance (TEER) and lower permeability in comparison to traditional transwell-based *in vitro* models, better representing the cerebromicrovascular environment [15,16] found *in vivo*.

Despite these advantages, dynamic *in vitro* models have not been widely accepted for BBB permeability screening in the pharmaceutical industry yet. Acceptance of *in vitro* models first requires a standard for translation of model results to the *in vivo* condition [17], in terms of its predictive ability of permeability to new compounds. Currently, none of the existing dynamic *in vitro* BBB models utilizing microfluidics [15,18-20] or hollow fibers [14,21] have been assessed for a large number (>2) of CNS drugs to elucidate a

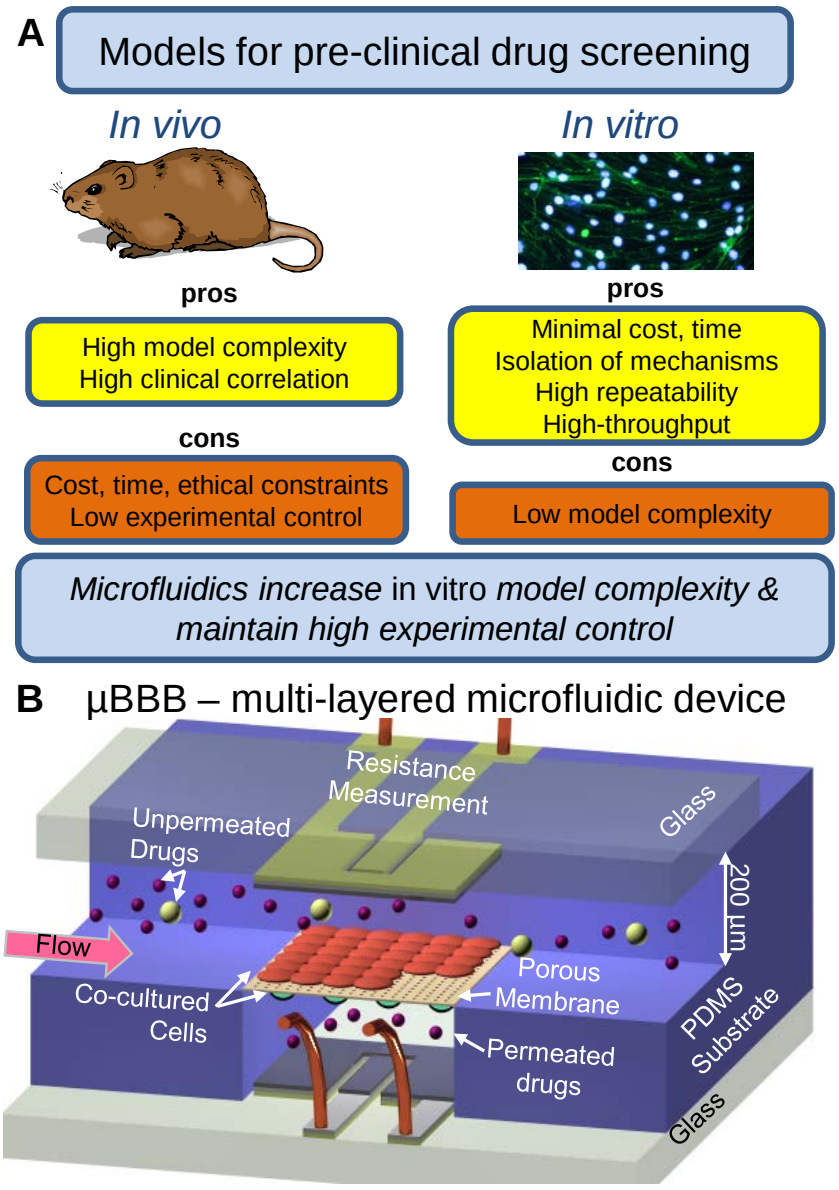

Figure 5.1 Microfluidic blood-brain barrier models. (A) The preclinical drug screening process would benefit from more innovative *in vitro* models. Though *in vitro* models are advantageous due to their low cost, time and ethical constraints, high experimental control over isolation of individual mechanisms, and allow a more repeatable and high-throughput approach, they lack the complexity of the *in vivo* environment. Microfluidic *in vitro* models allow higher model complexity by introducing a dynamic environment, while maintaining experimental control. (B) The illustration of the previously developed dynamic µBBB system that recreates the micro-cerebrovascular environment with dynamic flows and co-culture of endothelial and glial cells. Also included in the system is two sets of resistance-measuring AgCl electrodes. Graphic modified from previously published graphic [15].

translational standard for permeability. The successful assessment of permeability to multiple CNS drugs would establish quantitative correlation with *in vivo* permeability, and demonstrate the high-throughput potential for such a dynamic model.

We previously developed a dynamic *in vitro* microfluidic BBB model (μBBB, Figure 5.1B), and characterized the effects of chemical/pH modulation [15] and WSS [16] on BBB functions, such as cell morphology, fluorescent tracer permeability, TEER measurement by integrated electrodes, and BBB protein expression [16]. To establish quantitative correlation with *in vivo* permeability, this paper reports the permeability measurement of seven CNS drugs (Ethosuximide, Gabapentin, Sertraline Hydrochloride, Sunitinib Malate, Traxoprodil Mesylate, Varenicline Tartrate, PF-3084014) across the dynamic μBBB model as well as static *in vitro* transwell platforms prepared with both mono- and co-cultured BBB layers (endothelial and glial cells). Due to the abundance of evidence that drugs of small molecular weights (<500Da) better cross the BBB, the selected drugs were limited to similarly small molecular weight drugs. Then, to ensure inclusion of a diverse sample set, the selection preferences were given to drugs that cover a wide range of hydrophilicity (between -1.27 and 5.15 $\log P_{o/w}$), which generally dictates the compound's ability to cross the plasma membrane, and have a wide range of relevant clinical applications including treatments for depression, epilepsy, pain, nicotine addiction, and tumors. Additionally, concentration-dependent cytotoxicity on brain endothelial cells for each drug was analyzed. For quality control of prepared cultures, TEER was monitored before and after each permeability test to remove outliers and define cell contiguity. Finally, permeability coefficients were correlated to brain/plasma ratios from previous studies of each drug.

5.3 Structure and Fabrication of the Microfluidic BBB Model

The previously developed dynamic *in vitro* microfluidic BBB model has been utilized due to proven validation on TEER and permeability properties [15]. The microfluidic structure of the μBBB system (Figure 5.2A) comprised multiple layers of polydimethylsiloxane (PDMS) and glass substrates to form two crossing channels (4mm). At the junction of the crossing channels in different layers, a free-standing porous polycarbonate (PC) membrane [22] was embedded allowing the diffusion path from the top to the bottom fluidic channels. The PC membrane also provided the co-culture surface for both endothelial and glial cells, enabling the permeability testing through the co-cultured BBB cell layers. On both sides of the co-culture membrane, two sets of thin-film electrodes were microfabricated by depositing and patterning AgCl layers on a glass substrate. The distance from the membrane to each electrode, equivalent to the channel height, was only 200μm, allowing high-accuracy TEER measurement. Each channel layer was connected to separate pairs of fluidic inlets and outlets for individual permeability analysis.

Fabrication of the BBB model was similar to the processes described previously [15,16], with some modifications. First, top and bottom glass substrates were sputtered with layers of Cr/Au/Ag (20/80/800nm) that were patterned utilizing a lift-off process, forming TEER electrodes. Then the Ag surface was chlorinated chemically by dipping the substrate into 30mM $FeCl_3$ for 50s to form an oxidized surface of AgCl, which is non-toxic with high long-term stability [23]. Second, following 30s O_2 plasma oxidation at 125W glass substrates were pressed into uncured PDMS prepolymer (10:1 elastomer:curing agent ratio), which was then cured on a 110º hot-plate for thirty minutes.

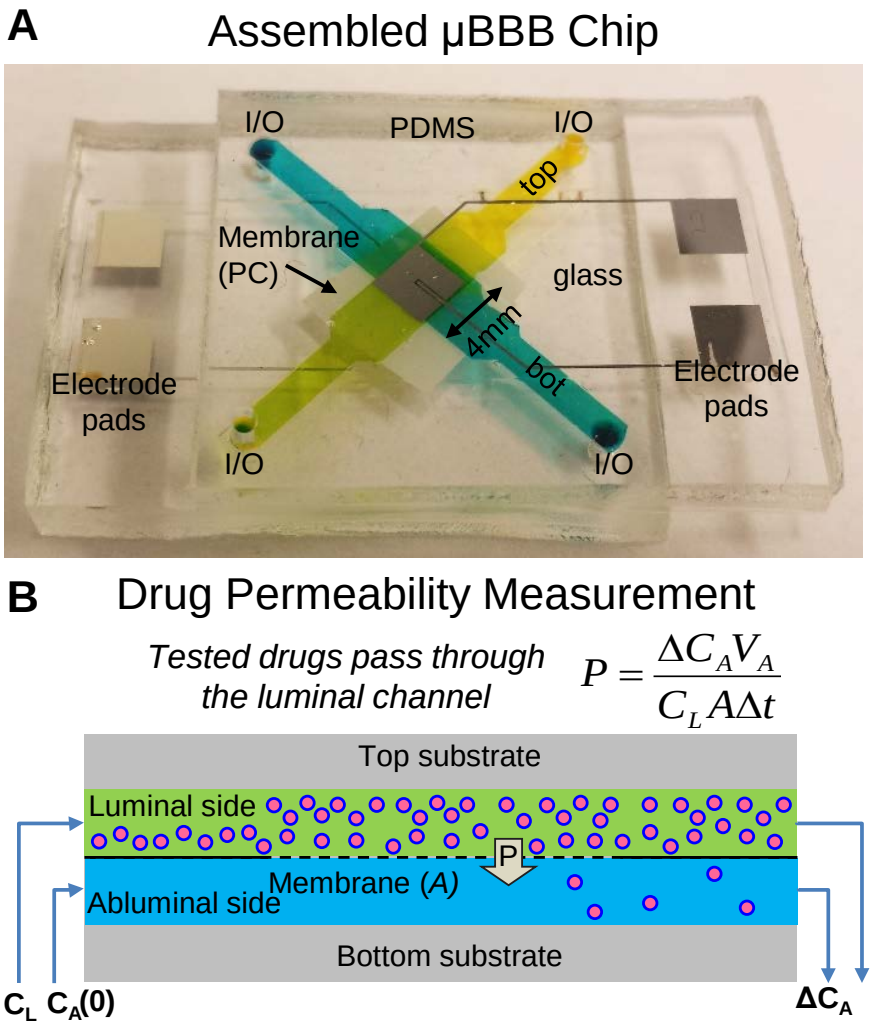

Figure 5.2: Microfluidic blood-brain barrier chip for permeability assays. (A) Multilayered channel structure made from patterned PDMS substrate with embedded glass electrode layers. Luminal (top, yellow) and abluminal (bottom, blue) channels are both 4mm wide and are seeded with bend.3 endothelial cells and C6 astrocytes, respectively, on either side of the free-standing PC membrane. Electrodes allow non-invasive TEER measurement. (B) To test permeability through the μBBB system, the drug is run of constant concentration C_L is run through the luminal channel for time Δt, and permeability is computed from the measured abluminal concentration ΔC_A in sample volume V_A, and the area A.

The replica mold was constructed on a Si substrate by lithographically patterning SU-8 2075 into defining top and bottom microchannel structures. For effective bonding, top and bottom PDMS channel layers (with embedded glass layers) and PC membrane were plasma oxidized for thirty seconds, and the PC membrane was treated for thirty minutes with 5% 3-aminopropyltriethoxysilane (APTES) on a hotplate set to 80°C [24]. Third, all three substrates were pressed together at room temperature, sandwiching the PC membrane in an irreversible bond. The APTES-based bonding method minimized occurrences of leaks compared with the PDMS pre-polymer "mortar" method [22].

5.4 Materials and Cell Culture

5.4.1 CNS-Targeting Compounds

Seven brain-targeting commercially-available drugs were utilized for permeability screening of the *in vitro* BBB models. The seven drugs were provided by the Compound Transfer Program (CTP) by Pfizer Inc., including Varenicline (PF-3430574), Gabapentin (PF-345043), Traxoprodil (PF-1486212), Sertraline (PF-579897), Ethosuximide (PF-344988), Sunitinib (PF-262192), and an unnamed compound (PF-3084014). The compounds have been proven to cross the *in vivo* BBB to some extent, and represent a wide range of applications, including treatment of pain, depression, seizures, nicotine addiction, and tumor suppression (Table 5.1). The compounds held small and comparable molecular weights between 141.17 and 489.65 Da, within the typically known size ranges (<500Da) for efficient diffusion through BBB, and ranged widely in hydrophobicity from -1.27 to 5.15 $\log P_{o/w}$. The compounds were provided in pure powder substances and were reconstituted in dimethylsiloxane (DMSO), ethanol,

Table 5.1: Compounds tested in this study. logP values are for the octanol/water partition coefficient $P_{o/w}$. B/P is the measured *in vivo* brain/plasma ratios derived from the cited sources [25-30].

	Name (Salt)	**MW**(Da) **(Salt)**	**logP**	**Action**	**B/P Ratio**	**Purpose**
PF-345043	Gabapentin	171.24	-1.27	GABA analog	0.75 [25]	Anti-convulsant
PF-1486212	Traxoprodil (Mesylate)	327.43 (423.53)	2.06	NDMA receptor antagonist	2.1 [26]	Analgesic
PF-579897	Sertraline (Hydrochloride)	(306.23) (342.70)	5.15	Selective serotonin re-uptake inhibitor	26.8 [27]	Anti-depressant
PF-3430574	Varenicline (Tartrate)	211.27 (361.37)	1.01	Nicotinic receptor partial agonist	3.24 [28]	Nicotine Substitute
PF-3084014	Unnamed	489.65	4.01	γ-secretase inhibitor	1 [29]	Anti-tumor
PF-344988	Ethosuximide	141.17	0.55	Succinimide	1.1 [27]	Anti-convulsant
PF-262192	Sunitinib (Malate)	398.48 (532.58)	2.93	RTK inhibitor	0.42 [30]	Anti-tumor

or methanol below the maximum solubility. The reconstituted solutions were kept at -20°C away from direct light to prepare stock solutions.

5.4.2 Cell Culture

Two immortalized cell lines were utilized for this permeability study, which have been widely accepted for BBB co-culture models, including the brain endothelial cell line bEnd.3 [31-33], and the glial cell line C6 [34,35], each of which was respectively derived from a mouse and a rat and was obtained from the ATCC. Both the cell lines were cultivated in DMEM/F12 media (Lonza) supplemented with 10% fetal bovine serum (Hyclone), with 1% Penicillin/Streptomycin and Amphotericin B (EMD) for contamination control. Media was buffered to 7.35 in all cases, and the cells for seeding experiments were taken from recently confluent subcultures only.

The cultivated cells were seeded in 6-well transwells in both the mono-culture and co-culture, serving as static control for comparison to dynamic experiments with the μBBB chips. For high adhesion cell seeding, both the transwells and the μBBB chips were coated overnight with poly-lysine (100 μg/mL) and Collagen IV/ Fibronectin (100 μg/mL each), respectively, to facilitate attachment of C6 and bEnd.3 cells. C6 astrocytes were seeded first on the underside of the membrane in both models at a density of $6x10^4$ cells/cm^2. After two days, bEnd.3 cells were seeded on the top surface of the membrane at the same density. The seeded cells reached stable confluence on day 6 for co-culture and day 4 for mono-culture, when permeability experiments were performed.

Primary brain endothelial cells were extracted from Sprague-Dawley rats for morphological comparisons to bEnd.3 cells [36]. Rats were euthanized with CO_2, and forebrains were removed, diced, and digested in 1mg/mL collagenase II and 15μg/mL DNAse I in DMEM with 50μg/mL gentamycin for 1.5h at 37°C under 250RPM rotation. Following centrifugation in 20% BSA for twenty minutes at 1000g, the re-suspended pellet was again digested in 1mg/mL collagenase-dispase and 6.7 μg/mL DNAse I in DMEM for one hour at 37°C under 200RPM rotation. Following the 2nd centrifugation for twenty minutes at 1000g, the further digested cells were separated on a 33% Percoll gradient and centrifuged a 3rd time for ten minutes at 1000g. Finally, isolated brain endothelial cells were plated for two days in DMEM supplemented with 10% plasma-derived serum, 1.5ng/mL bFGF, 5μg/mL insulin, 5μg/mL transferrin, 5ng/mL sodium selenite, 50μg/mL gentamycin, and 4μg/mL puromycin. 500nM hydrocortisone was added on day 1 to improve the tightness of the cell-cell junctions; and puromycin, added initially to selectively kill non-endothelial cells, was removed on day 3; and cells were

imaged on day 5. All supplements were obtained from Sigma-Aldrich.

5.5 Testing Methodology

5.5.1 Fluorescent Imaging of Endothelial Cell Morphology

To compare morphological properties of the bEnd.3 cell line to primary brain endothelial cells, the presence of tight junctions were visualized through immunostaining of ZO-1 expression, and all cell images were obtained in the models without electrodes. Following rinsing with phosphate buffered saline (PBS), confluent cells were fixed with 4% paraformaldehyde (Avantor) for 10min at room temperature. Cell membranes were permeabilized with 0.1% Triton X-100 in PBS for 10min and blocked with 5% goat serum in permeabilization buffer for one hour. Cultures were incubated with primary mouse anti-ZO-1 antibody (Santa Cruz) overnight at 4°C, then incubated with secondary Alexa-fluor goat anti-mouse antibody (Invitrogen) for one hour at room temperature. Following counterstaining with 1μg/ml 4',6-diamidino-2-phenylindole (DAPI, Enzo), the cells were imaged with a Nikon microscope.

5.5.2 Dynamic Flow Experiments

The μBBB chips were prepared for permeability experiments under fluid flow in a similar process to that previously described [15,16]. The fabricated μBBB chips were sterilized with 70% EtOH, and connected to a 205S cartridge pump (Watson-Marlow) via gas-permeable marprene tubing, and the entire setup, including the pump, chips, and media reservoirs, was placed in a humid incubator (37°C, 5% CO_2). Cells were seeded as described in the previous section. Chips were perfused at ~10μL/min until day 2 after

bEnd.3 seeding, and flow on the luminal side was increased to 2 mL/min, providing a level of WSS relevant to the BBB (3-20dyn/cm^2) [37]. WSS (τ_A) applied to the endothelial cells was ~15dyn/cm^2 according to the equation for WSS in a rectangular channel

$$\tau_A = \frac{6Q\mu}{h^2 w} \tag{5.1}$$

where Q is flow, μ is dynamic viscosity of the media (0.012 dyn·s/cm^2), and h and w are the channel height and width, respectively. The high aspect ratio (20:1) of the channel ensures that most of the cells experience a uniform WSS, except the high-drag regions near the side-walls [16].

5.5.3 Cytotoxicity Testing

To evaluate cytotoxicity levels of each drug and to establish permeability assay concentration limit, lactate dehydrogenase (LDH) assay (Pierce) was performed on bEnd.3 cells following exposure to various concentrations of each drug for twenty-four hours. Cells that undergo apoptosis release LDH in proportion to the level of toxicity, and the LDH assay reaction produces red formazan that can be measured via absorbance readings. To accurately quantify cytotoxicity, confluent cultures of bEnd.3 cells with a constant cell seeding number (9000/well) were respectively exposed to 1, 10, 100, and 1000 μM drug concentrations in DMEM/F12 media with controlled pH of 7.35 for twenty-four hours in a 98-well plate. Negative controls (untreated) and positive controls (lysis buffer) were added to each plate to establish a basepoint and maximum levels for LDH release, respectively. Following the LDH assay, absorbance values were recorded at wavelengths of 490nm and 680nm. LDH activity was derived from these measurements

according to:

$$\mathrm{LDH} = \mathrm{abs}(490\mathrm{nm}) - \mathrm{abs}(680\mathrm{nm}) \quad (5.2)$$

yielding responses proportional to the LDH expression in the cells. Results were reported as "% toxicity", as the ratio between sample LDH response and positive control LDH response (100%).

5.5.4 Trans-Endothelial Electrical Resistance (TEER)

To evaluate layer contiguity of the bEnd.3 cells, and to act as quality control for prepared BBB cultures, TEER was monitored prior to and following each permeability measurement. For the transwell-based static model, the transwells with seeded cells were moved to an EndOhm chamber (WPI) connected to an EVOM2 epithelial voltohmeter (WPI). For the μBBB dynamic model, the outputs of voltages and currents from the embedded electrodes were connected through an electrode adapter (WPI) to an EVOM2 epithelial voltohmeter. To calculate TEER, initial background resistances of the blank chip/membrane R_{blank} were subtracted from the measured resistance. The difference value was multiplied with the cell culture area A (0.16cm^2 or 4.67cm^2 for the chips and transwells, respectively), resulting in the TEER values of only the endothelial cells in Ωcm^2 from the following equation [33].

$$\mathrm{TEER} = (\mathrm{R} - \mathrm{R_{blank}})\mathrm{A} \quad (5.3)$$

5.5.5 Drug Permeability

To measure the BBB permeability of each drug, aforementioned seven drugs in various concentrations were perfused through the dynamic BBB models (Figure 5.2B) or

pipetted in the static models, and concentration change on the receiving side was measured. To minimize the presence of media serum components in downstream LC-MS measurements, drugs were diluted in PBS. Each drug was injected into the luminal (top) side of the membrane dissolved in PBS with pH of 7.4. The permeated drugs were collected at the abluminal side while being perfused with pure PBS. Transwell permeability assays were conducted for twenty minutes, and the 1.5 mL abluminal fluid was collected. Dynamic permeability assays for all replicates were conducted simultaneously at 10 µL/min, with assay times of twenty minutes, yielding 200 µL of sample. All the collected samples were stored at -20°C until concentration measurements. The permeability coefficient P was obtained from the measurement following the equation [38]:

$$P = \frac{\Delta C_A V_A}{C_L A \Delta t} \tag{5.4}$$

where C_L is the luminal concentration, ΔC_A is the abluminal concentration change, V_A is the abluminal sample volume, and Δt is the assay time. Finally, endothelial permeability P_e was calculated by subtracting the permeability through a blank PC membrane P_b, with the equation [33]:

$$\frac{1}{P_e} = \frac{1}{P} - \frac{1}{P_b} \tag{5.5}$$

The measured endothelial permeability P_e represents the rate of drug diffusion through the BBB layer, and was compared to the *in vivo* clearance from literature. For this correlation with *in vivo* results, measured *in vitro* P_e values were compared to brain/plasma ratios (B/P or K_p). A drug's B/P is an optimal metric for correlation with BBB permeability, because B/P calculation is typically part of the standard

pharmacokinetic (PK) profiling of compounds [39], and was thus consistently available for the drugs used in this study [25-30]. These values were calculated from the brain and plasma area under the curves (AUCs) from time/concentration profiles of *in vivo* biodistribution studies [27]. For consistency, all referenced B/P values are from PK studies in the rat (Sprague-Dawley), with the exception of Sunitinib (mouse, strain unspecified) and PF-3084014 (guinea pig).

5.5.6 Sample Compound Quantification (HPLC-UV/LC-MS)

To accurately quantify the concentrations from the tested samples, their quantitative concentrations (molarity) were measured by performing analysis with liquid chromatography (LC) and mass spectrometry (MS). First, the samples were mixed with mobile phases of either 0.1% formic acid in H2O or 0.1% formic acid in acetonitrile (ACN). The samples in the mobile phases were injected into a coupled LC-MS equipment setup: Agilent 1290 LC system, Agilent 6550 iFunnel Q-TOF mass spectrometer. The LC system utilized an Agilent Eclipse reversed-phase C-18 column. The separated compositions of the samples were then fed into the MS system where the samples were ionized (positive ion mode) through electro-spray ionization for detection. All the ionized compounds were detected as [M+H]+ species, intact compounds plus one proton. The obtained mass spectra were analyzed with Agilent Mass Hunter Quantitative Analysis software, where the AUC were calculated and utilized for quantification. Due to the structural closeness to an amino acid, the quantification of Gabapentin was performed utilizing a high-performance liquid chromatography (HPLC) method [40]. The HPLC-based protocol utilized the proportional fluorescence emission from o-phthalaldehyde

(OPA) to the amount of Gabapentin under the incident light with wavelengths of 340nm/455nm. The protocol analyzed the samples containing Gabapentin through reverse phase analysis utilizing an Insertsil PH 5µm column (4.0x150mm^2, GL Sciences) in an Agilent 1100 HPLC system. The samples were mixed with mobile phases that contain Buffer A (40 mM NaPhosphate, pH7.8) and Buffer B (ACN:MeOH:H_2O, 45:45:10). The samples were first mixed with fluoraldehyde OPA reagent in a ratio of 1:2 in the auto-injector system prior to the column injection. The mobile phase consisted of a gradient elution from 0% buffer B/100% buffer A to 65% buffer B/35% buffer A over twenty minutes, and the detector was set at the absorption wavelength of 338 nm.

5.6 Results and Discussion

5.6.1 Chromatographic Analysis

To establish defined linear ranges for chromatographic quantitation methods, standard solutions of each drug in known concentrations in PBS (pH buffered 7.4) were analyzed to provide an interpolation standard for sample quantification (Figure 5.3). The resultant absorbance curves defined very highly linear ranges (R^2>0.99) and were utilized to interpolate concentrations of each sample (Figure 5.3). In cases where a sample was found to be above the defined linear range, samples were diluted and run again to ensure accurate quantification.

We believe that the effects of serum components on downstream measurements were negligible. Downstream LC-MS measurements of each of these compounds in serum/plasma have been conducted in previous studies by several research groups resulting in negligible serum component interactions [29,41-46]. Furthermore, the

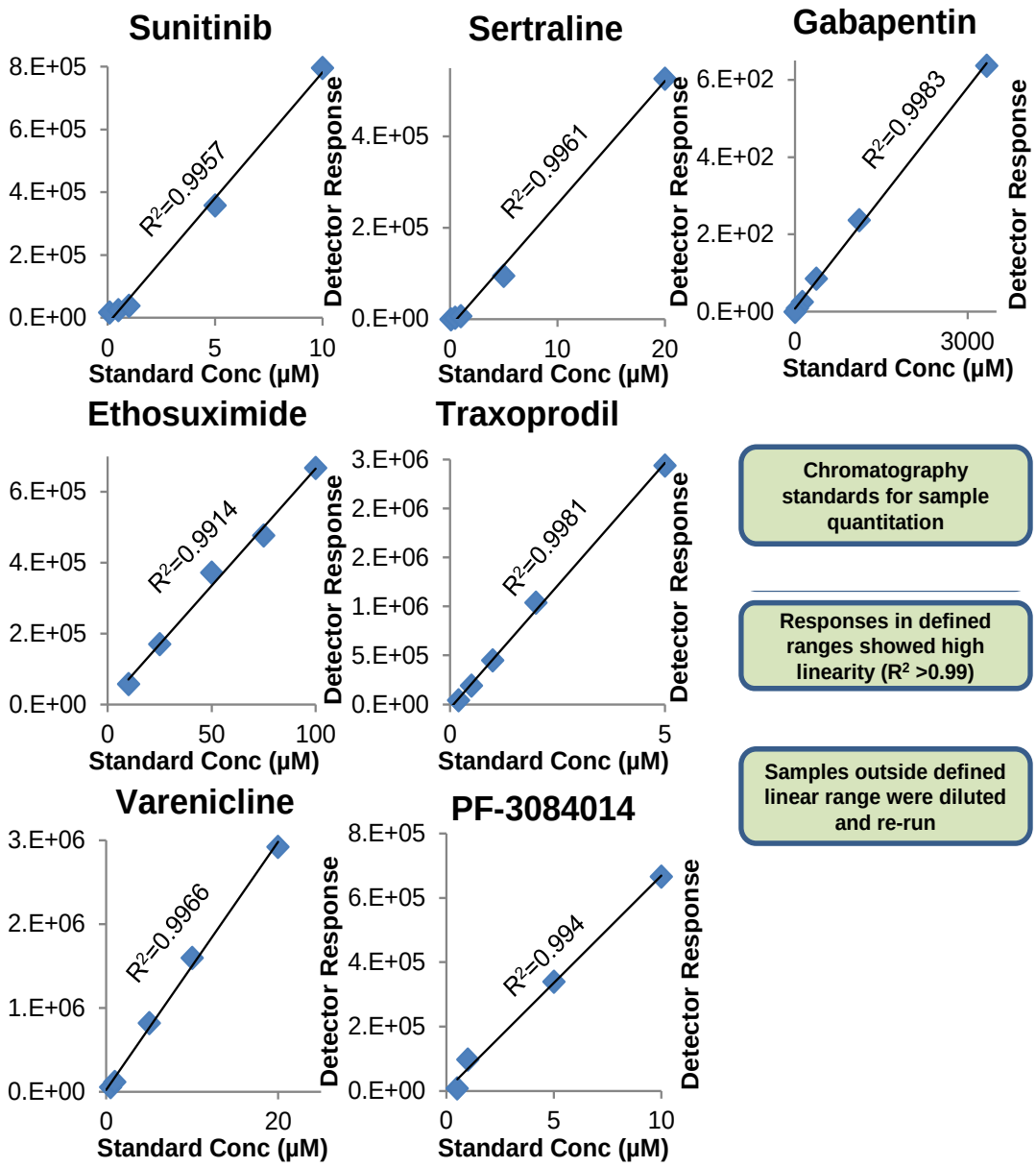

Figure 5.3: Linear standard curves for chromatographic detection. Standards were used to define a linear range, and as a quantitative standard for interpolation of sample results. Samples which were measured to fall above the defined linear range were diluted and re-run to ensure accurate interpolation. All standard curves defined a linear range with R^2 of higher than 0.99. Analysis methods for each drug were LC-MS, except for Gabapentin, which was HPLC-UV.

presence of media serum components was diluted by using phosphate-buffered saline (PBS) during permeability assays.

5.6.2 Morphology

The optical images of the immortalized bend.3 cells, obtained on day 4 of endothelial culture, did not show any significant dissimilarities in morphology from those of the primary rat brain endothelial cells (Figure 5.4). Particularly, cells from both sources clearly showed full confluence of highly elongated cells and strong tight junction expression of ZO-1 (green) among all adjacent cells. The images also showed that both the cell groups held comparable sizes of their highly elongated shape, typically ranging in 10-30μm width, and 50-80μm length. Since the monolayer of endothelial cells mainly determines the BBB permeability, such similarities in morphology validate the use of bEnd.3 cells to examine the diffusion properties of the BBB, such as TEER and permeability. As the zonal occludins are localized exclusively at the interface between cell membranes and tight junctions [47], we suspect that the background in these images are of secondary antibody, either nonspecifically bound or in unbound globules. Despite this background, the distinct boundaries where tight junctions are expressed are sufficiently clear from these images to conclude expression of tight junctions and observe cell shapes.

5.6.3 Cytotoxicity

The LDH measurement results (Figure 5.5) showed that all the seven drug compounds did not cause toxic effects to the brain endothelial cells in the dynamic BBB

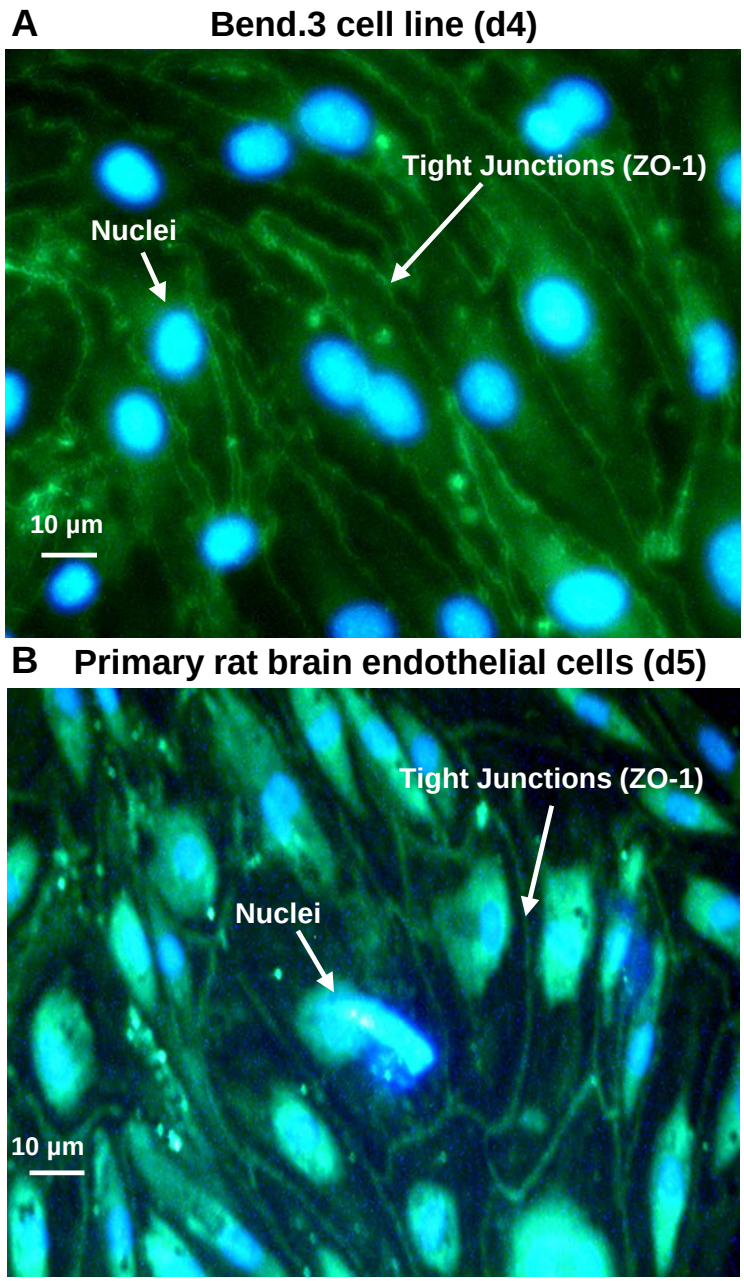

Figure 5.4: Immunostaining of the brain endothelial cell line bEnd.3 cell line used for the BBB models in this study (A) and extracted primary brain endothelial cells from the rat (B) for reference. Cells were fixed and permeabilized, and stained with antibodies targeting the ZO-1 and conjugated to Alexa-fluor 488 (green), and counterstained with DAPI nuclear stain (blue). Cell morphologies were qualitatively similar, with strong expression of tight junctions as indicated by ZO-1 expression, and with similar shape and size, suggesting correlation with the *in vivo* physiology.

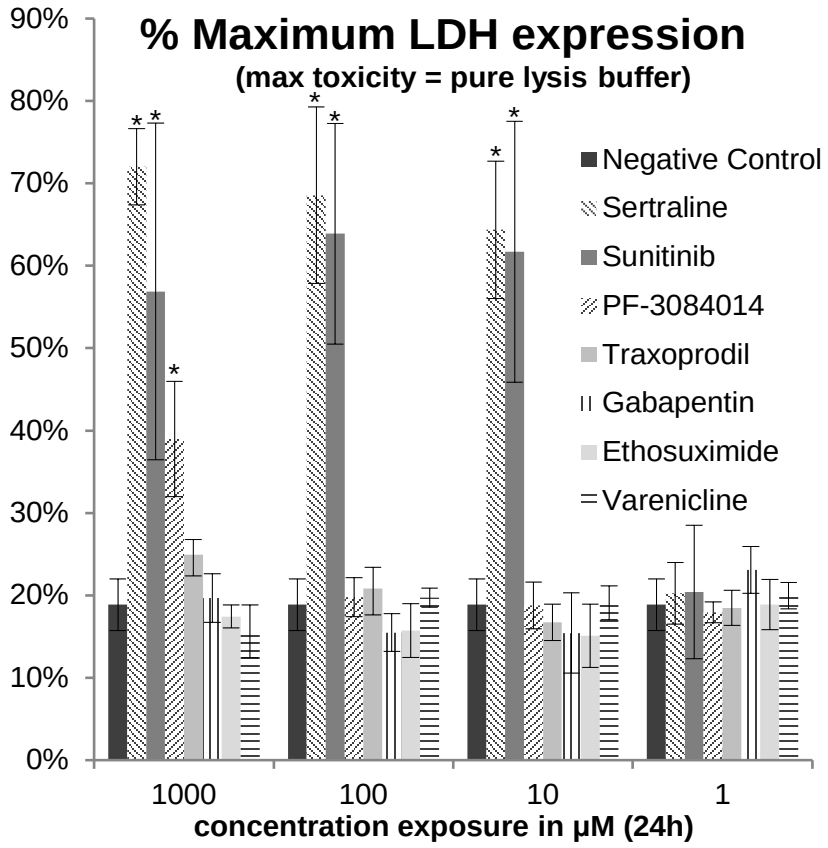

Figure 5.5: Cytotoxicity of each drug tested in this study as measured by LDH expression following twenty-four hour exposure to different concentrations. Data are reported as a ratio to LDH levels expressed by cells exposed to lysis buffer (100% toxicity). Also included is the negative control, or the LDH expression of untreated cells, indicating a baseline of negligible cytotoxicity. Standard deviations displayed with error bars. Conditions significantly higher than negative control denoted with *. All n=4.

model up to 10µM, defining the maximum range of testing in this study. Four compounds (Traxoprodil, Gabapentin, Ethosuximide, and Varenicline) did not induce any increased LDH expression over the negative control at any measured concentrations between 10µM and 1mM. Compound PF-3084014 induced toxic response of 39% of positive control at high concentrations of 1000µM or higher, while Sertraline and Sunitinib respectively induced toxic response of 62% and 64% at the concentrations of 10µM or higher. Thus,

these corresponding maximum acceptable concentration ranges were selected for the permeability assays to avoid the unrelated errors such as the loss of functioning cells due to toxicity. Only the selected concentrations were used as C_L during permeability assays. Note that some *in vivo* toxicological information was available from MSDS documentation for the seven drugs utilized in this study. However, these toxicological tests, such as LD50 (50% lethal dose) represent the potential concentrations to poison the individual entity of animals, thus not providing direct translation to cytotoxicity in the cellular environments concerned by this study.

5.6.4 Trans-Endothelial Electrical Resistance

For this study, cells were cultured in the device only until they had reached confluence and steady-state TEER was reached. As a result, cell cultures have been maintained in the device only for up to seven days, during which any observed changes in electrode performance or background resistance potentially caused by protein fouling was not observed. TEER measurement results (Figure 5.6) showed that the change in average TEER before and after permeability was within $5\Omega cm^2$ for all model conditions, and that outliers were observed with occurrence rates of 12.5% and 37.5% in 8 cases, respectively, for the dynamic BBB model and the static Transwell model, with an average standard deviation of 19% of the total steady-state TEER values. The outliers were defined as when datapoints were deviated from the average by more than 2X standard deviations. It was hypothesized that outliers were caused by pinholes in the bEnd.3 cell layer or by apoptosis due to cytotoxicity by the tested drugs. The TEER measurement results were utilized for quality precontrol for permeability assays by enabling the

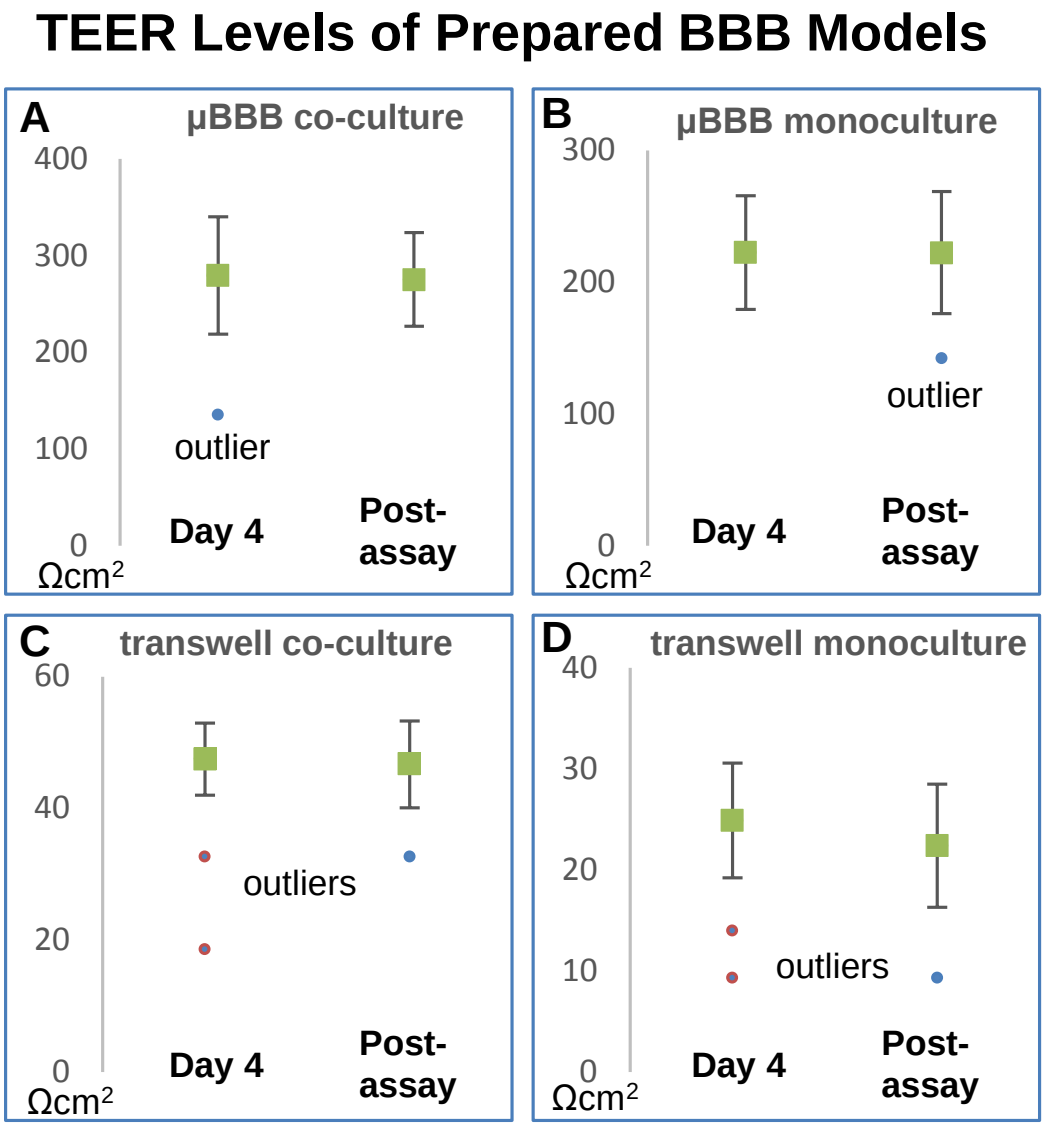

Figure 5.6: TEER level s of prepared BBB models, four days after endothelial cell seeding as quality control. TEER was measured before and after permeability assays, and outliers were selected and removed as unacceptable for permeability testing. TEER for co-cultures (A,C) were significantly higher than for mono-cultures (B,D), and TEER for the μBBB cultures (A,B) were significantly higher than static transwells (C,D). Standard deviations displayed with error bars. All n=8.

exclusion of outliers.

As shown previously [15], co-culturing bEnd.3 cells with astrocytes results in significantly elevated TEER levels of BBB models in both static (~90% increase) and dynamic (~25% increase) conditions. These TEER levels indicate more fully contiguous cell layers and more strongly expressed tight junctions [48], though they are not indicative of cell transcytotic activity [49], which is the primary path for compounds that cannot pass through tight junctions.

Finally, TEER levels were measured to be significantly higher for dynamic μBBB compared with static transwells for both co-cultured (5.9 fold increase) and mono-cultured (8.9 fold increase) BBB models. A consensus has been reached regarding BBB models that a minimum TEER level of 150Ωcm^2 is required for BBB models to achieve reasonably representative and consistent permeability characteristics [50], and this threshold was consistently reached for both monocultured (223 Ωcm^2) and co-cultured (280 Ωcm^2) embodiments of the dynamic μBBB model, but not for their static transwell counterparts (47 and 25 Ωcm^2). This indicates that the dynamic model represents a significant improvement in terms of monolayer tightness.

5.6.5 Drug Permeability

The feasibility of the BBB model as a predictive platform for drug screening was tested with peremability measurement of the seven drugs (Table 5.2, Figure 5.7). Comparison of the logP_e averages across all seven drugs appear to suggest two trends in permeability: (1) lower permeability in co-cultured models than in monocultured models, and (2) lower permeability through dynamic μBBB models than static transwells. First,

Table 5.2: Permeability results of each compound used in the study. Standard deviations displayed after each result. Data is presented in Figures 5.8-5.9 as $logP_e$ according to convention. All n=4. B/P ratios from previous studies [25-30].

Compound	B/P Ratio	µBBB P_e (Co-culture) ($10e^{-6}$ cm/s)	Transwell P_e (Co-culture) ($10e^{-6}$ cm/s)	µBBB P_e (Monoculture) ($10e^{-6}$ cm/s)	Transwell P_e (Monoculture) ($10e^{-6}$ cm/s)
PF-262192	0.42	87±13	97±4	104±29	104±7
PF-345043	0.75	109±7	119±18	110±17	118±27
PF-3084014	1	93±12	105±14	108±9	151±7
PF-344988	1.1	128±10	133±2	144±7	146±12
PF-1486212	2.1	131±37	153±43	162±49	175±28
PF-3430574	3.24	163±78	173±19	195±57	199±40
PF-579897	26.8	208±20	237±36	229±7	294±19

the drug $logP_e$ coefficents of monocultured models were, on average, 0.063 and 0.061 log(cm/s) lower than for co-cultured models in static and dynamic conditions, respectively, while the average $LogP_e$ coefficients were lower in the dynamic *in vitro* BBB models than static Transwell models by 0.050 and 0.052 log(cm/s) for co-cultured and monocultured models, respectively (Figure 5.8). These trends indicate that optimal model conditions in regards to highest barrier performance are achieved by dynamic co-cultures. These trends are consistent with the highest TEER values obtained in dynamic co-culture conditions.

For all model conditions, there was a strong correlation with *in vivo* B/P ratios with linear regression accuracy of R^2>0.85. As the B/P ratio increased from 0.42 to 26.8, the corresponding average $logP_e$ values of each drug proportionally increased from -4.06 to -3.63 log(cm/s) (Figure 5.9). Though multiple-drug correlation of brain clearance results between transwell-based *in vitro* models and *in vivo* animal models has been shown previously [17,51], this reports the first demonstration of *in vivo* correlation for pharmaceutical drug clearance in a dynamic microfluidic model of the BBB. These

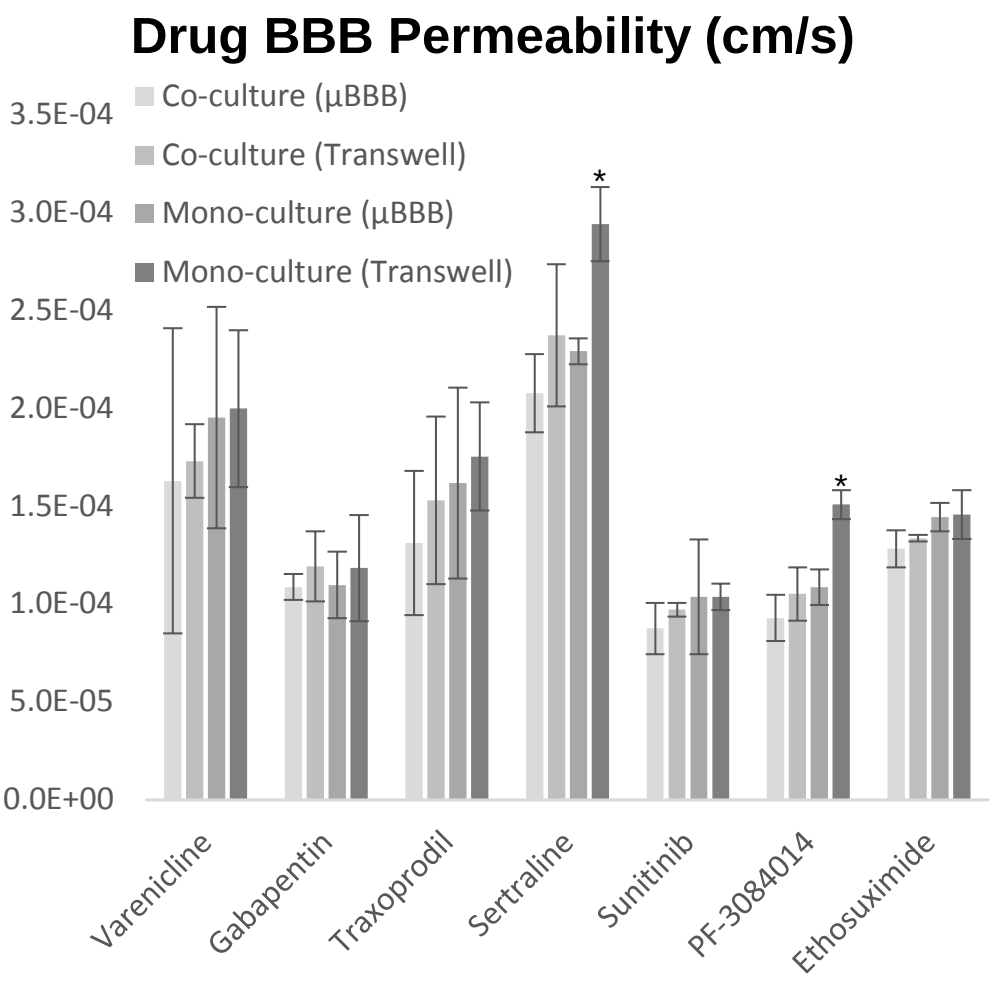

Figure 5.7: Permeability coefficients of each compound used in the study. Data are presented in Figure 5.8-5.9 as $\log P_e$ according to convention. Dynamic conditions significantly different than transwell controls denoted with *. All n=4.

confirmed correlation results, in addition to the practical advantages of the μBBB (high-throughput, material conservation, integrated sensing, controlled delivery), demonstrate that microfluidic models are a promising tool for pharmaceutical drug screening.

No correlative trend was deterministically exhibited between permeability profiles or B/P and $\log P_{o/w}$ (octanol/water coefficient) or molecular weight, implying the potential influence of other physicochemical properties on diffusive properties of the sample drugs through the BBB. The lack of public information on some physicochemical

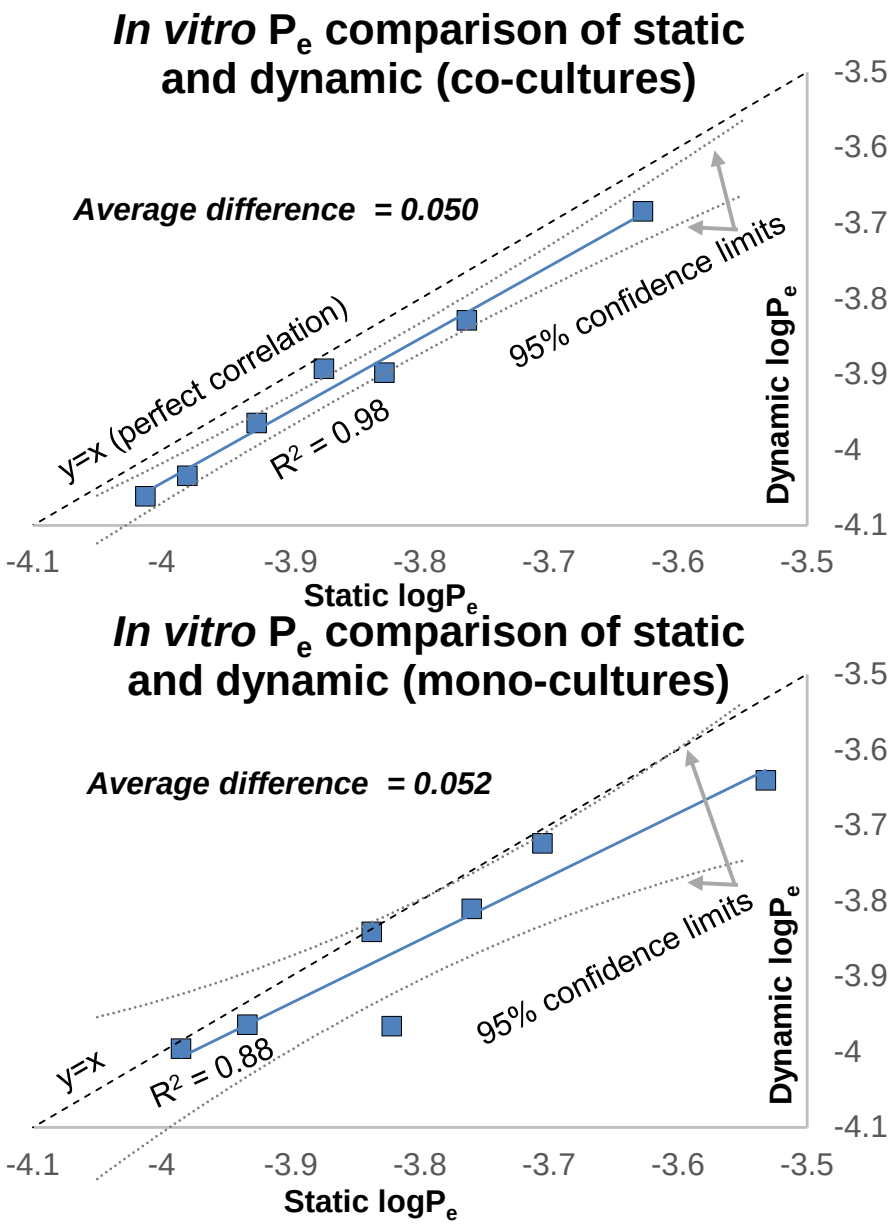

Figure 5.8: Comparison of average static/dynamic BBB permeability coefficients ($logP_e$) between static and dynamic models, where dynamic $logP_e$ corresponds to the y-axis, and static $logP_e$ corresponds to the x-axis. In the case of both co-culture (A) and mono-culture (B) versions of the models, drug logPe of static BBB models with otherwise similar culture conditions were higher than their corresponding logPe (dotted line), with an average offset of 0.050 and 0.052 for co-cultured and monocultured versions of the model, respectively. These results indicate that dynamic models provide higher barrier activity and better model performance, in agreement with the higher model TEER values. 95% confidence limits for the linear regression are displayed for comparison purposes.

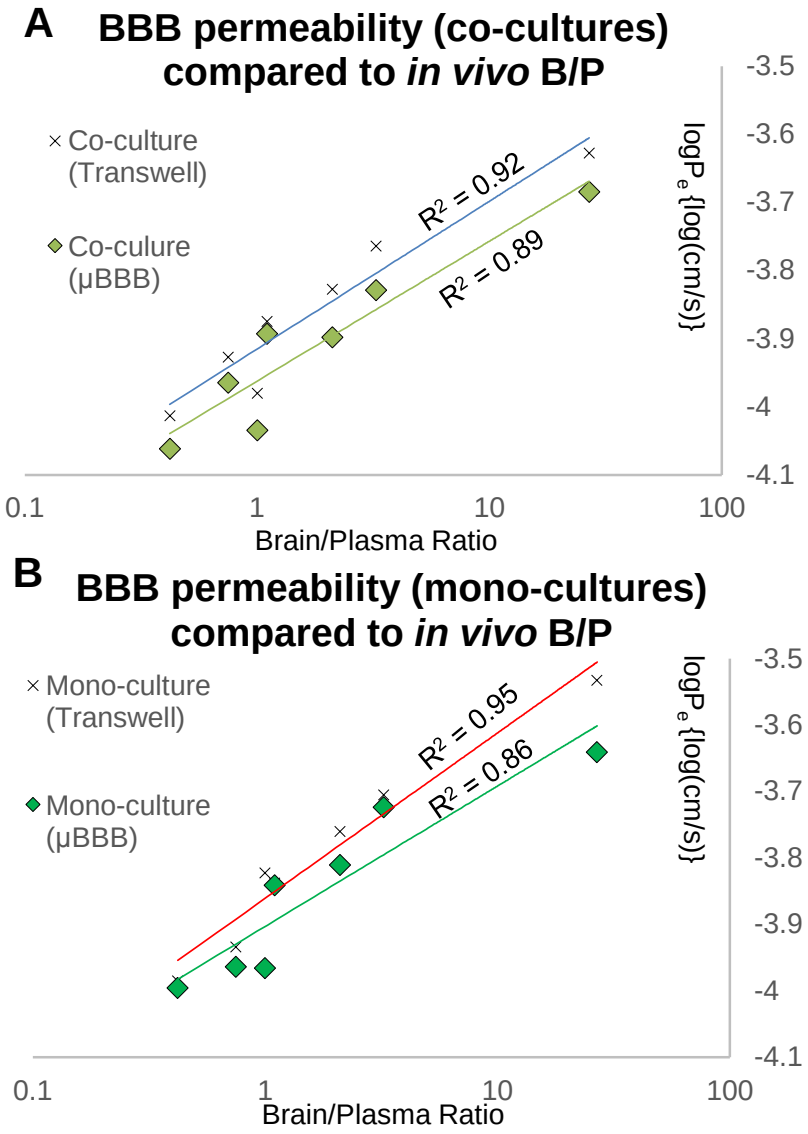

Figure 5.9: *In vivo* correlation of averaged permeability coefficients (see Table 5.2). Data are displayed as $logP_e$ according to convention. Drug brain/plasma ratios were referenced from literature. In the case of both co-culture (A) and monoculture (B) versions of the models, permeabilities were consistently lower for dynamic μBBB than static transwells, indicating increased barrier function. All cases showed a highly correlated positive trend with brain/plasma ratio, indicating that the BBB model is feasible for prediction of *in vivo* brain clearance.

properties of the tested compounds as well as requirement of a larger dataset of compounds tested in this study has currently limited more comprehensive, multi-descriptor quantitative structure-activity response (QSAR) analysis [52]. However, within the limited testing, Sertraline, which exhibited the best BBB clearance, showed both the highest $\log P_{o/w}$ (octanol/water coefficient), thus the highest lipophilicity, and the highest $\log P_{ch}$ (alkane/water coefficient), indicating a lack of polar interactions [53], likely explaining its comparatively excellent brain penetration in the test group. This is because capacity factors (polar interactions per surface unit) have exhibited a significantly-decreasing correlation with BBB permeability of compounds [54].

5.7 Conclusions

We have demonstrated the permeability analysis of neuroactive drugs and correlation with *in vivo* brain/plasma ratios in a dynamic microfluidic blood-brain barrier (BBB) model. Seven neuroactive drugs, including Ethosuximide, Gabapentin, Sertraline, Sunitinib, Traxoprodil, Varenicline, PF-3084014, were analyzed in terms of TEER and permeability in both dynamic (microfluidic) and static (transwell) BBB models either with brain endothelial cell line bEnd.3 in monoculture, or in co-culture with glial cell line C6. For all seven drugs, dynamic and co-culture models respectively resulted in lower permeability, and significantly higher TEER, than static and monoculture models, providing the justification for the dynamic co-culture microfluidic BBB model utilized in this study. Correlation of the resultant $\log P_e$ values (ranging from -4.06 to -3.63 log(cm/s)) with *in vivo* brain/plasma ratios (ranging from 0.42 to 26.8) showed highly linear correlation (R^2>0.85) for all model conditions, indicating the feasibility of the

dynamic microfluidic BBB model for prediction of BBB clearance of pharmaceuticals. Within our knowledge, this is the first reported drug clearance study in a microfluidic BBB model.

5.8 Acknowledgements

This project has been supported by the Utah Science Technology and Research Initiative (USTAR). Microfabrication was performed at the University of Utah Nano Fabrication Facility located in the Sorenson Molecular Biotechnology Building. CNS drugs were provided by Pfizer through the compound transfer program. LC-MS and HPLC-UV was performed at the University of Utah Health Sciences Center (HSC) Core Lab.

5.9 References

[1] Ferri, C. P., M. Prince, C. Brayne, H. Brodaty, L. Fratiglioni, M. Ganguli, K. Hall, K. Hasegawa, H. Hendrie, and Y. Huang. Global prevalence of dementia: A delphi consensus study. *The Lancet*. **366**(9503):2112-2117, 2006.

[2] Bynum, J., *Unpublished tabulations based on data from the medicare current beneficiary survery for 2008.* Nov 2011: Dartmouth Medical School.

[3] Hebert, L. E., L. A. Beckett, P. A. Scherr, and D. A. Evans. Annual incidence of alzheimer disease in the united states projected to the years 2000 through 2050. *Alzheimer Dis Assoc Disord*. **15**(4):169-173, 2001.

[4] Pangalos, M. N., L. E. Schechter, and O. Hurko. Drug development for cns disorders: Strategies for balancing risk and reducing attrition. *Nature Reviews Drug Discovery*. **6**(7):521-532, 2007.

[5] Adams, C. P. and V. V. Brantner. Estimating the cost of new drug development: Is it really 802 million dollars? *Health Aff (Millwood)*. **25**(2):420-428, 2006.

[6] Pardridge, W. M., W. H. OLDENDORF, P. CANCILLA, and H. J. FRANK. Blood-brain barrier: Interface between internal medicine and the brain. *Annals*

of internal medicine. **105**(1):82-95, 1986.

[7] Pardridge, W. M. The blood-brain barrier: Bottleneck in brain drug development. *NeuroRx*. **2**(1):3-14, 2005.

[8] Reichel, A. Addressing central nervous system (cns) penetration in drug discovery: Basics and implications of the evolving new concept. *Chem Biodivers*. **6**(11):2030-2049, 2009.

[9] Kola, I. and J. Landis. Can the pharmaceutical industry reduce attrition rates? *Nature reviews Drug discovery*. **3**(8):711-716, 2004.

[10] Cecchelli, R., V. Berezowski, S. Lundquist, M. Culot, M. Renftel, M. P. Dehouck, and L. Fenart. Modelling of the blood-brain barrier in drug discovery and development. *Nat Rev Drug Discov*. **6**(8):650-661, 2007.

[11] Tzima, E., M. Irani-Tehrani, W. B. Kiosses, E. Dejana, D. A. Schultz, B. Engelhardt, G. Cao, H. DeLisser, and M. A. Schwartz. A mechanosensory complex that mediates the endothelial cell response to fluid shear stress. *Nature*. **437**(7057):426-431, 2005.

[12] Chien, S., S. Li, and Y. J. Shyy. Effects of mechanical forces on signal transduction and gene expression in endothelial cells. *Hypertension*. **31**(1 Pt 2):162-169, 1998.

[13] Chien, S. Molecular basis of rheological modulation of endothelial functions: Importance of stress direction. *Biorheology*. **43**(2):95-116, 2006.

[14] Cucullo, L., M. Hossain, V. Puvenna, N. Marchi, and D. Janigro. The role of shear stress in blood-brain barrier endothelial physiology. *BMC Neurosci*. **12**(40, 2011.

[15] Booth, R. and H. Kim. Characterization of a microfluidic in vitro model of the blood-brain barrier (μbbb). *Lab on a Chip*. **12**(10):1784-1792, 2012.

[16] Booth, R., S. Noh, and H. Kim. A multiple-channel, multiple-assay platform for characterization of full-range shear stress effects on vascular endothelial cells. *Lab on a Chip*. 2014.

[17] Pardridge, W. M., D. Triguero, J. Yang, and P. A. Cancilla. Comparison of in vitro and in vivo models of drug transcytosis through the blood-brain barrier. *Journal of Pharmacology and Experimental Therapeutics*. **253**(2):884-891, 1990.

[18] Griep, L., F. Wolbers, B. de Wagenaar, P. Ter Braak, B. Weksler, I. A. Romero, P. Couraud, I. Vermes, A. van der Meer, and A. van den Berg. Bbb on chip: Microfluidic platform to mechanically and biochemically modulate blood-brain

barrier function. *Biomedical microdevices*. **15**(1):145-150, 2013.

[19] Prabhakarpandian, B., M.-C. Shen, J. B. Nichols, I. R. Mills, M. Sidoryk-Wegrzynowicz, M. Aschner, and K. Pant. Sym-bbb: A microfluidic blood brain barrier model. *Lab on a Chip*. **13**(6):1093-1101, 2013.

[20] Achyuta, A. K. H., A. J. Conway, R. B. Crouse, E. C. Bannister, R. N. Lee, C. P. Katnik, A. A. Behensky, J. Cuevas, and S. S. Sundaram. A modular approach to create a neurovascular unit-on-a-chip. *Lab on a Chip*. **13**(4):542-553, 2013.

[21] Cucullo, L., M. S. McAllister, K. Kight, L. Krizanac-Bengez, M. Marroni, M. R. Mayberg, K. A. Stanness, and D. Janigro. A new dynamic in vitro model for the multidimensional study of astrocyte–endothelial cell interactions at the blood–brain barrier. *Brain research*. **951**(2):243-254, 2002.

[22] Chueh, B. H., D. Huh, C. R. Kyrtsos, T. Houssin, N. Futai, and S. Takayama. Leakage-free bonding of porous membranes into layered microfluidic array systems. *Anal Chem*. **79**(9):3504-3508, 2007.

[23] Polk, B. J., A. Stelzenmuller, G. Mijares, W. MacCrehan, and M. Gaitan. Ag/agcl microelectrodes with improved stability for microfluidics. *Sensors and Actuators B: Chemical*. **114**(1):239-247, 2006.

[24] Aran, K., L. A. Sasso, N. Kamdar, and J. D. Zahn. Irreversible, direct bonding of nanoporous polymer membranes to pdms or glass microdevices. *Lab Chip*. **10**(5):548-552, 2010.

[25] Wang, Y. and D. F. Welty. The simultaneous estimation of the influx and efflux blood-brain barrier permeabilities of gabapentin using a microdialysis-pharmacokinetic approach. *Pharm Res*. **13**(3):398-403, 1996.

[26] Peeters, M., M. J. Gunthorpe, P. J. Strijbos, P. Goldsmith, N. Upton, and M. F. James. Effects of pan- and subtype-selective n-methyl-d-aspartate receptor antagonists on cortical spreading depression in the rat: Therapeutic potential for migraine. *J Pharmacol Exp Ther*. **321**(2):564-572, 2007.

[27] Summerfield, S. G., A. J. Lucas, R. A. Porter, P. Jeffrey, R. N. Gunn, K. R. Read, A. J. Stevens, A. C. Metcalf, M. C. Osuna, P. J. Kilford, J. Passchier, and A. D. Ruffo. Toward an improved prediction of human in vivo brain penetration. *Xenobiotica*. **38**(12):1518-1535, 2008.

[28] Rollema, H., A. Shrikhande, K. M. Ward, F. D. Tingley, 3rd, J. W. Coe, B. T. O'Neill, E. Tseng, E. Q. Wang, R. J. Mather, R. S. Hurst, K. E. Williams, M. de Vries, T. Cremers, S. Bertrand, and D. Bertrand. Pre-clinical properties of the alpha4beta2 nicotinic acetylcholine receptor partial agonists varenicline, cytisine and dianicline translate to clinical efficacy for nicotine dependence. *Br J Pharmacol*. **160**(2):334-345, 2010.

[29] Wood, K. M., T. A. Lanz, K. J. Coffman, S. L. Becker, J. van Deusen, C. E. Nolan, K. E. Richter, J. E. Finley, T. M. Brown, and M. A. Brodney. P2-375: Efficacy of the novel γ-secretase inhibitor, pf-3084014, in reducing aβ in brain, csf, and plasma in guinea pigs and tg2576 mice. *Alzheimer's & Dementia*. **4**(4):T482-T483, 2008.

[30] Oberoi, R. K., R. K. Mittapalli, J. Fisher, and W. F. Elmquist. Sunitinib lc-ms/ms assay in mouse plasma and brain tissue: Application in cns distribution studies. *Chromatographia*. **76**(23-24):2013.

[31] Zehendner, C. M., H. J. Luhmann, and C. R. Kuhlmann. Studying the neurovascular unit: An improved blood-brain barrier model. *J Cereb Blood Flow Metab*. **29**(12):1879-1884, 2009.

[32] Omidi, Y., L. Campbell, J. Barar, D. Connell, S. Akhtar, and M. Gumbleton. Evaluation of the immortalised mouse brain capillary endothelial cell line, b.End3, as an in vitro blood-brain barrier model for drug uptake and transport studies. *Brain Res*. **990**(1-2):95-112, 2003.

[33] Li, G., M. J. Simon, L. M. Cancel, Z. D. Shi, X. Ji, J. M. Tarbell, B. Morrison, 3rd, and B. M. Fu. Permeability of endothelial and astrocyte cocultures: In vitro blood-brain barrier models for drug delivery studies. *Ann Biomed Eng*. **38**(8):2499-2511, 2010.

[34] Neuhaus, W., V. E. Plattner, M. Wirth, B. Germann, B. Lachmann, F. Gabor, and C. R. Noe. Validation of in vitro cell culture models of the blood-brain barrier: Tightness characterization of two promising cell lines. *J Pharm Sci*. **97**(12):5158-5175, 2008.

[35] Neuhaus, W., R. Lauer, S. Oelzant, U. P. Fringeli, G. F. Ecker, and C. R. Noe. A novel flow based hollow-fiber blood-brain barrier in vitro model with immortalised cell line pbmec/c1-2. *J Biotechnol*. **125**(1):127-141, 2006.

[36] Nakagawa, S., M. A. Deli, H. Kawaguchi, T. Shimizudani, T. Shimono, A. Kittel, K. Tanaka, and M. Niwa. A new blood–brain barrier model using primary rat brain endothelial cells, pericytes and astrocytes. *Neurochemistry international*. **54**(3):253-263, 2009.

[37] Desai, S. Y., M. Marroni, L. Cucullo, L. Krizanac-Bengez, M. R. Mayberg, M. T. Hossain, G. G. Grant, and D. Janigro. Mechanisms of endothelial survival under shear stress. *Endothelium*. **9**(2):89-102, 2002.

[38] Yuan, W., G. Li, E. S. Gil, T. L. Lowe, and B. M. Fu. Effect of surface charge of immortalized mouse cerebral endothelial cell monolayer on transport of charged solutes. *Ann Biomed Eng*. **38**(4):1463-1472, 2010.

[39] Abbott, N. J. Prediction of blood–brain barrier permeation in drug discovery

from *in vivo*, *in vitro* and *in silico* models. *Drug Discovery Today: Technologies*. **1**(4):407-416, 2004.

[40] Henderson, J., R. D. Ricker, B. A. Bidlingmeyer, and C. Woodward. Rapid, accurate, sensitive, and reproducible hplc analysis of amino acids. *Amino acid analysis using Zorbax Eclipse-AAA columns and the Agilent*. **1100**(1-10, 2000.

[41] Couchman, L., M. Birch, R. Ireland, A. Corrigan, S. Wickramasinghe, D. Josephs, J. Spicer, and R. Flanagan. An automated method for the measurement of a range of tyrosine kinase inhibitors in human plasma or serum using turbulent flow liquid chromatography–tandem mass spectrometry. *Analytical and bioanalytical chemistry*. **403**(6):1685-1695, 2012.

[42] Kushnir, M. M., J. Crossett, P. I. Brown, and F. M. Urry. Analysis of gabapentin in serum and plasma by solid-phase extraction and gas chromatography-mass spectrometry for therapeutic drug monitoring. *Journal of Analytical Toxicology*. **23**(1):1-6, 1999.

[43] Galan-Valiente, J., R. Soto-Otero, and G. Sierra-Marcuño. Simultaneous measurement of ethosuximide and phenobarbital in brain tissue, serum and urine by hplc. *Biomedical Chromatography*. **3**(2):49-52, 1989.

[44] Obach, R. S., A. E. Reed-Hagen, S. S. Krueger, B. J. Obach, T. N. O'Connell, K. S. Zandi, S. Miller, and J. W. Coe. Metabolism and disposition of varenicline, a selective α4β2 acetylcholine receptor partial agonist, in vivo and in vitro. *Drug metabolism and disposition*. **34**(1):121-130, 2006.

[45] Johnson, K., A. Shah, S. Jaw-Tsai, J. Baxter, and C. Prakash. Metabolism, pharmacokinetics, and excretion of a highly selectiven-methyl-d-aspartate receptor antagonist, traxoprodil, in human cytochrome p450 2d6 extensive and poor metabolizers. *Drug metabolism and disposition*. **31**(1):76-87, 2003.

[46] Jain, D. S., M. Sanyal, G. Subbaiah, U. Pande, and P. Shrivastav. Rapid and sensitive method for the determination of sertraline in human plasma using liquid chromatography–tandem mass spectrometry (lc–ms/ms). *Journal of Chromatography B*. **829**(1):69-74, 2005.

[47] Wolburg, H., S. Noell, A. Mack, K. Wolburg-Buchholz, and P. Fallier-Becker. Brain endothelial cells and the glio-vascular complex. *Cell and tissue research*. **335**(1):75-96, 2009.

[48] Gloor, S. M., M. Wachtel, M. F. Bolliger, H. Ishihara, R. Landmann, and K. Frei. Molecular and cellular permeability control at the blood–brain barrier. *Brain research reviews*. **36**(2):258-264, 2001.

[49] De Boer, A., I. Van Der Sandt, and P. Gaillard. The role of drug transporters at the blood-brain barrier. *Annual review of pharmacology and toxicology*.

43(1):629-656, 2003.

[50] Vastag, M. and G. M. Keseru. Current in vitro and in silico models of blood-brain barrier penetration: A practical view. *Curr Opin Drug Discov Devel*. **12**(1):115-124, 2009.

[51] Zhang, Y., C. S. Li, Y. Ye, K. Johnson, J. Poe, S. Johnson, W. Bobrowski, R. Garrido, and C. Madhu. Porcine brain microvessel endothelial cells as an in vitro model to predict in vivo blood-brain barrier permeability. *Drug metabolism and disposition*. **34**(11):1935-1943, 2006.

[52] Zhang, L., H. Zhu, T. I. Oprea, A. Golbraikh, and A. Tropsha. Qsar modeling of the blood–brain barrier permeability for diverse organic compounds. *Pharmaceutical research*. **25**(8):1902-1914, 2008.

[53] Deak, K., K. Takacs-Novak, K. Tihanyi, and B. Noszal. Physico-chemical profiling of antidepressive sertraline: Solubility, ionisation, lipophilicity. *Medicinal Chemistry*. **2**(4):385-389, 2006.

[54] Crivori, P., G. Cruciani, P.-A. Carrupt, and B. Testa. Predicting blood-brain barrier permeation from three-dimensional molecular structure. *Journal of medicinal chemistry*. **43**(11):2204-2216, 2000.

CHAPTER 6

CONCLUSIONS

6.1 Summary and Impact

The purpose of this project was to develop and characterize an innovative chip-based platform for blood-brain barrier (BBB) modeling with advantages over the state-of-the-art: Compared with *in vivo* models, (A) lower costs, timescales, and ethical issues than *in vivo* studies; (B) Massively-parallel, controlled and repeatable environments, and easier elucidation of molecular mechanisms; Compared with transwell models, (C) a dynamic microenvironment providing shear stress stimulation to the constituent cells, also allowing controlled delivery of test compounds and improved permeability analysis; Compared with hollow fiber models, (D) much thinner culture membrane, decreasing the distance between co-cultured cells for compound diffusion, and (E) smaller functional volumes for quicker media exchange, material conservation, and scales closer to true *in vivo* dimensions, and (F) a 2D culture surface allowing complete initial seeding and shorter times to steady-state barrier resistance for a more rapid turn-around time, shortening experiments and allowing a more high-throughput approach to experimentation. The systems primary applications include (1) use as a platform to test responses of the cultured cells to chemical and physical stimuli, and (2) use as a drug delivery test platform for predicting clinical clearance through the BBB. The described

studies in the preceding chapters fully demonstrated these applications.

Chapter 3 demonstrated the first publication of a microfluidic BBB model (μbbb) [1]. However, since its publication, three other groups have published chip-based microfluidic BBB models, though the publications in this dissertation remain the most comprehensive in comparison. Indeed, the μBBB remains the only microfluidic BBB which has simultaneously measured trans-endothelial electrical resistance (TEER) and permeability within the same system, and the only system to test more than a single magnitude of on-chip discrete shear stress, or to test the passage of actual drugs through the system (Table 6.1). The first, "BBB-ON-CHIP" [2] focused on modulation of BBB properties (TEER) in response to tumor necrosis factor alpha (TNF-α); however, they did

Table 6.1 Comparison of microfluidic BBB studies reported at the time of this dissertation. *Drug data currently unpublished (under review)

Microfluidic Device	**μBBB [1,3]***	BBB-ON-CHIP [2]	Neurovascular unit-on-a-chip [4]	SyM-BBB (Synthetic microvascular model) [5]
Constituent Cells	**bEnd.3 + C8-D1A or C6**	hCMEM/ D3	RBE4 + Rat cortical cells (4% neuron/ 96% glial)	RBE4
TEER Measurement	**Yes**	Yes	No	No
Permeability Measurement	**Yes**	No	Yes	Yes
Co-culture	**Yes**	No	Yes	No
Real drugs tested	**Yes**	No	No	No
TEER achieved	**250 cm^2**	120 Ωcm^2	N/A	N/A
Shear Stresses Tested	**0.02-86 dyn/cm^2 (wide range)**	5.8 dyn/cm^2	Flowrate unspecified	0.00006 dyn/cm^2
Barrier Modulation	**Shear stress, Histamine, pH**	TNF-α	TNF-α	N/A
Proteins Measured	**ZO-1, GFAP, P-gp**	ZO-1	ZO-1, vWF	ZO-1, Claudin-1, P-gp
Permeability Compounds tested	**FITC-Dextran (4, 20, 70kD), PI, 7 CNS compounds***	N/A	Alexafluor-Dextran	FITC
Published	**April 2012**	Feb 2013	Feb 2013	Mar 2013

not measure permeability, and did not co-culture the cells with astrocytes, though they did run experiments within the physiologically relevant range of shear stresss ($5.8 dyn/cm^2$). Notably, they used nearly identical structures and methods to a previous paper on resistance measurement across epithelial barriers by the Takayama group [6]. The second, "neurovascular unit-on-a-chip" [4] focused on constructing a co-cultured system with the RBE4 cell line and a mixture of primary neurons and astrocytes at 4% and 96% population, respectively. Though they tested permeability of the fluorescent marker Alexafluor-dextran through the co-culture and also looked at modulation of permeability by TNF-α, the system cannot measure TEER, is a noncontact co-culture, and was not operated under specified shear stress levels. The third, "synthetic microvascular model (SyM-BBB)" [5] differs in concept in that it uses micropillar gaps in the walls between two adjacent chambers instead of a porous membrane, and measured permeability of fluorescent tracer fluorescein isothiocyanate (FITC) with microscopy rather than with a plate reader. However, the system is not feasible for TEER measurement, only extremely low shear stress was used, and barrier modulation was not demonstrated. In short, the described μBBB system remains the best characterized microfluidic BBB model to date.

6.2 Unpublished Results

In Chapter 3, the cell lines selected for study in the presented μBBB were observed for key morphological properties, confirming expression of glial fibrillary acidic protein (GFAP) by C8-D1A astrocytes, and localized expression of key tight junction component zonal occludin-1 (ZO-1) by bEnd.3 cells, by fluorescence

microscopy. An additional key component that should be expressed by BBB endothelial cells is P-glycoprotein (P-gp) [7], because it acts in concert with tight junctions to exclude trans-cellular passage of compounds by efflux transport. While protein expression by bEnd.3 cells under static and dynamic conditions was tested by western blot in Chapter 4, we conducted a biochemical assay to confirm significant quantifiable activity of P-gp in bEnd.3 cells. To quantify P-gp activity, we used the Multi-Drug Resistance (MDR) assay made by Cayman Chemical. The assay allows measurement of cellular uptake of Calcein AM (acetomethoxy), which loses its AM group when exposed to intracellular esterases, both emitting fluorescence and trapping the Calcein within the cell. Populations of bEnd.3 cells were seeded in 96-well plates at $5x10^4$ cells/well, and were assayed for MDR activity on the next day. To act as a control group representing zero efflux activity, 20 μM Cyclosporin A, a competitive inhibitor of P-gp and other MDR efflux transporters, was treated to one set of wells for thirty minutes to simulate cells with no efflux activity. Following Cyclosporin A treatment, both groups and media-only background control were incubated with Calcein AM staining solution for twenty minutes, when fluorescence was measured with a plate reader at 485nm and 535nm excitation and emission, respectively. Results indicated that the untreated bEnd.3 cells uptook approximately 32% less Calcein AM than the Cyclosporin A-treated control (Figure 6.1). Thus, in the 20 minute biochemical assay time, efflux transporters on the bEnd.3 cell membrane reduced Calcein AM entry by 32%. This result confirms quantitatively significant P-gp expression by bEnd.3 cells used in this dissertation, supporting justification of its use in these studies.

Two different astrocyte-type cell lines were used in Chapters 3 and 5 of this dissertation. The immortalized rat glial cell line C8-D1A was used in the initial

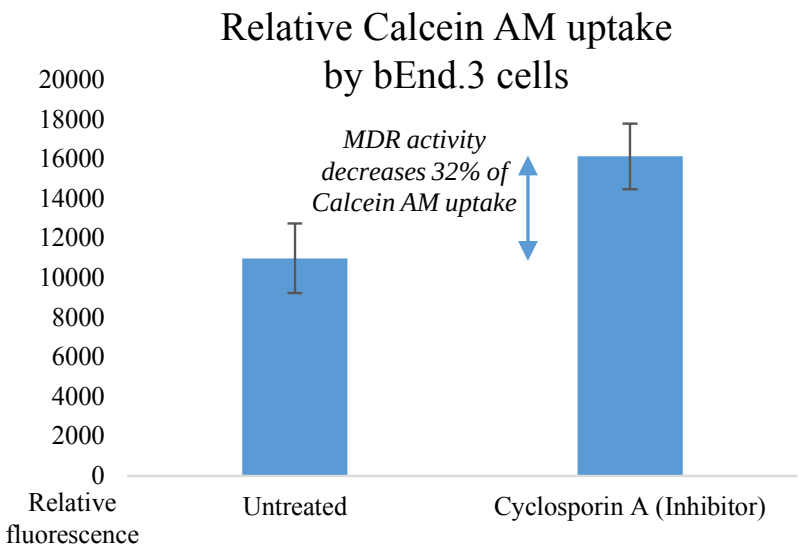

Figure 6.1 Relative Calcein AM uptake by bEnd.3 cells. 96-wells seeded with equal number of bEnd.3 cells ($5x10^4$ cells/well) were treated on day 1 with 20 µM Cyclosporin A for thirty minutes to inhibit efflux activity for comparison with untreated control. Results indicated significantly lower Calcein AM uptake by the untreated cells, at approximately 32% lower amounts than cells inhibited with Cylcosporin A. All n>3.

characterization study; however, its proliferative properties were inferior to bEnd.3 making evenly developed co-cultures tedious; therefore subsequently, the C6 glial cell line was used because it was commonly used in previous co-culture BBB models [8,9] and to generate astrocyte-conditioned medium [10], and because its proliferative properties were comparable to bEnd.3, typically reaching confluence in less than 4 days. To compare their morphologies, immunostaining was done to label GFAP as follows: Cells were fixed with 4% paraformaldehyde for 10m at room temperature. Cells were permabilized with 0.1% Triton X-100 in PBS for 10m and blocked with 5% bovine serum albumin permeabilization buffer for one hour. Cultures were incubated with primary antibody in blocking solution overnight at 4ºC. Cultures were rinsed with blocking

solution and left in secondary antibody for one hour, counter-stained with DAPI (blue) or propidium iodide (red) for 5m, and imaged with a Nikon fluorescence microscope. Rabbit anti-GFAP (Invitrogen) was used in conjunction with Alexa Fluor 488 goat anti-rabbitt secondary antibody (Invitrogen). Morphological analysis of cell lines indicated that both cell types showed comparable morphology and size, with process arms branching outward from small somata (Figure 6.2). Nucleui is counterstained with DAPI (blue) or propidium iodide (red). These comparable morphologies, the excellent growth properties, and heavy amount of previous studies with the cell line support the use of the C6 cell line in the more optimized μBBB co-culture model.

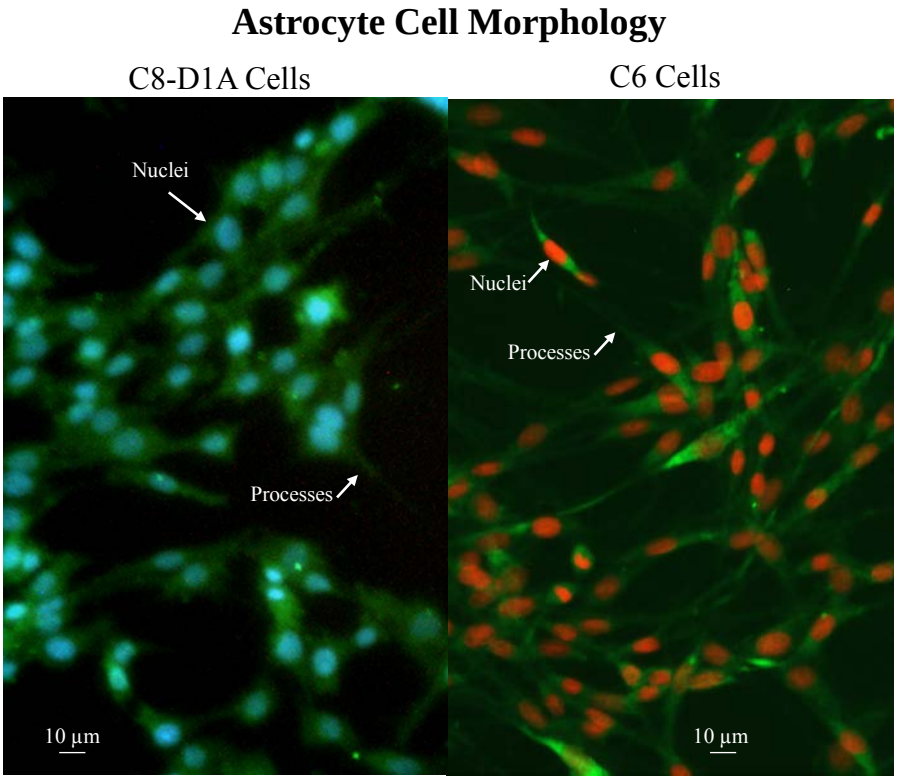

Figure 6.2 Morphological images of both astrocyte cell lines used in this dissertation, stained on day 2 of culture. Both cell types were fluorescently stained with anti-GFAP antibody, a glial marker (green). Both cell types showed comparable morphology and size, with process arms branching outward from small somata. Nucleus is counterstained with DAPI (blue) or propidium iodide (red). Scale bars for reference.

With the aim of retroactively measuring size exclusion characteristics of the three different types of FITC-conjugated dextrans used in Chapter 3, equal concentrations (500 µg/ml) of each size diluted in DMEM/F12 media were run through a standard FPLC column to test for differences in size distribution and confirm the accuracy of the supplier-provided average molecular weights for each type of compound (4, 20, and 70 kDa average molecular weight). The elution profiles of each solution are displayed in Figure 6.3. Size-exclusion measurements of each type of compound showed 5 distinct peaks at the same elution time; however, it was expected that distinct peak locations would be present for each compound of different size. It is likely that this is due to degradation of

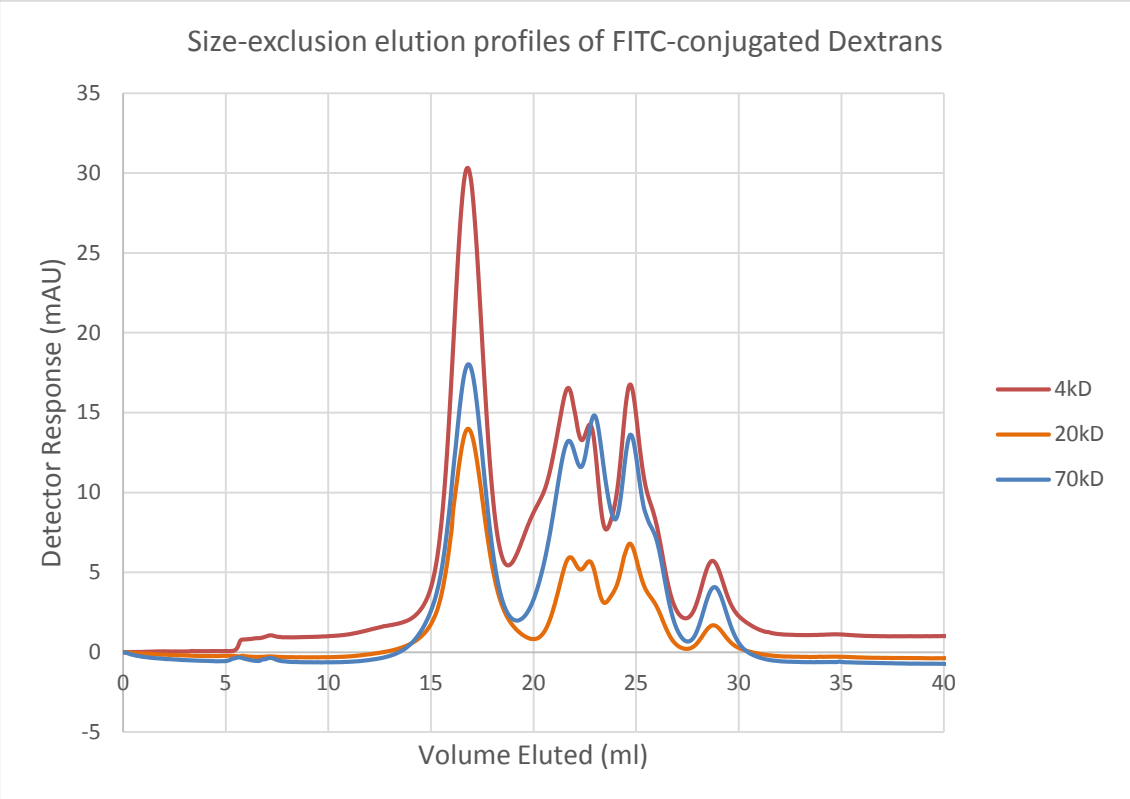

Figure 6.3 Size-exclusion elution profiles of FITC-conjugated dextrans used in Chapter 3 permeability assays following 3 years of storage in aqueous solution. Elution profiles, with five distinct peaks located at the same elution time, indicate significant sample degradation due to low-stability storage conditions in high passage of time.

the compounds to their commonly stable polymeric fragments, because the tested samples were stored as solutions in DMEM/F12 media (5°C) for more than 3 years following permeability measurements, before the size exclusion tests were conducted. Dextran's stability in aqueous solutions is not well described, but is not suggested by the manufacturer (Sigma-Aldrich) for long-term storage. This result demonstrates the importance of sample characterization at approximately the same time-frame as sample permeability analysis.

6.3 Further Commentary

Further commentary supporting the studies in the previous chapters will be discussed in this section, in addition to that discussed within the chapter discussions themselves. First, discussion is necessary on the highly significant difference in TEER observed between the chip-based studies and the transwell controls under identical cell culture conditions, resulting in nearly an order of magnitude difference. There is a high body of evidence that the mechanotrasductive response of endothelial cells to shear stress includes significant increases in tight junction expression [11-15], and this increase in tight junction expression was observed in Chapter 4, indicated by western blots of dynamic cultures and static controls. These evidences support the explanation that the presence of shear stress in the system induce significant changes in the endothelial cells, even at very low flows (0.02 dyn/cm^2). It is also possible that part of the increase in TEER can be explained by the large area differences between the two systems (0.16 cm^2 for the microchip, and 4.67 cm^2 for transwells), perhaps due to higher occurrences of "pinholes" in larger area cultures. However, previous transwell studies with variable areas did not

show a significant difference: transwell cultures of bEnd.3 cells have shown comparable results to our 6-well static control (4.67cm^2, 20-30 Ωcm^2) in both 12-well formats [16] (1.13cm^2, 29-31 Ωcm^2) and 24-well formats [17] (0.33cm^2, 30-34 Ωcm^2). These differences between areas are not significant, so it is most likely not a notable contributing factor to discrepancies in TEER between systems used in this dissertation.

The relationship between TEER and permeability was not discussed explicitly in the preceding chapters either. Differences between permeability results in chip-based cultures and static controls were not as significant as differences in TEER. However, it should be noted that the relationship between TEER and solute transport is not necessarily linear, because solute transport depends on a combination of paracellular transport (which is effectively described by TEER) and transcellular transport, which is independent of TEER [18]. It has been shown before that at TEER values higher than about 130 Ωcm^2, solute permeability was independent of TEER status [19], so the relationship between TEER and permeability are not directly correlated, except at very low levels of TEER.

Little justification was provided in Chapter 3 for modifying pH. In ischemic conditions, the pH in the brain can change significantly, resulting in pH changes and increased permeability through those particular regions. Thus, studying the relationship between pH and BBB permeability is relevant to studying pathological conditions of the BBB. In addition, heightened pH has been suggested as a permeability enhancer for delivered drugs. For example, significant increases in nicotine and the marker mannitol have been shown *in vivo* and *in vitro* under increases in pH, particularly at pH levels higher than 9 [20,21]. Thus, the feasibility of testing pH effects in the microfluidic model was investigated in Chapter 3.

Finally, more in-depth physic-chemical descriptions of the selection of drugs tested in Chapter 5, and the macromolecules and small fluorescent molecules tested in Chapter 3 and 4, are provided in Table 6.2. The seven Pfizer CNS drugs exhibited the highest permeability compared with the fluorescent tracers, but there is no clear physicochemical correlation across all drugs. Sertraline, the compound having both the highest logP (octanol/water coefficient) and thus the highest lipophilicity, the highest biologically relevant logD (distribution coefficient at pH7.4), and the lowest polar surface area, had the highest BBB model permeability results. Each of these physicochemical characteristics have been shown to contribute to BBB permeability [22,23]. Finally, the

Table 6.2 Physicochemical properties and dynamic *in vitro* results of each of the compounds tested in this dissertation. Properties are referenced from the chemical database ChEMBL.

Compound	MW	LogP	LogD pH7.4	H-Bond Acceptors /Donors	Polar Surface Area	Arom. Rings	Perm.	Toxicity
Sertraline	306.2	5	3.04	1/1	12.03	2	208±20	High
Varenicline	211.3	1.04	-1.06	3/1	37.81	2	163±78	Low
Traxoprodil	327.4	2.4	-0.16	4/3	63.93	2	131±37	Low
Ethosuximide	141.2	0.54	0.25	2/1	46.17	0	128±10	Low
Gabapentin	171.2	-1.49	-1.42	3/3	63.32	0	109±7	Low
Unnamed	489.6	5.04	2.75	4/3	70.98	2	93±12	Low
Sunitinib	398.5	3	0.44	4/3	77.23	2	87±13	High
Propidium Iodide	414.6	3.4	-1.89	2/2	55.92	4	7.9±2.9	Low
FITC-Dextran 4kD	4k	-6.29	-6.19	16/11 (per unit)	276.52 (per unit)	0	3.08±0.16	Low
FITC-Dextran 20kD	20k	-6.29	-6.19	16/11 (per unit)	276.52 (per unit)	0	1.84±0.97	Low
FITC-Dextran 70kD	70k	-6.29	-6.19	16/11 (per unit)	276.52 (per unit)	0	0.70±0.13	Low

FITC-Dextrans have the lowest permeability due to their significantly higher molecular weight and highly hydrophilic and polar physicochemical properties.

6.4 Future Work

This dissertation has demonstrated the feasibility of such a system for both applications: (1) measurement of barrier properties and testing of barrier modulation; (2) predictive assay platform for the clearance of compounds targeting the central nervous system. However, this dissertation represents an introductory pilot study to the novel concept of the microfluidic BBB model, which is intended to act as a launching point for several focused projects that will both benefit from and contribute to the foundations it has provided with the presented studies.

6.4.1 μBBB Model Optimization

The studies described in this dissertation have successfully accomplished considerable progress toward validating the feasibility of this type of system for use in the pharmaceutical industry. However, there are further characteristics of the model which can be optimized, in order to further hone the achieved barrier properties of the system and increase its practical efficacy. Further research is required to optimize the design of the system and further assess its benefits.

6.4.1.1 Primary Cells and Cell Culture Properties

The immortalized cell lines used in this dissertation have provided extremely valuable information, and indeed have several practical advantages that were described

in Chapter 2. However, primary cells are recognized as an optimal standard for BBB models. This is because relatively high correlations with *in vivo* models in terms of TEER and tight junction expression have been observed, though this advantage diminishes after only a few passages [24]. Furthermore, to achieve the ideal *in vitro* condition for translation of *in vitro* prediction to clinical efficacy, primary human cells rather than animal cells should be used. Since their origin is the brain, such endothelial cell culture isolations can only be obtained from surgical resections during autopsy or temporal lobectomy. Cerebral cortex fragments will be minced, homogenized in dextran, digested using collagenase/dispase, and isolated with a Percoll gradient procedure as has been described previously [25]. Results with the model are expected to exhibit significant increases in TEER, since in previous studies, TEER levels with significantly higher results have been achieved within the same laboratory with the same physical model and TEER measurement techniques in comparison with immortalized cells. However, limitations of adhesion are expected, and optimization of flow conditions and adhesion protein coatings will be required to ensure successful cell culture upon integration into the microfluidic device.

In addition to endothelial cells and astrocytes, a third cell type, the perictye, is present *in vivo* and covers approximately a quarter of the abluminal endothelial surface, playing a role in endothelial proliferation and inflammatory processes [26], though there have been difficulties in isolating this cell type due to lack of specific markers, therefore its use in BBB models have been somewhat limited. It would be pertinent to include pericytes in future studies with the μBBB.

6.4.1.2 Membrane Materials

The track-etched polycarbonate membranes used in this study were primarily used because they are identical to those used in transwells, providing experimental consistency with the static controls used, though they are one of many options for porous membrane materials which could be used in the model. Track-etched polyetheyle terephthalate (PET) are transparent, allowing light-based microscopy during cultures [27]. These track-etched membranes are not flexible, and tend to tear under too much mechanical stress. Other, highly flexible materials such as polydimethylsiloxane (PDMS) could be used instead to allow application of stretching mechanics to cell layers [28]. Such an approach could, for example, be used for testing of barrier modulation under conditions of physical trauma to brain vascular systems.

6.4.1.3 Electrode Properties

While the thin-film Ag/AgCl electrodes fabricated for the described μBBB were sufficient for the short-term experiments from this dissertation, they will need to be characterized for long-term stability and drift for long-term cultures to increase the throughput potential of the system. Optimization of electrode properties will be pertinent for future study. Electroplated AgCl has been shown to have improved long-term performance over sputtered AgCl [29]. Conversely to the microfabricated AgCl thin-film electrodes used in these studies, many different types of electrodes have been used for measuring TEER of endothelial or epithelial cells, including commercial silver/silver chloride electrodes [6,30], or alternate materials such as platinum [2], aluminum and copper [31], and stainless steel [32]. Additional strategies, such as KCl gel [33] or agar

[34] coatings on electrode systems could potentially improve their stability and long-term performance. Finally, to remove the need for integrating glass substrates, print-and-peel fabrication methods have been demonstrated to deposit copper and silver electrodes directly onto flexible PDMS substrates with reasonable performance [35].

6.4.1.4 Direct Comparison with an Animal Model

Though multiple-drug correlation of brain clearance results between transwell-based *in vitro* models and *in vivo* animal models has been shown previously [37,38], Chapter 5 reports the first demonstration of *in vivo* correlation for pharmaceutical drug clearance in a dynamic microfluidic model of the BBB. Though strong quantitative correlation between *in vivo* brain/plasma ratios (B/P) and *in vitro* permeability (P_e) was observed, B/P is not exclusively defined by BBB permeability, as it also involves other factors such as protein binding and brain metabolism [39,40]. Thus, a more direct, calculable correlation between *in vitro* and *in vivo* permeability for accurate quantitative prediction using the microfluidic model would best be achieved by calculating the *in vivo* BBB permeability-surface area product (P_S) for each compound.

To measure P_S with the animal model (Figure 6.4) [41], animals will need to be anesthetized with ketamine and xylazine, and body temperature will be maintained at 37°C with a heating pad. The right common carotid artery, which runs directly to the brain, will be exposed and ligated with the occipital artery, and cannulated with tubing connected to a syringe pump. Next, the heart is stopped by severing the ventricles, and the perfusion of the test compound diluted in a bicarbonate-buffered saline solution is initiated. Physiologically-relevant perfusion rates of about 9-10 mL/min should be used

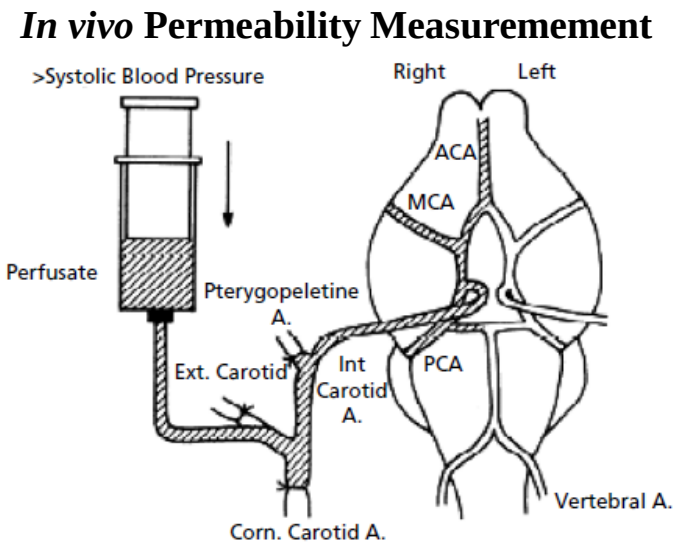

Figure 6.4 Permeability measurement of the BBB *in vivo*. Direct short-term permeability of the BBB can be measured *in vivo* by exposing and cannulating one of the carotid arteries, and perfusing a test compound prior to decapitation and measurement. From Nicolazzo [36].

[42], for a short duration >60s. Following the perfusion, the animal is immediately decapitated, and the brain tissue is excised, weighed, and digested in tissue solubilizer for scintillation counting. The measured brain concentration C_B is related to the initial uptake clearance Cl_{up} [43] by the equation

$$C_B/C_p = Cl_{up}T + V_v \tag{6.1}$$

where C_p is the perfused concentration, T is perfusion time, and V_v is the brain's vascular volume. Finally, the permeability coefficient P_S is computed from the following equation where F is the regional flow rate [42]:

$$P_S = -Fln\left(1 - Cl_{up}/F\right) \tag{6.2}$$

Thus, a more direct, calculable correlation between *in vitro* and *in vivo* permeability for more direct quantitative prediction could be achieved for characterizing correlation of

BBB permeability between the developed microfluidic model and the physiological condition.

6.4.1.5 Adoption of the Model by Industry

Adoption of such microfluidic models by the pharmaceutical industry for early-stage *in vitro* drug permeability screening is supported by the currently rapid increase of microfluidics in industry. The global microfluidics market was valued at $1.59 billion, attributed largely to the growing adoption of *in vitro* diagnostics for point of care, and is projected to reach $3.57 billion by 2018, with the drug delivery devices market expected to undergo the fastest growth during that time [44]. Adoption of microfluidic models for mainstream drug research and development has not yet occurred, though AstraZeneca has recently announced a collaboration with Harvard's Wyss Institute to research the integration of microfluidic cell culture models into their drug development process [45]. The primary challenge for adoption of organ-on-chips in this process is establishment of reliablie *in vivo* correlation. The effective *in vivo* correlation requires side-by-side studies between model results and *in vivo* results in terms of permeability, toxicity, as well as drug efficacy. The proof-of-concept for this *in vivo* correlation was demonstrated in this dissertation.

In addition, commercialization of the μBBB devices will require device fabrication and process design to optimize the robustness of the model for use by various researchers, and to allow large-scale manufacturing. While many of the fabrication processes in this dissertation were conducted by hand, automation of device fabrication processes will allow chip-to-chip consistency for extremely large batches of fabricated

chips. For consistency of such large-scale experiments, automation should be integrated into the system in every feasible way. For example, microfluidic chips have been designed that are capable of performing fully automated cell culture, including cell seeding and treatment with growth factors [46], allowing high versatility and repeatability, independent of the researcher performing experimentation. Such automation processes are key to large-scale mainstream industry adoption.

6.4.2 Screening of Novel BBB-Crossing Macromolecules

Up to date macromolecular drug delivery carriers have not proven to reach the CNS in effective pharmacological concentrations, though such routes are promising for future clinical application because they take advantage of specific receptors bound to endothelial cells. There is considerable interest in testing the effectiveness of such macromolecules for BBB passage, and the use of the microfluidic BBB model for this purpose is a potential future direction for this work, especially when various forms of the compound are available with a wide range of physicochemical properties. Novel drug delivery systems can be tailored for their physicochemical properties, making them potentially valuable vectors for targeting the blood-brain barrier. Poly (amidoamine) (PAMAM) dendrimers have been extensively studied for drug delivery applications [47]. First, they are available in a number of sizes, dependent on generation number, resulting in incremental increases in size. Furthermore, generation number increases molecular weight, the number of branches, and thus the number of terminal amine surface groups, each with their own diffusion times based on size and polarity. Second, surface modification onto the surface amine groups with different types of chemical groups, such as acetyl, lauroyl groups [48], amino acids, or PEG [49], as well as modification of

surface charge, number of lipid chains, and concentration, have been shown to lead to changes in permeability, functionality, and toxicity in Caco-2 epithelial cells [50,51]. It is reasonable to assume that such correlations of physicochemical properties of dendrimers with transport across epithelial and endothelial barriers such as the BBB are similar, nevertheless high-throughput testing of permeability of these compounds through the μBBB model and transwell/animal controls will be needed.

6.4.3 Toward a Complete Neurovascular Unit

The complete neurovascular unit is considered to comprise of the BBB multi-cellular component, the capillary and connected astrocytes, in addition to the adjacent neurons in the surrounding parenchyma [52], which are typically the target of CNS drugs (Figure 6.5A). Though neuron processes do not directly contact the capillaries as astrocyte processes do, there is sufficient evidence that neurons influence the BBB [53]. Co-culturing neurons or neural progenitor cells with endothelial cells in BBB models can have similar influence on barrier function as astrocyte co-culture [54,55], presumably through cell-cell signaling. Thus, further investigation of the interplay between neurons and the BBB is warranted.

A compartmentalized microfluidic model would allow isolation of the BBB and cultured neurons in separate compartments to permit integration of specialized microsensors in each chamber, and allows diffusion of test compounds and secreted cell signaling factors between the chambers in a tunable manner (Figure 6.5B). Though chambers are separated spatially in the mm scale, the channel height is in the μm scale, the Reynolds number remains under the laminar threshold [56], and particle motion is

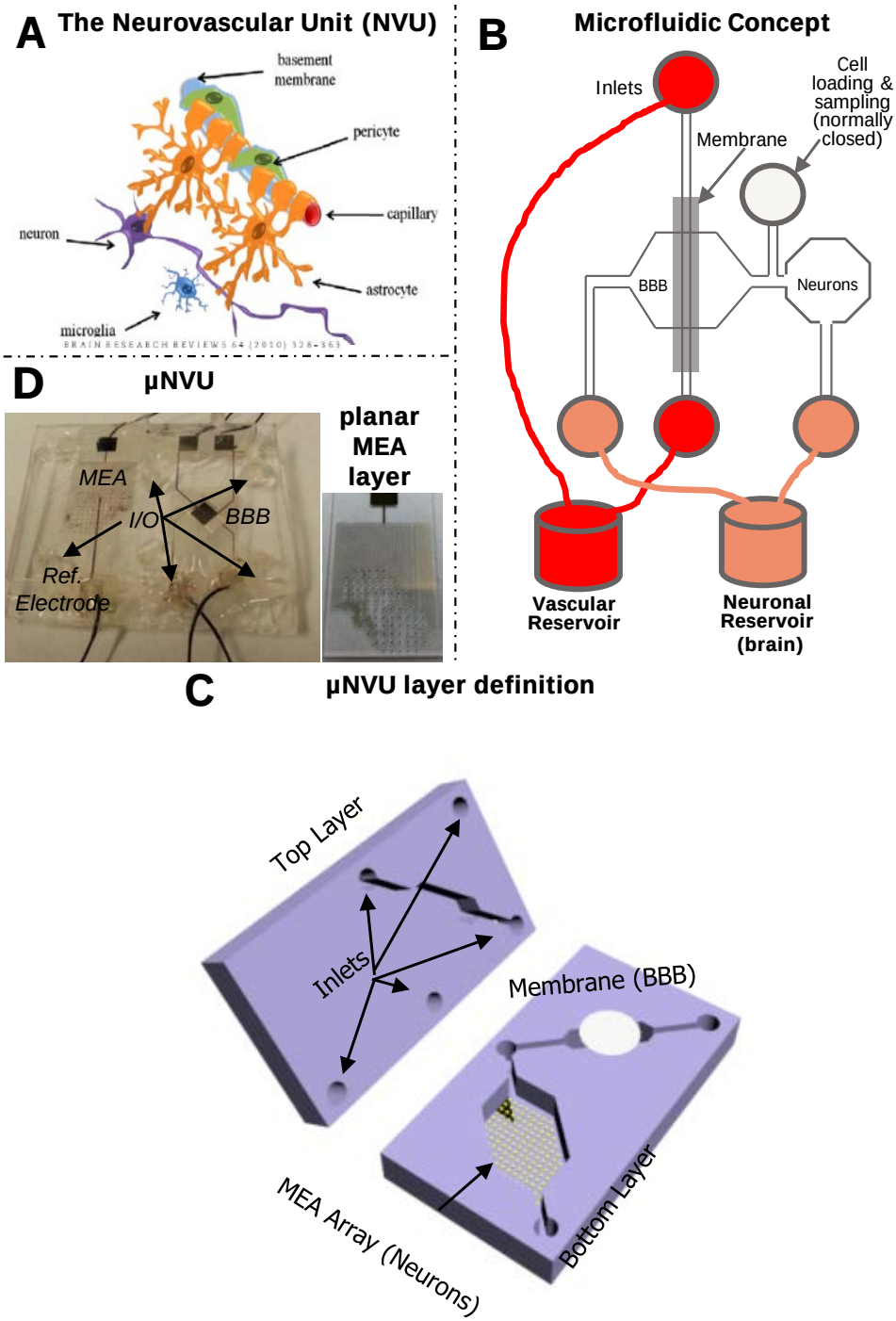

Figure 6.5 The microfluidic neurovascular unit concept (μNVU). (A) The neurovascular unit comprises of the BBB and the adjacent neurons. It is possible that these neurons play a role in BBB function. (B-C) To model the interplay between neurons and the BBB, a compartmentalized microfluidic device can isolate neurons from the BBB, while allowing diffusion of soluble factors and enabling independent monitoring/manipulation. (D) Prototype μNVU has been built; not yet characterized.

dominated by diffusion, as in brain tissue. Such a microfluidic neurovascular unit (μNVU, Figure 6.4C) has two applications: (1) BBB clearance and PD effect on (or cellular uptake by) neurons can be investigated simultaneously. (2) Secondary influence of neuron stimulation on BBB function can be observed. Electrical stimulation of neurons has been seen to induce neuronal activity *in vitro* [57-59] and *in vivo* [60-62]. Opening of the BBB has been observed in tissue surrounding implanted recording electrodes [63,64], though this has been attributed to the injury related to insertion trauma. It was recently shown that fifteen minutes of 50-100μA subcutaneous electrical stimulation at rat whisker pads induced transient BBB passage of IGF-1 *in vivo*, localized to the stimulated region, and the authors attributed this effect to the stimulated increase in neuronal activity [65], not electrical damage as has been previously attributed following several days of continuous stimulation [66]. This indicates BBB modulation through neurovascular coupling, and could have significant clinical implications for drug delivery. To our knowledge, the relationship between neuronal stimulation and BBB function has not been examined *in vitro*; therefore, a prototype was fabricated to test this relationship, though it has not yet been characterized or tested (Figure 6.4D). A second application of this design is recording changes in neuron activity in response to a perfused drug, thus allowing simultaneous monitoring of pharmacokinetic BBB clearance and pharmacodynamic neuron response.

6.4.4 Integration into a Body-on-a-Chip

An emerging branch of microfluidics uses compartmentalization to allow facilitated interaction between different organs/cell types, while allowing independent

manipulation and observation of the respective cell populations [67-69]. Shuler and colleagues previously developed the concept utilizing microfluidics to compartmentally model physiologically-based pharmacokinetic models (PBPK) [70], allowing effective elucidation of absorption, distribution, metabolism, excretion, and toxicity (ADMET) properties relating to multiple organs. These body-on-a-chip platforms, also coined microscale cell culture analogues (μCCAs), have been developed to model multiple organs, such as lung, liver, fat, or marrow into isolated chambers, while allowing integration of biosensors such as oxygen sensors [71,72]. Thus, these single systems allow modeling of realistic metabolism, distribution, and toxicities of tested compounds in a manner not possible with simpler models.

Though body-on-chips have been developed to include barrier components representing the gastrointestinal tract to model oral adsorption in combination with interaction with individual organs on the same chip [67-69] or in a separate module in connection with peripheral organs [73], such a system is yet to be integrated with a BBB component to allow simultaneous monitoring of systemic interaction and BBB passage.

6.5 References

[1] Booth, R. and H. Kim. Characterization of a microfluidic in vitro model of the blood-brain barrier (μbbb). *Lab on a Chip*. **12**(10):1784-1792, 2012.

[2] Griep, L., F. Wolbers, B. de Wagenaar, P. Ter Braak, B. Weksler, I. A. Romero, P. Couraud, I. Vermes, A. van der Meer, and A. van den Berg. Bbb on chip: Microfluidic platform to mechanically and biochemically modulate blood-brain barrier function. *Biomedical microdevices*. **15**(1):145-150, 2013.

[3] Booth, R., S. Noh, and H. Kim. A multiple-channel, multiple-assay platform for characterization of full-range shear stress effects on vascular endothelial cells. *Lab on a Chip*. **14**(11):1880-1890, 2014.

[4] Achyuta, A. K. H., A. J. Conway, R. B. Crouse, E. C. Bannister, R. N. Lee, C. P.

Katnik, A. A. Behensky, J. Cuevas, and S. S. Sundaram. A modular approach to create a neurovascular unit-on-a-chip. *Lab on a Chip*. **13**(4):542-553, 2013.

[5] Prabhakarpandian, B., M.-C. Shen, J. B. Nichols, I. R. Mills, M. Sidoryk-Wegrzynowicz, M. Aschner, and K. Pant. Sym-bbb: A microfluidic blood brain barrier model. *Lab on a Chip*. **13**(6):1093-1101, 2013.

[6] Douville, N. J., Y.-C. Tung, R. Li, J. D. Wang, M. E. El-Sayed, and S. Takayama. Fabrication of two-layered channel system with embedded electrodes to measure resistance across epithelial and endothelial barriers. *Analytical chemistry*. **82**(6):2505-2511, 2010.

[7] Schinkel, A. H., E. Wagenaar, C. Mol, and L. van Deemter. P-glycoprotein in the blood-brain barrier of mice influences the brain penetration and pharmacological activity of many drugs. *Journal of Clinical Investigation*. **97**(11):2517, 1996.

[8] Raub, T. J. Signal transduction and glial cell modulation of cultured brain microvessel endothelial cell tight junctions. *American Journal of Physiology-Cell Physiology*. **271**(2):C495-C503, 1996.

[9] Smith, M., Y. Omidi, and M. Gumbleton. Primary porcine brain microvascular endothelial cells: Biochemical and functional characterisation as a model for drug transport and targeting. *Journal of drug targeting*. **15**(4):253-268, 2007.

[10] Fu, C. T., J. F. Bechberger, M. A. Ozog, B. Perbal, and C. C. Naus. Ccn3 (nov) interacts with connexin43 in c6 glioma cells possible mechanism of connexin-mediated growth suppression. *Journal of Biological Chemistry*. **279**(35):36943-36950, 2004.

[11] Grabowski, E., E. Jaffe, and B. Weksler. Prostacyclin production by cultured endothelial cell monolayers exposed to step increases in shear stress. *J Lab Clin Med*. **105**(1):36-43, 1985.

[12] Ott, M. J. and B. J. Ballermann. Shear stress-conditioned, endothelial cell-seeded vascular grafts: Improved cell adherence in response to in vitro shear stress. *Surgery*. **117**(3):334-339, 1995.

[13] Chen, J., B. Fabry, E. L. Schiffrin, and N. Wang. Twisting integrin receptors increases endothelin-1 gene expression in endothelial cells. *American Journal of Physiology-Cell Physiology*. **280**(6):C1475-C1484, 2001.

[14] Ando, J. and K. Yamamoto. Vascular mechanobiology: Endothelial cell responses to fluid shear stress. *Circulation journal: official journal of the Japanese Circulation Society*. **73**(11):1983, 2009.

[15] Colgan, O. C., G. Ferguson, N. T. Collins, R. P. Murphy, G. Meade, P. A. Cahill, and P. M. Cummins. Regulation of bovine brain microvascular

endothelial tight junction assembly and barrier function by laminar shear stress. *American Journal of Physiology-Heart and Circulatory Physiology*. **292**(6):H3190-H3197, 2007.

[16] Simon, M. J., W. H. Kang, S. Gao, S. Banta, and B. Morrison III. Tat is not capable of transcellular delivery across an intact endothelial monolayer in vitro. *Annals of biomedical engineering*. **39**(1):394-401, 2011.

[17] Wuest, D. M., A. M. Wing, and K. H. Lee. Membrane configuration optimization for a murine< i> in vitro</i> blood–brain barrier model. *Journal of neuroscience methods*. **212**(2):211-221, 2013.

[18] Madara, J. L. Regulation of the movement of solutes across tight junctions. *Annual review of physiology*. **60**(1):143-159, 1998.

[19] Gumbleton, M. and K. L. Audus. Progress and limitations in the use of in vitro cell cultures to serve as a permeability screen for the blood-brain barrier. *Journal of pharmaceutical sciences*. **90**(11):1681-1698, 2001.

[20] Nielsen, H. M. and M. R. Rassing. Nicotine permeability across the buccal tr146 cell culture model and porcine buccal mucosa in vitro: Effect of ph and concentration. *Eur J Pharm Sci*. **16**(3):151-157, 2002.

[21] Nielsen, H. M. and M. R. Rassing. Tr146 cells grown on filters as a model of human buccal epithelium: Iii. Permeability enhancement by different ph values, different osmolality values, and bile salts. *Int J Pharm*. **185**(2):215-225, 1999.

[22] Deak, K., K. Takacs-Novak, K. Tihanyi, and B. Noszal. Physico-chemical profiling of antidepressive sertraline: Solubility, ionisation, lipophilicity. *Medicinal Chemistry*. **2**(4):385-389, 2006.

[23] Crivori, P., G. Cruciani, P.-A. Carrupt, and B. Testa. Predicting blood-brain barrier permeation from three-dimensional molecular structure. *Journal of medicinal chemistry*. **43**(11):2204-2216, 2000.

[24] Yoo, J.-W., Y.-S. Kim, S.-H. Lee, M.-K. Lee, H.-J. Roh, B.-H. Jhun, C.-H. Lee, and D.-D. Kim. Serially passaged human nasal epithelial cell monolayer for in vitro drug transport studies. *Pharmaceutical research*. **20**(10):1690-1696, 2003.

[25] Bowman, P. D., S. R. Ennis, K. E. Rarey, A. Lorris Betz, and G. W. Goldstein. Brain microvessel endothelial cells in tissue culture: A model for study of blood-brain barrier permeability. *Annals of neurology*. **14**(4):396-402, 1983.

[26] Dore-Duffy, P. Pericytes: Pluripotent cells of the blood brain barrier. *Current Pharmaceutical Design*. **14**(16):1581-1593, 2008.

[27] Perrière, N., S. Yousif, S. Cazaubon, N. Chaverot, F. Bourasset, S. Cisternino, X. Declèves, S. Hori, T. Terasaki, and M. Deli. A functional in vitro model of

rat blood–brain barrier for molecular analysis of efflux transporters. *Brain research*. **1150**(1-13, 2007.

[28] Huh, D., B. D. Matthews, A. Mammoto, M. Montoya-Zavala, H. Y. Hsin, and D. E. Ingber. Reconstituting organ-level lung functions on a chip. *Science*. **328**(5986):1662-1668, 2010.

[29] Polk, B. J., A. Stelzenmuller, G. Mijares, W. MacCrehan, and M. Gaitan. Ag/agcl microelectrodes with improved stability for microfluidics. *Sensors and Actuators B: Chemical*. **114**(1):239-247, 2006.

[30] Ma, S. H., L. A. Lepak, R. J. Hussain, W. Shain, and M. L. Shuler. An endothelial and astrocyte co-culture model of the blood–brain barrier utilizing an ultra-thin, nanofabricated silicon nitride membrane. *Lab on a Chip*. **5**(1):74-85, 2005.

[31] Vogel, P. A., S. T. Halpin, R. S. Martin, and D. M. Spence. Microfluidic transendothelial electrical resistance measurement device that enables blood flow and postgrowth experiments. *Analytical chemistry*. **83**(11):4296-4301, 2011.

[32] Wegener, J., D. Abrams, W. Willenbrink, H.-J. Galla, and A. Janshoff. Automated multi-well device to measure transepithelial electrical resistances under physiological conditions. *Biotechniques*. **37**(590):592-594, 2004.

[33] Huang, I.-Y., R.-S. Huang, and L.-H. Lo. Improvement of integrated ag/agcl thin-film electrodes by kcl-gel coating for isfet applications. *Sensors and Actuators B: Chemical*. **94**(1):53-64, 2003.

[34] Hassel, A. W., K. Fushimi, and M. Seo. An agar-based silver| silver chloride reference electrode for use in micro-electrochemistry. *Electrochemistry communications*. **1**(5):180-183, 1999.

[35] Hong, C., D. Bao, M. S. Thomas, J. M. Clift, and V. I. Vullev. Print-and-peel fabrication of microelectrodes. *Langmuir*. **24**(16):8439-8442, 2008.

[36] Nicolazzo, J. A., S. A. Charman, and W. N. Charman. Methods to assess drug permeability across the blood-brain barrier. *Journal of pharmacy and pharmacology*. **58**(3):281-293, 2006.

[37] Zhang, Y., C. S. Li, Y. Ye, K. Johnson, J. Poe, S. Johnson, W. Bobrowski, R. Garrido, and C. Madhu. Porcine brain microvessel endothelial cells as an in vitro model to predict in vivo blood-brain barrier permeability. *Drug metabolism and disposition*. **34**(11):1935-1943, 2006.

[38] Pardridge, W. M., D. Triguero, J. Yang, and P. A. Cancilla. Comparison of in vitro and in vivo models of drug transcytosis through the blood-brain barrier. *Journal of Pharmacology and Experimental Therapeutics*. **253**(2):884-891,

1990.

[39] Liu, X., C. Chen, and B. J. Smith. Progress in brain penetration evaluation in drug discovery and development. *Journal of Pharmacology and Experimental Therapeutics*. **325**(2):349-356, 2008.

[40] Cornford, E. The blood-brain barrier, a dynamic regulatory interface. *Molecular physiology*. **7**(3):219-260, 1985.

[41] Liu, X., M. Tu, R. S. Kelly, C. Chen, and B. J. Smith. Development of a computational approach to predict blood-brain barrier permeability. *Drug metabolism and disposition*. **32**(1):132-139, 2004.

[42] Smith, Q. R., *Brain perfusion systems for studies of drug uptake and metabolism in the central nervous system*, in *Models for assessing drug absorption and metabolism*. 1996, Springer. p. 285-307.

[43] Dagenais, C., C. Rousselle, G. M. Pollack, and J.-M. Scherrmann. Development of an in situ mouse brain perfusion model and its application to mdr1a p-glycoprotein-deficient mice. *Journal of Cerebral Blood Flow & Metabolism*. **20**(2):381-386, 2000.

[44] Rohan, *Microfluidics market by materials, pharmaceuticals, drug delivery devices, ivd - global trends & forecast to 2018*, in *Microfluidics Market worth $3.5 Billion by 2018*, Rohan, Editor. 2013: Markets and Markets.

[45] Sackmann, E. K., A. L. Fulton, and D. J. Beebe. The present and future role of microfluidics in biomedical research. *Nature*. **507**(7491):181-189, 2014.

[46] Gómez-Sjöberg, R., A. A. Leyrat, D. M. Pirone, C. S. Chen, and S. R. Quake. Versatile, fully automated, microfluidic cell culture system. *Analytical Chemistry*. **79**(22):8557-8563, 2007.

[47] Sadekar, S. and H. Ghandehari. Transepithelial transport and toxicity of pamam dendrimers: Implications for oral drug delivery. *Adv Drug Deliv Rev*. 2011.

[48] Jevprasesphant, R., J. Penny, D. Attwood, and A. D'Emanuele. Transport of dendrimer nanocarriers through epithelial cells via the transcellular route. *Journal of controlled release*. **97**(2):259-267, 2004.

[49] Sweet, D. M., R. B. Kolhatkar, A. Ray, P. Swaan, and H. Ghandehari. Transepithelial transport of pegylated anionic poly(amidoamine) dendrimers: Implications for oral drug delivery. *J Control Release*. **138**(1):78-85, 2009.

[50] Tomalia, D. A., A. M. Naylor, and W. A. Goddard III. Starburst dendrimers: Molecular-level control of size, shape, surface chemistry, topology, and flexibility from atoms to macroscopic matter. *Angewandte Chemie International Edition in English*. **29**(2):138-175, 1990.

[51] Jevprasesphant, R., J. Penny, D. Attwood, N. B. McKeown, and A. D'Emanuele. Engineering of dendrimer surfaces to enhance transepithelial transport and reduce cytotoxicity. *Pharm Res*. **20**(10):1543-1550, 2003.

[52] Cardoso, F. L., D. Brites, and M. A. Brito. Looking at the blood-brain barrier: Molecular anatomy and possible investigation approaches. *Brain Res Rev*. **64**(2):328-363, 2010.

[53] Bauer, H. C. and H. Bauer. Neural induction of the blood-brain barrier: Still an enigma. *Cell Mol Neurobiol*. **20**(1):13-28, 2000.

[54] Schiera, G., S. Sala, A. Gallo, M. P. Raffa, G. L. Pitarresi, G. Savettieri, and I. Di Liegro. Permeability properties of a three-cell type in vitro model of blood-brain barrier. *J Cell Mol Med*. **9**(2):373-379, 2005.

[55] Weidenfeller, C., C. N. Svendsen, and E. V. Shusta. Differentiating embryonic neural progenitor cells induce blood-brain barrier properties. *J Neurochem*. **101**(2):555-565, 2007.

[56] Stone, H. A. and S. Kim. Microfluidics: Basic issues, applications, and challenges. *AIChE Journal*. **47**(6):1250-1254, 2001.

[57] Takenaga, S., Y. Tamai, K. Hirai, K. Takahashi, T. Sakurai, S. Terakawa, M. Ishida, K. Okumura, and K. Sawada. *Label-free real time imaging of neural communication using acetylcholine image sensor*. in *Solid-State Sensors, Actuators and Microsystems Conference (TRANSDUCERS), 2011 16th International*. 2011: IEEE.

[58] Blake, A. J., F. C. Rodgers, A. Bassuener, J. A. Hippensteel, T. M. Pearce, T. R. Pearce, E. D. Zarnowska, R. A. Pearce, and J. C. Williams. A microfluidic brain slice perfusion chamber for multisite recording using penetrating electrodes. *Journal of neuroscience methods*. **189**(1):5-13, 2010.

[59] Erickson, J., A. Tooker, Y. C. Tai, and J. Pine. Caged neuron mea: A system for long-term investigation of cultured neural network connectivity. *J Neurosci Methods*. **175**(1):1-16, 2008.

[60] Cogan, S. F. Neural stimulation and recording electrodes. *Annu. Rev. Biomed. Eng.* **10**(275-309, 2008.

[61] Pagé, P. L., N. Dandan, P. Savard, R. Nadeau, J. A. Armour, and R. Cardinal. Regional distribution of atrial electrical changes induced by stimulation of extracardiac and intracardiac neural elements. *The Journal of Thoracic and Cardiovascular Surgery*. **109**(2):377-388, 1995.

[62] Robin, S., M. Sawan, M. Abdel-Gawad, T. Abdel-Baky, and M. Elhilali. Implantable stimulation system dedicated for neural selective stimulation. *Medical and Biological Engineering and Computing*. **36**(4):490-492, 1998.

[63] Winslow, B. D. and P. A. Tresco. Quantitative analysis of the tissue response to chronically implanted microwire electrodes in rat cortex. *Biomaterials*. **31**(7):1558-1567, 2010.

[64] Zhong, Y. and R. V. Bellamkonda. Dexamethasone-coated neural probes elicit attenuated inflammatory response and neuronal loss compared to uncoated neural probes. *Brain Res*. **1148**(15-27, 2007.

[65] Nishijima, T., J. Piriz, S. Duflot, A. M. Fernandez, G. Gaitan, U. Gomez-Pinedo, J. M. Verdugo, F. Leroy, H. Soya, A. Nunez, and I. Torres-Aleman. Neuronal activity drives localized blood-brain-barrier transport of serum insulin-like growth factor-i into the cns. *Neuron*. **67**(5):834-846, 2010.

[66] Pudenz, R. H., L. Bullara, S. Jacques, and F. Hambrecht. Electrical stimulation of the brain. Iii. The neural damage model. *Surgical neurology*. **4**(4):389, 1975.

[67] Imura, Y., E. Yoshimura, and K. Sato. Micro total bioassay system for oral drugs: Evaluation of gastrointestinal degradation, intestinal absorption, hepatic metabolism, and bioactivity. *Anal Sci*. **28**(3):197-199, 2012.

[68] Esch, M. B., T. L. King, and M. L. Shuler. The role of body-on-a-chip devices in drug and toxicity studies. *Annu Rev Biomed Eng*. **13**(55-72, 2011.

[69] Esch, M. B., J. H. Sung, and M. L. Shuler. Promises, challenges and future directions of muccas. *J Biotechnol*. 2010.

[70] Sweeney, L., M. Shuler, J. Babish, and A. Ghanem. A cell culture analogue of rodent physiology: Application to naphthalene toxicology. *Toxicology in vitro*. **9**(3):307-316, 1995.

[71] Viravaidya, K., A. Sin, and M. L. Shuler. Development of a microscale cell culture analog to probe naphthalene toxicity. *Biotechnology Progress*. **20**(1):316-323, 2004.

[72] Viravaidya, K. and M. L. Shuler. Incorporation of 3t3-l1 cells to mimic bioaccumulation in a microscale cell culture analog device for toxicity studies. *Biotechnology progress*. **20**(2):590-597, 2004.

[73] Mahler, G. J., M. B. Esch, R. P. Glahn, and M. L. Shuler. Characterization of a gastrointestinal tract microscale cell culture analog used to predict drug toxicity. *Biotechnology and bioengineering*. **104**(1):193-205, 2009.